Thesis

Revealing entanglement and nonlocality in few photon states

CAPRARA VIVOLI, Valentina

Abstract

In the past two decades, the union of quantum mechanics and information science has led to significant progress in our understanding of the quantum world and in our ability to coherently control individual quantum systems. New technologies have appeared, and some of them, such as quantum key distribution (QKD), are now commercially available. We are now envisioning quantum networks that could allow us to communicate over intercontinental scales, as the internet does, but with a provable security. An open question in this framework is how to certify that a given quantum network performs well, i.e. how to detect entanglement between 2, 5, 10 or 100 nodes located far away from each other. Bell tests are appealing for such a task as they allow one to certify the presence of entanglement deviceindependently, i.e. without assumptions on the Hilbert space dimension or on the proper alignment of the measurement devices. In the first chapter, I start by examining in depth the most standard approach to perform a Bell test in which a source based on spontaneous parametric down conversion (SPDC) is used to create photon pairs [...]

Reference

CAPRARA VIVOLI, Valentina. *Revealing entanglement and nonlocality in few photon states*. Thèse de doctorat : Univ. Genève, 2015, no. Sc. 4876

URN : urn:nbn:ch:unige-839792
DOI : 10.13097/archive-ouverte/unige:83979

Université de Genève
Groupe de Physique Appliquée

Faculté des Sciences
Professeur Nicolas Gisin

Revealing Entanglement And Nonlocality In Few Photon States

Thèse

présentée à la Faculté des Sciences de l'Université de Genève pour obtenir le grade de Docteur ès Sciences, mention physique

par

Valentina Caprara Vivoli

d'Italie

Thèse N° 4876

GENÈVE
2015

UNIVERSITÉ DE GENÈVE

FACULTÉ DES SCIENCES

Doctorat ès sciences
Mention physique

Thèse de *Madame Valentina CAPRARA VIVOLI*

intitulée :

"Revealing Entanglement and Nonlocality in Few Photons States"

La Faculté des sciences, sur le préavis de Monsieur N. GISIN, professeur ordinaire et directeur de thèse (Groupe de Physique Appliquée), Monsieur R. THEW, docteur (Groupe de Physique Appliquée), Monsieur A. MARTIN, docteur (Groupe de Physique Appliquée), Monsieur N. SANGOUARD, professeur (Département de physique, Université de Bâle, Suisse) et Madame Stephanie WEHNER, professeure (Centre QuTech, Delft University of Technology, The Netherlands), autorise l'impression de la présente thèse, sans exprimer d'opinion sur les propositions qui y sont énoncées.

Genève, le 16 décembre 2015

Thèse - 4876 -

Le Doyen

N.B. - La thèse doit porter la déclaration précédente et remplir les conditions énumérées dans les "Informations relatives aux thèses de doctorat à l'Université de Genève".

Abstract

In the past two decades, the union of quantum mechanics and information science has led to significant progress in our understanding of the quantum world and in our ability to coherently control individual quantum systems. New technologies have appeared, and some of them, such as quantum key distribution (QKD), are now commercially available. We are now envisioning quantum networks that could allow us to communicate over intercontinental scales, as the internet does, but with a provable security. An open question in this framework is how to certify that a given quantum network performs well, i.e. how to detect entanglement between 2, 5, 10 or 100 nodes located far away from each other. Bell tests are appealing for such a task as they allow one to certify the presence of entanglement device-independently, i.e. without assumptions on the Hilbert space dimension or on the proper alignment of the measurement devices. In the first chapter, I start by examining in depth the most standard approach to perform a Bell test in which a source based on spontaneous parametric down conversion (SPDC) is used to create photon pairs entangled in polarization. I show, in particular, that in this case the Bell inequality violation is fundamentally limited by vacuum and multi-photon emissions. In the second part of this thesis, I show how to overcome this limitation by using the SPDC source to create single photon entanglement, i.e. entanglement between two paths sharing a single photon, or two-mode squeezed states. Here, the non local content of the states is revealed using photon counting techniques preceded by small displacements in phase space. In the third part, I show how these measurements can be used for an optomechanical Bell test. This opens the way for device-independent quantum information processing with optomechanical systems and might be relevant to test collapse models in a theory independent manner. In the fourth chapter, the same measurements are used to build up a witness that can reveal genuine path entanglement. This witness has triggered an experiment which highlights its potential for network certification. I conclude the thesis by showing how path entanglement can be revealed with the human eye by exploiting these displacement operations.

Résumé

Pendant les deux dernières décennies, l'union de la mécanique quantique et des sciences de l'information a conduit à des progrès significatifs dans notre compréhension du monde quantique et pour le contrôle cohérent des systèmes quantiques individuels. Des nouvelles technologies ont fait leur apparition et certaines d'entre elles, comme la distribution de clés quantiques (QKD), sont même commercialisée. Maintenant, il semble envisageable de faire des réseaux quantiques qui pourraient nous permettre d'échanger des bits quantiques sur des échelles intercontinentales, c'est-à-dire une sorte d'internet mais avec une sécurité prouvée. Une question demeure: comment certifier qu'un réseau quantique donne de bons résultats, ou plus précisément comment détecter de l'intrication entre 2, 5, 10 ou 100 nodes situés loin les uns des autres. Les tests de Bell sont attractifs pour une telle tâche car ils permettent de certifier la présence d'intrication "device-independently", c'est-à-dire sans hypothèses sur la dimension de l'espace de Hilbert ou sur le bon alignement des appareils de mesure. Dans le premier chapitre, je commence par examiner en profondeur l'approche la plus commune pour effectuer un test de Bell dans lequel une source basée sur des processus non-linéaire de conversion paramétrique spontannée (SPDC) est utilisée pour créer des paires de photons intriqués en polarisation. Je montre, en particulier, que dans ce cas la violation des inégalités de Bell est fondamentalement limitée par les contribution du vide et des multi-photons. Dans la deuxième partie de cette thèse, je montre comment surmonter cette limitation en utilisant la source SPDC pour créer de l'intrication entre des modes optiques où des états comprimés. Le contenu non local de ces états est révélé en utilisant des techniques de comptage de photons précédées par des petits déplacements dans l'espace des phases. Dans la troisième partie, je montre comment ces mesures peuvent être utilisées pour un test de Bell sur des systèmes optomécanique. Cela ouvre la voie pour l'information quantique device-independent dans ces systèmes et pourrait être pertinent pour tester des modèles de collapse sans hypothèse quantique. Dans le quatrième chapitre, les mêmes mesures sont utilisées pour construire un témoin qui peut révéler de l'intrication entre des modes optiques. Ce témoin a déclenché une expérience qui a mis en évidence son potentiel pour la certification des réseaux quantiques du futur. De plus, je montre comment á l'aide d'une approche similaire il serait possible d'observer de l'intrication avec un oeil humain à travers la loupe d'une opération de déplacement des modes quantiques.

Contents

List of publications **49**

Introduction

In the last two decades a wide range of discoveries have been made in the field of quantum information (Nielsen and Chuang 2000). In this broad context the implementations of quantum networks and their potential have inspired my thesis. In a quantum network information is generated, processed and stored in quantum nodes that are linked by quantum channels. These nodes and channels are used to distribute the information, stored in entangled states, over the entire network.
The advantage of quantum channels when compared to classical channels is given by the properties of composed quantum systems. Classically, a network composed of k n-bit nodes is a system of dimension $k2^n$. A quantum network of the same type, i.e. k n-qubit nodes, however has dimension 2^{kn} (Kimble 2008). This already alone hints at the fact that quantum information processing can have an exponential advantage when compared to the classical case.
Another advantage of quantum networks is the improvement of security protocols. It would allow the implementation of quantum key distribution (QKD), i.e. it would allow two parties to generate a secret key in the presence of an eavesdropper (Gisin 2002).
Amongst the various aspects of the implementation of such a network, my work focuses on detecting entanglement and nonlocality in a distributed scenario, i.e. using only local measurements. The long term goal of my work is to provide operational methods to certify the proper functioning of these networks. The underlying question is how can we reveal entanglement in 3, 10, 100 modes separated by tens or hundreds or more kilometers? Bell tests are appealing for such an endeavor because they can reveal entanglement device independently, i.e. without any assumption on the functioning of the devices.
Let us recall the principle of such a test. In its simplest form, a Bell test requires two protagonists, Alice and Bob. They each receive a particle that they analyze with a measurement device. They can ask two questions with such a device, labeled x for Alice and y for Bob, $x, y, \in \{0, 1\}$. For a given question, the measurement device provides two answers $a(b) = \pm 1$. By repeating the experiment many times, Alice and Bob can estimate the joint probability distribution $p\left(ab|xy\right)$ and subsequently compute the CHSH value Clauser et al. 1969

$$\mathrm{CHSH} = \sum_{x,y=0}^{1} (-1)^{xy} \left(p\left(a = b|xy\right) - p\left(a \neq b|xy\right)\right). \tag{1}$$

If CHSH > 2, Alice and Bob share correlations that cannot be explained by local hidden variables. Interestingly, the conclusion holds in a theory-independent manner, i.e. we do not need quantum mechanics to get to such a conclusion. Realizing a proper Bell test is important from a practical point of view since it would allow device-independent random number generation (DI-RNG) and device-independent quantum key distribution (DI-QKD). In the first case the idea relies on the fact that the entropy produced per run depends on the Bell violation, i.e. every ϵ of violation translates into ϵ' of entropy (Pironio et al. 2010). For this purpose, two experiments have already been realized (Christensen et al. 2013; Pironio et al. 2010).
In the same way, concerning DIQKD, the amount of violation tells us how many random bits can be used to distribute a secret key in a device-independent way. There are already theoretical (Acin et al. 2007) and experimental (Gisin et al. 2010; Lim et al. 2013; Sangouard et al. 2011) proposals.
Since the amount of violation is the relevant parameter for these applications it is worth studying what can be observed in a standard protocol where a photon source based on a parametric down conversion source is used to create photon pairs entangled in polarization. We can confidently state that nowadays this is the only device suited for such applications: it is well integrated, commercially available and operates at room temperature. Furthermore, the physics behind optical systems is well known, both in the classical and in the quantum regimes. The drawback is the detection efficiency, but recent improvements (Fukuda et al. 2011; Lita et al. 2008; Miller et al. 2011; Verma et al. 2014) led to the first detection loophole-free photonic Bell tests recently (Christensen et al. 2013; Giustina et al. 2013).
Given that the CHSH inequality considers two outcomes, qubit-pairs, for example two polarization entangled photons are a natural choice. Such a system is, however, very difficult to realize in practice and SPDC sources only provide an approximation of two qubit entangled states. These sources are indeed probabilistic and have the drawback to inherently produce vacuum states and multi-pairs. Thus the maximal violation can be greatly reduced by these factors. Yet, all the theoretical studies are based on the assumption of having two photons entangled in polarization. It is, then, necessary to make the link between theory and experiment.
Another approach could be to use other degrees of freedom. Optical-path entanglement, i.e. the entanglement relying on the sharing of one or more photons between several modes, is another kind of entanglement that has recently gained interest both from the theoretical (Banaszek and Wodkiewicz 1998; Bohr Brask et al. 2013; Chaves and Bohr Brask 2011; Hessmo et al. 2004) and the experimental (Ho et al. 2014; Kuzmich et al. 2000; Morin et al. 2013) point of view. Optical-path entangled states have the appealing potential to extend known point-to-point quantum repeaters to richer topologies for quantum networks. Indeed a single photon can generate entanglement between an arbitrary large number of spatial modes using beam splitters. The local network can subsequently be entangled with others using 50:50 beam splitters and photon counting techniques. Furthermore two-qubit

states can now be almost perfectly created with SPDC sources and photon counting techniques.
Optical-path entanglement is, however, difficult to measure. One cannot, for example, use only photon-counting techniques in order to detect correlations between states with a different number of photons. A measurement that has already been used for this degree of freedom is the homodyne measurement. It consists of a 50:50 beam splitter, a coherent state and two photo-diodes per arm. It has been shown that this measurement with a suitable binning acts in the $\{|0\rangle, |1\rangle\}$ subspace as a noisy Pauli matrix on the equator of the Bloch sphere (Morin et al. 2013). Unfortunately this measurement is not suitable for nonlocality tests, since the noise strongly affects the maximal CHSH value. An alternative measurement has been proposed in Banaszek and Wodkiewicz 1998 consisting of a small displacement in phase space followed by a non-photon number resolving (NPNR) detector. This allows for high Bell violations that can be realized in optical-path setups.
Studies about optical-path entanglement could, in principle, be very attractive since they could be adapted to detect nonlocality in optomechanical systems. Indeed a recent study (Galland et al. 2014) showed how it is possible to generate a two-mode squeezed state by means of an optomechanical cavity. Optomechanical cavities are raising more and more interest since they could also be used to generate macroscopic quantum states. Realizing an optomechanical Bell test could possibly open the way to the detection of macroscopic quantum features.
Nevertheless the possibility of violating a Bell test in a optical-path scenario with low efficiencies is rather unlikely. There is also the possibility to test entanglement instead of nonlocality. The requirements needed in this case are less demanding in terms of efficiency and noise, as one can apply, for example, the PPT criterion to a Bell inequality to lower the minimal required efficiency. In this case the Bell inequality serves as witness of entanglement. The latter is defined as an observable W such that, if for a given state its value is bigger than a certain threshold value, then that state is entangled. If it is smaller than the threshold, we cannot conclude anything. Witnesses of entanglement also have the appealing feature of being scalable, i.e. to be extendable to the multimode case.
Another interesting topic is how we can apply all our discoveries to the detection of quantum features with the human eye. It has been shown in Hecht et al. 1942 that human eyes can be modelled as low efficiency detectors ($\eta = 0.08$) with a threshold between 7 and 8 photons. It is worth to see if adding a small displacement before an eye could allow the detection of optical-path entanglement.
In this thesis, I report on my work of how to detect non-local and entangled correlations for photonic quantum networks. The thesis is organised as follows.
In the first chapter, I studied the implementation of a CHSH-Bell test in the case of polarization-entangled states. I show that even though this case has already been studied in several works, a deeper study of a setup based on SPDC sources is required.

In the second chapter, I move to the study of a CHSH-Bell implementation using optical-path entanglement. Here, I introduce the displacement-based (DB) measurement relying on a small displacement and a NPNR detector. I show how with the use of this measurement it is possible to obtain better results than in the polarization case both in terms of violation and randomness generation. Secondly, I show that it is possible to use the DB measurement also for Bell tests on two-mode squeezed states generated by SPDC sources and compare the results with the previous implementations.
In the third chapter, I show that the DB measurement is able to show photon-phonon nonlocal correlations for states generated by optomechanical cavities. I, then, show that it is possible to implement the experiment also with imperfect initial conditions, i.e. if the optomechanical cavity is initially not in its ground state.
In the fourth chapter, I pass to study if it is possible to implement an experiment with the aim of revealing genuine multipartite optical-path entanglement relying on local measurements. I show that this is possible using two DB measurements per party for high losses and low quantity of entanglement.
Finally in chapter 5, I report the study performed on the human eye. I show that using a small displacement before the eye, as for the DB measurement, it is theoretically possible to detect entanglement.
As a last note, I add in the Appendix a proposal for quantum storage studied during my PhD. The intuition behind it is to exploit the coherent free-induced decay type re-emission which occurs naturally when a photon with a broadband spectrum is absorbed by a narrow atomic transition in an optically dense ensemble. In this regime it is reasonable to expect high retrieval efficiencies and fidelities. I will not provide any other comment about it, but instead I refer the interested reader to the paper.

1 Challenging preconceptions about Bell tests with photon pair sources

1.1 Introduction.

Several studies have been made on how to realize a loophole-free Bell test. Recently all the loopholes have been closed together in a CHSH experiment exploiting the entanglement between the spins of two electrons (Hensen et al. 2015) proving that Nature is nonlocal.
Nevertheless loophole free Bell tests are also important for technological applications. Indeed they would allow random number generation (Brunner et al. 2014; Colbeck and Kent 2011; Pironio et al. 2010) device-independently. To this end, the CHSH inequality is the most known and easiest to implement inequality.
Since the randomness generated per run is a monotonic function of the violation for CHSH tests (Pironio et al. 2010), it is of primary importance to implement experiments that can maximize the violation. The maximal violation $2\sqrt{2}$ for the CHSH inequality is given for maximally entangled two-qubit states. In photonic systems such states can be realized using two photons entangled in polarization such as in the state $\frac{1}{\sqrt{2}}(|HV\rangle + |VH\rangle)$, where H and V represents the horizontal and vertical polarization.
A SPDC source is used to implement such a state; it is further analysed by means of two wave-plates per mode, polarizing beam splitters, and photon counting techniques. The theoretical studies rely on three intuitions, i.e. 1. that for systems with no loss we can obtain the maximal violation $2\sqrt{2}$ for 2. maximally entangled states in 3. two well defined polarization modes.
In this chapter these beliefs are challenged. Indeed I show that a full analytical analysis of the experimental setup brings rather different results.

1.2 Experimental setup

The experimental setup is shown in Fig. 1.1. It consists in the following steps:

1. A SPDC source produces photons entangled in polarization in spatial modes

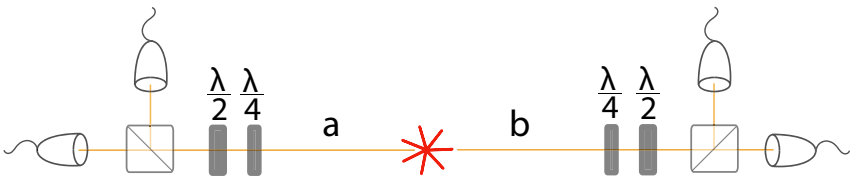

Figure 1.1: Experimental setup for a CHSH-Bell test with photon pairs entangled in polarization. An SPDC source generates photon-pairs entangled in polarization. The photonic modes a and b are analysed in polarization through a set of wave-plates, polarizing beam splitters and NPNR detectors.

a and b according to the Hamiltonian $\mathcal{H} = i\sum_{k=1}^{N}(\chi a_k^\dagger b_{k,\perp}^\dagger - \bar{\chi} a_{k,\perp}^\dagger b_k^\dagger + h.c.)$ where χ and $\bar{\chi}$ are proportional to the susceptibility of the crystal and to the power of the pump laser, even though they are independent to mode k. The final generated state is given by the equation (Sekatski et al. 2010)

$$|\psi\rangle = (1-T_g^2)^{\frac{N}{2}}(1-T_{\bar{g}}^2)^{\frac{N}{2}}\Pi_{k=1}^{N} e^{T_g a_k^\dagger b_{k,\perp}^\dagger - T_{\bar{g}} a_{k,\perp}^\dagger b_k^\dagger}|\underline{0}\rangle\,, \tag{1.1}$$

where T_g stands for $\tanh(g) = \tanh(\chi t)$.

2. Alice and Bob rotate modes a and b respectively through a series of wave-plates according to the following equations

$$a_k = \quad \cos\alpha\ A_k + e^{i\phi_\alpha}\sin\alpha\ A_{k,\perp} \tag{1.2}$$
$$a_{k,\perp} = \quad e^{-i\phi_\alpha}\sin\alpha\ A_k - \cos\alpha\ A_{k,\perp}. \tag{1.3}$$

3. Finally a polarizing beam splitter and two non-photon number resolving (NPNR) detectors per mode are used to detect the absence or presence of a photon in each polarization. Given the efficiency η of the detector, and the probability p_{dc} of dark counts, the no-click operator P_{nc}^a is

$$P_{\text{nc}}^a = (1-p_{\text{dc}})\,\Pi_{k=1}^{N}(1-\eta)^{a_k^\dagger a_k}. \tag{1.4}$$

1.3 Calculation of the joint probabilities

There are four possible results per side per run. Thus Alice and Bob have to bin their results in order to have just two outcomes ± 1. In the following I will maximize the CHSH value over all the binnings and the variables of the system as a function of the efficiency η. I have, then, to derive all the joint and local probabilities. I

here explain how to derive $p(\mathrm{nc}_A)$, the local probability of having no detections in Alice's mode. This probability is equal to

$$p(\mathrm{nc}_A) = (1 - p_{\mathrm{dc}}) \left(\mathrm{tr}\ R^{\frac{A_k^\dagger A_k}{2}} |\psi^k_{\alpha,\beta}\rangle\langle\psi^k_{\alpha,\beta}| R^{\frac{A_k^\dagger A_k}{2}} \right)^N, \tag{1.5}$$

where $R = 1 - \eta$, and $|\psi_{\alpha,\beta}\rangle$ is obtained by introducing the expressions of a_k, $a_{k,\perp}$, b_k, $b_{k,\perp}$ as a function of A_k, $A_{k,\perp}$, B_k, $B_{k,\perp}$, given in the previous paragraph, in $|\psi\rangle$. Let's focus on a single mode. We have the relation

$$R^{\frac{A_k^\dagger A_k}{2}} |\psi^k_{\alpha,\beta}\rangle = \left(1 - T_g^2\right)^{\frac{1}{2}} \left(1 - T_{\bar{g}}^2\right)^{\frac{1}{2}} e^{(A_k^\dagger, A_{k,\perp}^\dagger) M \begin{pmatrix} B_k^\dagger \\ B_{k,\perp}^\dagger \end{pmatrix}} |\underline{0}\rangle, \tag{1.6}$$

where

$$M = \begin{pmatrix} R^{\frac{1}{2}}(T_g C_\alpha S^\star_\beta - T_{\bar{g}} S^\star_\alpha C_\beta) & R^{\frac{1}{2}}(-T_g C_\alpha C_\beta - T_{\bar{g}} S^\star_\alpha S_\beta) \\ T_g S_\alpha S^\star_\beta + T_{\bar{g}} C_\alpha C_\beta & -T_g S_\alpha C_\beta + T_{\bar{g}} C_\alpha S_\beta \end{pmatrix}, \tag{1.7}$$

C_α and S_α (C_β and S_β) being $\cos\alpha$ and $e^{i\phi_\alpha}\sin\alpha$ ($\cos\beta$ and $e^{i\phi_\beta}\sin\beta$) respectively. Using the singular value decomposition $M = U \begin{pmatrix} \lambda_1 & 0 \\ 0 & \lambda_2 \end{pmatrix} V^\star$, we end up with the solution

$$p(\mathrm{nc}_A) = (1-p_{\mathrm{dc}}) \left(\frac{\left(1 - T_g^2\right)\left(1 - T_{\bar{g}}^2\right)}{(1-\lambda_1^2)(1-\lambda_2^2)} \right)^N = (1-p_{\mathrm{dc}}) \left(\frac{2}{2 - \eta + \eta(C_{2g} C_\alpha^2 + C_{2\bar{g}} |S_\alpha|^2)} \right)^N, \tag{1.8}$$

with $C_g = \cosh(g)$. All the other probabilities are derived following the same procedure.

1.4 Results and conclusion

The results of the optimization of the CHSH value as a function of the efficiency η are shown in Fig. 1.2. The full curve represents the final result obtained optimizing over the squeezing parameter g, the number of modes, α, ϕ_α, β, and ϕ_β. The dashed line (dotted line) has been obtained restraining the optimization over the cases where just one mode is involved (just one mode and maximally-entangled states are involved). The optimization shows very interesting results:

- The maximal violation for $\eta = 1$ is only 2.35 and not $2\sqrt{2}$. This is due to the presence of both vacuum and multiple pairs which limits the maximal violation;

- The maximal violation is obtained when $N \to \infty$ and not for a single mode;

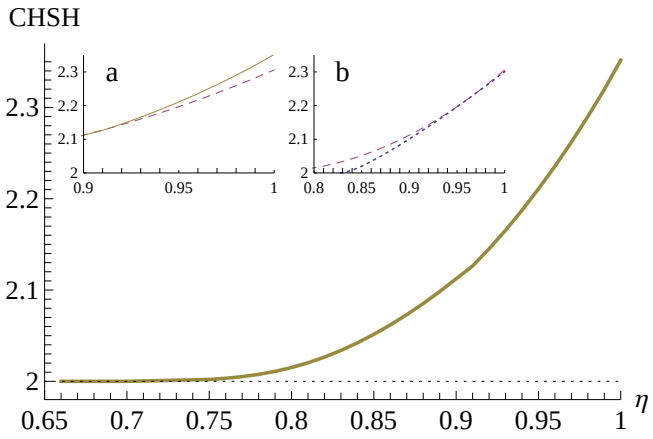

Figure 1.2: CHSH values as a function of the detection efficiency η. The golden full curve is the optimization over the squeezing parameters, the number of modes and all the possible measurements. The dashed (dotted) line represents the optimization restrained to the case of only one mode (only one mode and $g = \bar{g}$).

- The maximal violation is not obtained for maximally entangled states. This is probably due to the fact that vacuum and multiple pairs operate as losses;
- The minimal required efficiency is 2/3, as for the case of two photons entangled in polarization.

The results obtained show that the standard optimization (Eberhard 1993) is not suitable for such kind of experiments.
In the next chapter, I will show how the Bell violation can be improved in the setup using the same source but different states and measurements.

2 Bell tests with optical-path entangled states

2.1 Introduction

In the previous chapter, I have shown that in a standard setup involving photon pairs entangled in polarization, produced by a SPDC source, it is not possible to maximally violate the CHSH inequality.
This raises the question of whether other implementations could be more efficient, i.e. how to use the same photon source to get higher Bell violations. We here discuss two possible implementations relying on path-entanglement and two-mode squeezed entanglement.
In the first case we analyze a setup initially proposed in Banaszek and Wodkiewicz 1998. The authors focused on entangled states of the form $\frac{1}{\sqrt{2}}(|01\rangle + |10\rangle)$ and showed that their non local content can be revealed using measurements combining photon counting and small displacement operations.
I present a full characterization of this measurement showing that it is able to span the entire Bloch sphere, even though with non extremal length.
Subsequently I extend the study to the setup involving a SPDC source and I maximize the CHSH violation.
In the second part of the chapter, I discuss another setup where states of the form $\frac{1}{\sqrt{2}}(|00\rangle + |11\rangle)$ are analyzed with the same measurement. I show that it is possible to implement a Bell experiment relying on two-mode squeezed states generated by a SPDC source and maximize the violation as well.
Finally, I analyze and compare the randomness per run and the rate of randomness generation for the three experimental setups presented so far.

2.2 Displacement-based (DB) measurement

In this section we present the measurement that will be used in all what follows. As shown in Fig. 2.1 the measurement consists in a non-photon number resolving (NPNR) detector of efficiency η preceded by a small displacement operation in phase space with argument α. Associating the outcome $+1$ to a no-click and -1 to

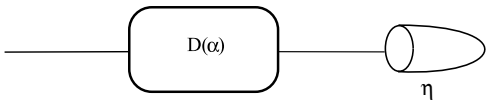

Figure 2.1: Displacement-based measurement. It consists of a displacement of the phononic mode followed by a NPNR detector.

a click and knowing that for a NPNR detector

$$P^{\eta}_{\text{no-click}} = (1-\eta)^{a^\dagger a}, \;\; P^{\eta}_{\text{click}} = \mathbb{1} - (1-\eta)^{a^\dagger a}, \tag{2.1}$$

the observable for the overall detection setup is given by

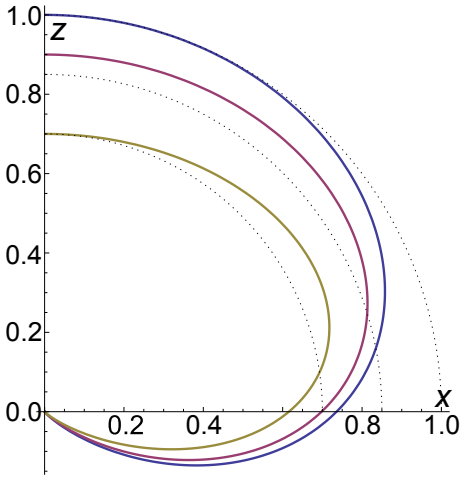

Figure 2.2: Displacement-based measurement in the Bloch sphere for different values of the detector efficiency ($\eta = 1, 0.8, 0.6$) varying the amplitude of the displacement α.

$$\mathfrak{o}^{\eta}_{\alpha} = D^\dagger(\alpha)\,(P^{\eta}_{\text{no-click}} - P^{\eta}_{\text{click}})\,D(\alpha). \tag{2.2}$$

Note that the matrix form of $\mathfrak{o}^{\eta}_{\alpha}$ restricted to the subspace $\{|0\rangle\text{-}|1\rangle\}$ reduces to

$$\mathfrak{o}^{\eta}_{\alpha} = \begin{pmatrix} 2e^{-\eta|\alpha|^2} - 1 & -2\alpha^*\eta e^{-\eta|\alpha|^2} \\ -2\alpha\eta e^{-\eta|\alpha|^2} & 2\left(\eta^2|\alpha|^2 + 1 - \eta\right)e^{-\eta|\alpha|^2} - 1 \end{pmatrix}. \tag{2.3}$$

The no click/click events are associated to two elements of a POVM $\{P^{\eta,\alpha}_{\text{no-click}}, P^{\eta,\alpha}_{\text{click}}\}$ which satisfy $P^{\eta,\alpha}_{\text{no-click}} + P^{\eta,\alpha}_{\text{click}} = \mathbb{1}$. For non-unit efficiency $\eta < 1$, the POVM $\{P^{\eta,\alpha}_{\text{no-click}}, P^{\eta,\alpha}_{\text{click}}\}$ is not extremal (D'Ariano et al. 2005)

$$\{P^{\eta,\alpha}_{\text{no-click}}, P^{\eta,\alpha}_{\text{click}}\} = \mu\{\Pi_{\vec{n}}, \Pi_{-\vec{n}}\} + (1-\mu)\{r_{\text{no-click}}\mathbb{1}, r_{\text{click}}\mathbb{1}\}. \tag{2.4}$$

The measurement corresponds to a non-extremal measurement in the Bloch sphere in the direction

$$\vec{n} \propto \begin{pmatrix} -e^{-\eta|\alpha|^2}|\alpha|\eta\cos\varphi \\ e^{-\eta|\alpha|^2}|\alpha|\eta\sin\varphi \\ \frac{1}{2}e^{-\eta|\alpha|^2}\eta(1-|\alpha|^2\eta) \end{pmatrix}, \tag{2.5}$$

where $\alpha = |\alpha|e^{i\varphi}$, with probability

$$\mu = \sqrt{\eta^2 e^{-2|\alpha|^2\eta}\left(|\alpha|^2\left(|\alpha|^2\eta^2 - 2\eta + 4\right) + 1\right)}. \tag{2.6}$$

In Fig. 2.2 it is represented the projective part of the measurement in the Bloch sphere as a function of α and different values of $\eta = 1$, 0.9 and 0.7, where the length of the vector and the direction are μ and $\vec{n}$, respectively. For $\alpha = 0$ the vector points along the z direction, while for $\alpha \to \infty$ the vector tends to 0. The vector lies on the equator of the Bloch sphere for $\alpha = \frac{1}{\sqrt{\eta}}$. The phase of α allows to rotate the vector around the z axis. In particular for real values of α, the measurement does not have a y component, while for imaginary values the x component is null.

2.3 Revealing nonlocality of optical-path entangled states

2.3.1 Experimental setup for optical-path states

I here analyse the experimental setup represented in Fig. 2.3. A SPDC source

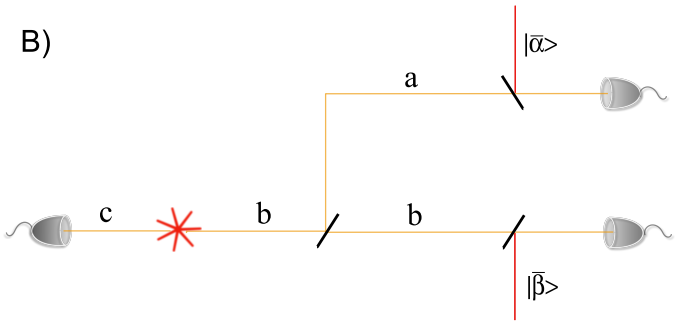

Figure 2.3: Experimental setup for optical-path states. An SPDC source generates a two-mode squeezed state. the detection of a photon in mode c heralds the presence of at least a photon in mode b. Then, a beam splitter generates entanglement between modes a and b. The photonic modes are analysed by mean of displacement-based measurements.

produces photon pairs. The detection of a photon in mode c heralds the presence

of at least one photon in mode b. The latter is sent through a beam splitter of transmittivity T. The state generated is entangled in the Fock space. Finally, each path is analysed after the beam splitter through a DB measurement.

2.3.2 Derivation of Bell-CHSH correlators

I, here, derive the correlators for the setup showed in Fig. 2.3. The state given by the SPDC source is given by $|\psi\rangle = \sqrt{1-T_g^2}\sum_n \frac{T_g^n}{n!} b^{\dagger n} c^{\dagger n} |00\rangle$, where $T_g = \tanh(g)$, g being the squeezing parameter. The state resulting from a detection in mode c is

$$\rho_h = \frac{1-R_h^2 T_g^2}{T_g^2\left(1-R_h^2\right)}\left[\rho_{\text{th}}\left(\bar{n}=\frac{T_g^2}{1-T_g^2}\right) - \frac{1-T_g^2}{1-R_h^2 T_g^2}\rho_{\text{th}}\left(\bar{n}=\frac{R_h^2 T_g^2}{1-R_h^2 T_g^2}\right)\right], \quad (2.7)$$

where $R_h = \sqrt{1-\eta_h}$, η_h being the efficiency in mode c and $\rho_{\text{th}}(\bar{n}) = \frac{1}{1+\bar{n}}\sum_k \left(\frac{\bar{n}}{1+\bar{n}}\right)^k |k\rangle\langle k|$ is a thermal state. Using the decomposition of a thermal state in terms of coherent states, $\rho_{\text{th}}(\bar{n}) = \int d^2\gamma P^{\bar{n}}(\gamma)|\gamma\rangle\langle\gamma|$, where $P^{\bar{n}}(\gamma) = \frac{1}{\pi\bar{n}} e^{-\frac{|\gamma|^2}{\bar{n}}}$, one can easily manipulate the expression of the density matrix ρ. In particular we know that a beam splitter splits a coherent state into two, i.e. $|\gamma\rangle \to |\sqrt{R}\gamma\rangle_a |\sqrt{T}\gamma\rangle_b$, and that $(1-\eta)^{\frac{a^\dagger a}{2}} |\bar{\gamma}\rangle = e^{-\frac{\eta|\bar{\gamma}|^2}{2}} |\sqrt{1-\eta}\bar{\gamma}\rangle$. We find that the local and joint probabilities for a thermal state are, then,

$$P_\alpha^{\text{nc}} = \frac{e^{-\frac{|\alpha|^2\eta_a}{\eta_a\bar{n}R+1}}}{\eta_a\bar{n}R+1}, \quad (2.8)$$

$$P_{\alpha,\beta}^{\text{nc,nc}} = \frac{e^{-\eta_a|\alpha|^2-\eta_b|\beta|^2+\frac{\bar{n}|\alpha\eta_a\sqrt{R}+\beta\eta_b\sqrt{T}|^2}{\bar{n}(\eta_a R+(1-R)\eta_b)+1}}}{\bar{n}(R\eta_a+T\eta_b)+1}. \quad (2.9)$$

The expression of the correlator $E_{\alpha,\beta}^{\text{th}} = \langle \sigma_\alpha^{\eta_a}\sigma_\beta^{\eta_b}\rho_{th}\rangle$ is

$$E_{\alpha\beta}^{\text{th}} = 1 + 4P_{\alpha,\beta}^{\text{nc,nc}} - 2P_\alpha^{\text{nc}} - 2P_\beta^{\text{nc}}. \quad (2.10)$$

From this last expression, we deduce the correlator $E_{\alpha_i\beta_j}$ for the state (2.7)

$$E_{\alpha_i\beta_j} = \frac{1-R_h^2T_g^2}{T_g^2\left(1-R_h^2\right)}\left[E_{\alpha_i\beta_j}^{\text{th}}\left(\bar{n}=\frac{T_g^2}{1-T_g^2}\right) - \frac{1-T_g^2}{1-R_h^2T_g^2}E_{\alpha_i\beta_j}^{\text{th}}\left(\bar{n}=\frac{R_h^2T_g^2}{1-R_h^2T_g^2}\right)\right]. \quad (2.11)$$

2.3.3 Results of the optimization

The optimization over the CHSH value reproduces the same values of the single-photon case presented in Chaves and Bohr Brask 2011 and Bohr Brask et al. 2013. Indeed the best squeezing parameter values are small, showing that the best state

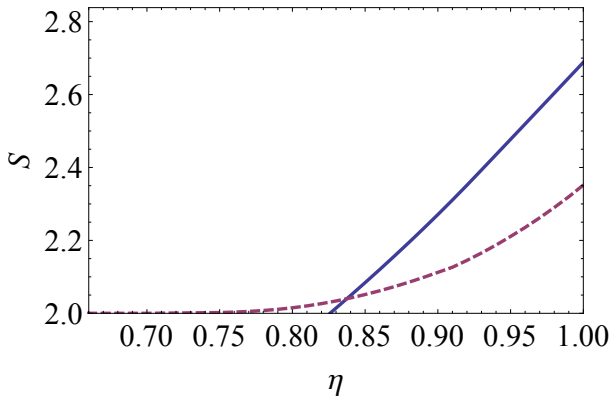

Figure 2.4: Optimal CHSH value as a function of the efficiency η. The full (dashed) curve is obtained in the case of optical-path entanglement (polarization entanglement).

for such a test is a single-photon state, a state where two spatial modes share a single delocalized photon. Moreover the optimal state is always obtained from a 50-50 beam splitter ($R = T = \frac{1}{2}$), i.e. a two-qubit maximally entangled state. Finally, the minimal required detector efficiency is $\eta_{\min} = 0.826$.

2.3.4 Comparing the randomness generation

In this section, I present the results of the optimization of the CHSH-Bell value. I am particularly interested in the randomness generation per run and the rate of random bits as a function of the efficiency η. I also compare this approach with the one of the previous chapter.
Let's focus now on the amount of randomness generated in both setups (Fig. 2.5). The expression of the minimal entropy generated (amount of randomness per bit) (Pironio et al. 2010) is the following

$$H_{\min}(S) = 1 - \log_2\left(1 + \sqrt{2 - \frac{S^2}{4}}\right). \tag{2.12}$$

Since $H_{\min}(S)$ (Fig. 2.5) is a monotonic function of the violation S, its maximal value is obtained in the case of the optical-path entanglement. On the other hand it is possible to have randomness generation for low values of the efficiency (under 0.826) only for the polarization setup. Let us now focus on the rate of randomness generation. It is given by

$$R(S) = rH_{\min}(S) \tag{2.13}$$

where r is the rate at which the states are analyzed. There are two cases that have

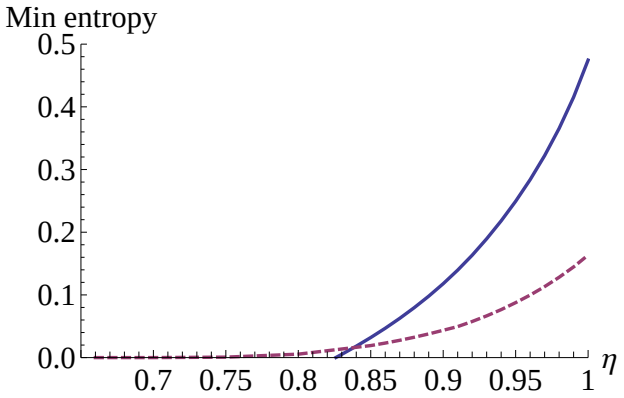

Figure 2.5: Min entropy per experimental run as a function of the efficiency η. The full (dashed) curve corresponds to the case of optical-path entanglement (polarization entanglement.

to be considered, 1. when it is set by the detectors deadtime (Fig. 2.5) and 2. when the repetition rate is set by the pump laser (Fig. 2.6). The first case is more likely to happen since superconductor detectors, that present the highest efficiencies at the moment, have also very long deadtimes.

2.4 Nonlocality for two-mode squeezed states

2.4.1 Nonlocality detection for GHZ states

Let us consider a GHZ-like state, i.e.

$$|\mathrm{GHZ}\rangle = \cos\theta\,|00\rangle + \sin\theta\,|11\rangle\,, \tag{2.14}$$

and let us study the CHSH-violation of this state using a DB measurement of efficiency η for each mode. The optimization over θ of this value as a function of the detector efficiency η, in Fig. 2.7, shows that

- the maximal violation 2.69 for $\eta = 1$ is obtained for maximally entangled states. This is the same result derived for the W-state $\frac{1}{\sqrt{2}}(|01\rangle + |10\rangle)$;
- The minimal efficiency is $\eta = \frac{2}{3}$.

These results are very interesting as with these states we have high violations with no loss and the minimal required efficiency is low. In the next paragraph, I will show how to implement a setup that can reproduce a GHZ-like state.

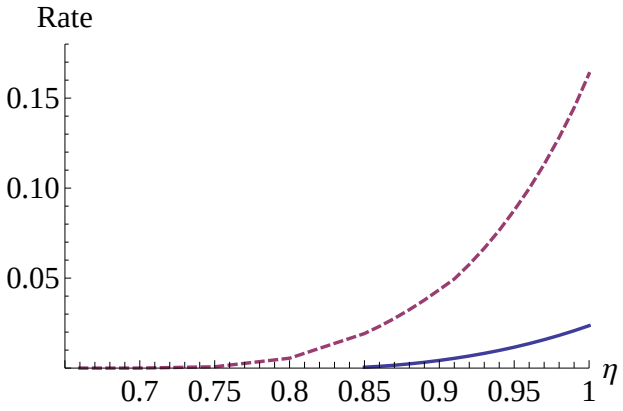

Figure 2.6: Rates of randomness generation as a function of the efficiency η. The full (dashed) curve corresponds to the case of optical-path entanglement (polarization entanglement).

2.4.2 Experimental setup

The experimental setup that I envision is represented in Fig. 2.8. A SPDC source produces a two-mode squeezed state between modes a and b. The modes are, then, analyzed by DB measurements.

2.4.3 Derivation of the correlators

In order to find the correlator of the system we have to calculate the probabilities $P^{\alpha,\beta}_{\text{no-click,no-click}}$, $P^{\alpha}_{\text{no-click}}$, and $P^{\beta}_{\text{no-click}}$ of having a no-click in both arms, in Alice's arm, and in Bob's arm respectively. The $P^{\alpha,\beta}_{\text{no-click,no-click}}$ is given by the formula

$$(1-\tanh^2(g))\,\langle 0|\,e^{\tanh(g)ab}D^\dagger(\alpha)D^\dagger(\beta)(1-\eta)^{a^\dagger a+b^\dagger b}D(\alpha)D(\beta)e^{\tanh(g)a^\dagger b^\dagger}\,|0\rangle$$

$$=(1-\tanh^2(g))\frac{1}{\pi^2}\int d^2\gamma'\int d^2\gamma\left|\langle 0|\,e^{\tanh(g)ab}D^\dagger(\alpha)D^\dagger(\beta)(1-\eta)^{\frac{a^\dagger a+b^\dagger b}{2}}\,|\gamma,\gamma'\rangle\right|^2. \tag{2.15}$$

Using the equivalence $e^{\tanh(g)ab}\,|\alpha,\beta\rangle = e^{\tanh(g)\alpha\beta}\,|\alpha,\beta\rangle$, we end up with the following equation

$$P^{\alpha,\beta}_{\text{no-click,no-click}}=(1-\tanh^2(g))\frac{e^{-\frac{\eta(|\alpha|^2+|\beta|^2)(1-\tanh^2(g)(1-\eta))-\tanh(g)\eta^2(\alpha^*\beta^*+\alpha\beta)}{1-\tanh^2(g)(1-\eta)^2}}}{1-\tanh^2(g)(1-\eta)^2}. \tag{2.16}$$

Similarly we can derive the other two probabilities

$$P^{\alpha}_{\text{no-click}}=(1-\tanh^2(g))\frac{e^{-\frac{\eta(1-\tanh^2(g))|\alpha|^2}{1-\tanh^2(g)(1-\eta)}}}{1-\tanh^2(g)(1-\eta)}, \tag{2.17}$$

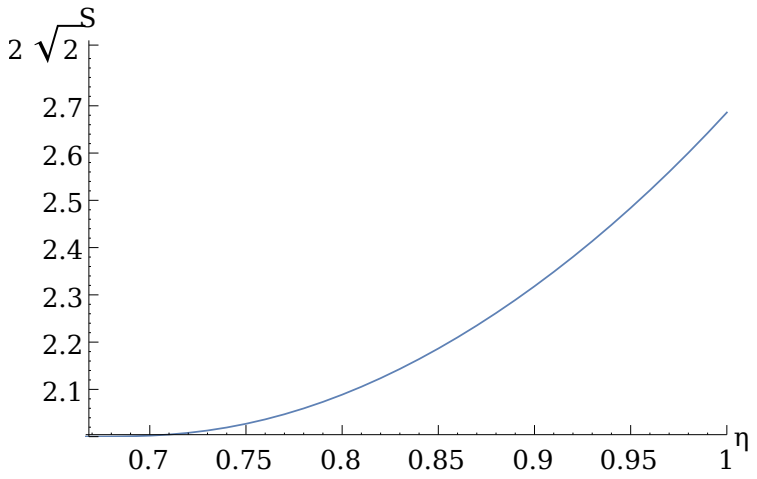

Figure 2.7: CHSH violation for a GHZ-like state $|\mathrm{GHZ}\rangle = \cos\theta\,|00\rangle + \sin\theta\,|11\rangle$ using DB measurements.

Figure 2.8: Setup for a CHSH Bell test for a two-mode squeezed state. A two-mode squeezed state is generated by an SPDC source. The state is, then, analysed with DB measurements.

and

$$P^{\beta}_{\text{no-click}} = (1-\tanh^2(g))\frac{e^{-\frac{\eta(1-\tanh^2(g))|\beta|^2}{1-\tanh^2(g)(1-\eta)}}}{1-\tanh^2(g)(1-\eta)}. \tag{2.18}$$

The expression of the correlator is the following

$$E^{\alpha,\beta} = 1 - 2P^{\alpha}_{\text{no-click}} - 2P^{\beta}_{\text{no-click}} + 4P^{\alpha,\beta}_{\text{no-click,no-click}}. \tag{2.19}$$

The result of the optimization of the CHSH value over α, β, and g, together with other CHSH value maximizations, are shown in Fig. 2.9. In the following subsection I discuss the results of the maximization.

2.4.4 Results

The expression for the CHSH value is $\mathrm{CHSH} = |E^{\alpha_1,\alpha_2} + E^{\alpha_1',\alpha_2} + E^{\alpha_1,\alpha_2'} - E^{\alpha_1',\alpha_2'}|$. The results of the optimization of the CHSH value over α_1, α_2, and g are shown in Fig. 2.9. We can summarize the results in three points:

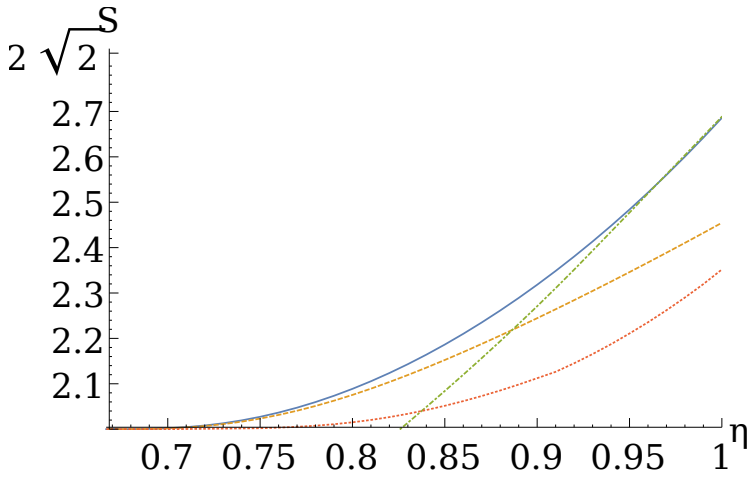

Figure 2.9: CHSH violation for different Bell tests as a function of the detection efficiency η. The blue full curve (green dot-dashed curve, yellow dashed curve, red dotted curve) is given by the optimization on a GHZ-like state (optical-path entangled state, two mode squeezed state with DB measurement, photon pairs entangled in polarization)

- The maximal value of the violation for $\eta = 1$ is 2.4. This value is bigger than 2.35, that is the result predicted for the case exploiting the standard polarization entanglement, and smaller than 2.69, that is the value for the optical-path entanglement setup. The result can be explained observing first that in this case the presence of vacuum is a resource and not a loss. From this we obtain a higher violation than in the polarization setup. Nevertheless, it is impossible to have a value of the squeezing parameter for which we obtain a good approximation of a maximally entangled state without producing several multi-pairs. This results in a loss of violation from 2.69 to 2.4.

- The minimal required efficiency of having a violation is $\eta = 0.668$. This result is slightly bigger than the efficiency $\eta = \frac{2}{3}$ for the GHZ state. My intuition is that the presence of multi-photon pairs accounts as loss and reduces the efficiency of the setup.

- Given that the repetition rate is always the same as the polarization setup, the randomness generated in the case of a two-mode squeezed state is very competitive if compared with the latter both in terms of randomness generation per run and rate of random bits. Concerning the optical-path setup, the two-mode squeezed state setup is better than this setup only when the detectors deadtime is long and, then, the rate of random bits is higher.

2.5 Conclusion

We can summarize the chapter recapitulating the following results:

- I fully characterized a measurement relying on a small displacement followed by NPNR detectors and showed that it is a resource for measurements in the Fock basis for photonic modes.
- I presented and analysed two different experimental setups relying on a SPDC source and entanglement lying in the Fock space.
- In the first case, the maximal violation is 2.69, as for single-photon states. The minimal detector efficiency for any violation for maximally entangled states is 0.826 and not 0.828 as expected from previous theory (Eberhard 1993).
- The maximal violation for two-mode squeezed states is strongly reduced from 2.69 to 2.4. The minimal detector efficiency is 0.668.
- I compared the three experimental Bell tests and I showed that when one analyses them in terms of the randomness generation the polarization setup is not the most promising.

In the next chapter, I am going to explain how the last approach opens the way to the first proposal of an optomechanical Bell test.

3 Optomechanical Bell test

3.1 Introduction

In the previous chapter, I have introduced the DB measurement, composed by a

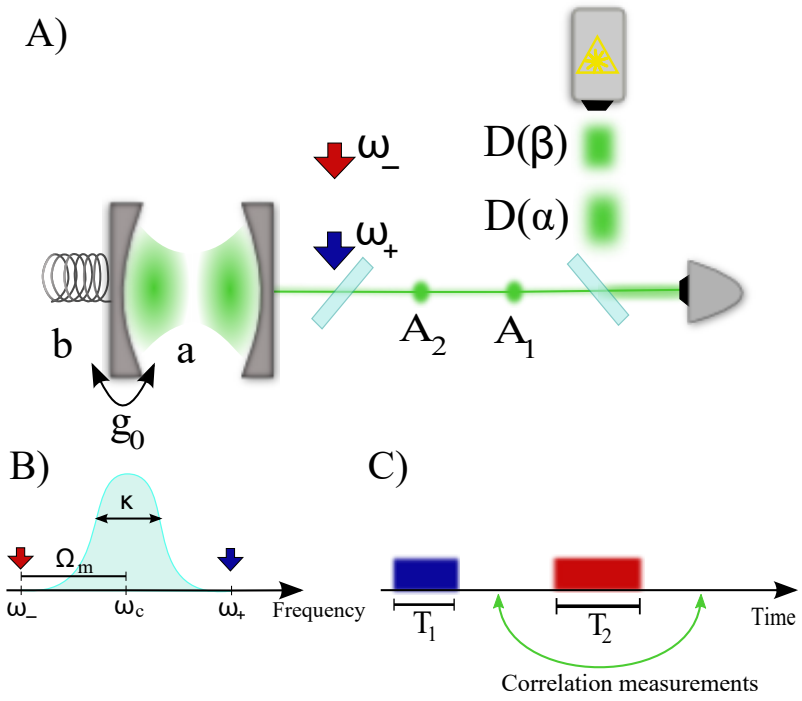

Figure 3.1: Schematics of the experimental setup for a Bell test with optomechanical cavities (A), of the Cavity linewidth and its two sidebands (B), and of the pulse sequence (C). A laser pulse at time T_1 of frequency $\omega_+ = \omega_c + \Omega_m$ generates a photon-phonon pair of frequencies ω_c and Ω_m respectively. The photon is, then, emitted in mode A_1 At time T_2 a second laser pulse of frequency $\omega_- = \omega_c - \Omega_m$ is sent into the cavity, allowing the mapping of the phononic mode in the photonic mode A_2.

displacement in phase space and photon counting techniques, suitable for detecting

quantum features. I have also shown that a setup consisting in a SPDC source that generates a two-mode squeezed state can reveal nonlocality when two DB measurements are performed per side. Interestingly, this test can be adapted to other systems where the two-mode squeezed state is generated through alternative sources.
While we have focused on a source based on a parametric process, these states can be generated by various systems. For example, Galland et al. 2014 have shown how a laser drives the blue sideband of an optomechanical cavity system leading to the generation of a photon-phonon two-mode squeezed state. The phononic mode can subsequently be converted into a photonic mode by driving the blue sideband of the optomechanical cavity. Consequently it is worth wondering if the use of DB measurements on both photonic modes could be exploited for an optomechanical experiment texting nonlocality.
This would be of great importance since it would allow one to test nonlocality on phononic systems. Furthermore, as optomechanical cavities are macroscopic objects in terms of mass, one could argue that the states that are generated through them are macroscopic. It is, then, interesting to adapt the Bell test studied in the previous chapter to optomechanical cavities.

3.2 Experimental setup

The experimental setup that we envision is represented in Fig. 3.1 . The optomechanical cavity produces first a photon-phonon pair at time T_1. The phononic is is, then, mapped into a photonic mode at time T_2 thank to the process described in Galland et al. 2014. The photonic modes are analyzed with the DB measurement.

3.3 Describing the optomechanical cavity Hamiltonian

The Hamiltonian of the cavity is a sum of three terms, i.e. $H = H_0 + H_{\mathrm{OM}} + H_l$, describing the uncoupled system ($H_0 = \omega_c a^\dagger a + \Omega_m b^\dagger b$), the optomechanical interaction ($H_{\mathrm{OM}} = -g_0 a^\dagger a(b^\dagger + b)$), and the laser driving ($H_l = s_\pm^* e^{i\omega_\pm t} a + s_\pm e^{-i\omega_\pm t} a^\dagger$ with $|s_\pm| = \sqrt{kP_\pm/\hbar\omega_\pm}$ being $P_\pm$ the laser power and k the cavity decay rate) respectively. In the weak coupling ($g_0 \ll k$) and resolved sideband ($k \ll \Omega_m$) regime the whole process can be modelled as a sequence of well known interactions. The process of photon-pair production consists of two steps

1. A blue write pulse at angular frequency $\omega_+ = \omega_c + \Omega_m$, i.e. the sum of the uncoupled cavity (ω_c) and mechanical (Ω_m) frequencies, of duration T_1 is applied to create a correlated photon-phonon pair in modes $A_{1,\mathrm{out}}$ and b

respectively. The operator representing this process is (Galland et al. 2014)

$$\tilde{U}(T_1) = e^{i\sqrt{1-e^{-2\bar{g}_+ T_1}}A^\dagger_{1,\mathrm{in}}b^\dagger} e^{\bar{g}_+ T_1(-1-A^\dagger_{1,\mathrm{in}}A_{1,\mathrm{in}}-b^\dagger b)} e^{i\sqrt{1-e^{-2\bar{g}_+ T_1}}A_{1,\mathrm{in}}b}, \tag{3.1}$$

where $\bar{g}_+ = \frac{2g_+^2}{k}$, g_+ being the effective optomechanical rate.

2. a red readout pulse of duration T_2 at angular frequency $\omega_- = \omega_c - \Omega_m$ is used to map the phonons onto the optical cavity mode at frequency ω_c. A second photon is then produced in mode $A_{2,\mathrm{out}}$ with transmission $\sin^2(\bar{g}_- T_2)$, where $\bar{g}_- = \frac{2g_-^2}{k}$. The operator representing this process is $U_{\mathrm{BS}} = e^{\bar{g}_- T_2\left(A^\dagger_{2,\mathrm{out}}b - A_{2,\mathrm{out}}b^\dagger\right)} |0\rangle_b$.

The operator representing the perfect photon-pair source U is obtained replacing in Eq. (3.1) b with $iA_{2,\mathrm{in}}$ and is given by the following equation

$$U = e^{\sqrt{1-e^{-2\bar{g}_+ T_1}}A^\dagger_{1,\mathrm{in}}A^\dagger_{2,\mathrm{in}}} e^{\bar{g}_+ T_1(-1-A^\dagger_{1,\mathrm{in}}A_{1,\mathrm{in}}-A^\dagger_{2,\mathrm{in}}A_{2,\mathrm{in}})} e^{\sqrt{1-e^{-2\bar{g}_+ T_1}}A_{1,\mathrm{in}}A_{2,\mathrm{in}}}. \tag{3.2}$$

The total operator representing the photon-pairs process is, then, $U_{\mathrm{BS}}U$.

3.4 Joint probabilities for a mechanical system in a thermal state

The aim of this section is to derive the joint probabilities $p(+1+1|\alpha_1\alpha_2)$ and the marginals $p(+1|\alpha_i)$ when the mechanical system, the phononic mode, is prepared in a thermal state $\rho_b = (1-p_0)\sum_{n\geq 0} p_0^n |n\rangle\langle n|$ with mean occupation number n_{th}. Let us focus on a initial state $|0n\rangle$, i.e. a state with 0 photons and n phonons. The state generated by the source is

$$|\psi\rangle = e^{\sqrt{1-e^{-2\bar{g}_+ T_1}}A^\dagger_1 A^\dagger_2} e^{\bar{g}_+ T_1(-1-A^\dagger_1 A_1 - A^\dagger_2 A_2)} e^{\sqrt{1-e^{-2\bar{g}_+ T_1}}A_1 A_2} |0n\rangle\,, \tag{3.3}$$

that can be easily simplified as in the following expression

$$|\psi\rangle = \sqrt{1-p}^{1+n} e^{\sqrt{p}A^\dagger_1 A^\dagger_2} |0n\rangle\,, \tag{3.4}$$

where $p = 1 - e^{-2\bar{g}_+ T_1}$. The $P^{\alpha_1,\alpha_2}_{\text{no-click,no-click}|n\rangle}$ is given by the following formula

$$\begin{aligned}
&(1-p)^{1+n} \langle 0n| e^{\sqrt{p}A_1 A_2} D^\dagger(\alpha_1) D^\dagger\left(\sqrt{T}\alpha_2\right) (1-\eta)^{A^\dagger_1 A_1} (1-\eta')^{A^\dagger_2 A_2} D(\alpha_1) D\left(\sqrt{T}\alpha_2\right) e^{\sqrt{p}A^\dagger_1 A^\dagger_2} |0n\rangle \\
&= \frac{1}{\pi^2}(1-p)^{1+n} \int d^2\gamma' \int d^2\gamma \left| \langle 0n| e^{\sqrt{p}A_1 A_2} D^\dagger(\alpha_1) D^\dagger\left(\sqrt{T}\alpha_2\right) (1-\eta)^{\frac{A^\dagger_1 A_1}{2}} (1-\eta')^{\frac{A^\dagger_2 A_2}{2}} |\gamma,\gamma'\rangle \right|^2,
\end{aligned} \tag{3.5}$$

where I have used the closing relation $\frac{1}{\pi}\int d^2\gamma\,|\gamma\rangle\langle\gamma| = \mathbb{1}$, $\eta' = \eta T$, and the integral is performed over all the complex plane. Using the relation $e^{Gab}\,|\alpha,\beta\rangle = e^{G\alpha\beta}\,|\alpha,\beta\rangle$, we end up with the following equation

$$\begin{aligned} &p(+1+1|\alpha_1\alpha_2)_{|n\rangle} = \\ &\frac{1}{\pi^2 n!}(1-p)^{1+n}\int d^2\gamma'\int d^2\gamma e^{-\eta|\gamma|^2-\eta'|\gamma'|^2}\left|e^{\sqrt{p}(\sqrt{1-\eta}\gamma-\alpha_1)(\sqrt{1-\eta'}\gamma'-\sqrt{T}\alpha_2)}\right|^2 \\ &e^{-|\sqrt{1-\eta}\gamma-\alpha_1|^2-|\sqrt{1-\eta'}\gamma'-\sqrt{T}\alpha_2|^2}\left|\sqrt{1-\eta'}\gamma'-\sqrt{T}\alpha_2\right|^{2n}. \end{aligned} \tag{3.6}$$

Given the relation $p(+1+1|\alpha_1\alpha_2) = (1-p_0)\sum_{n\geq 0} p_0^n p(+1+1|\alpha_1\alpha_2)_{|n\rangle}$ we end up

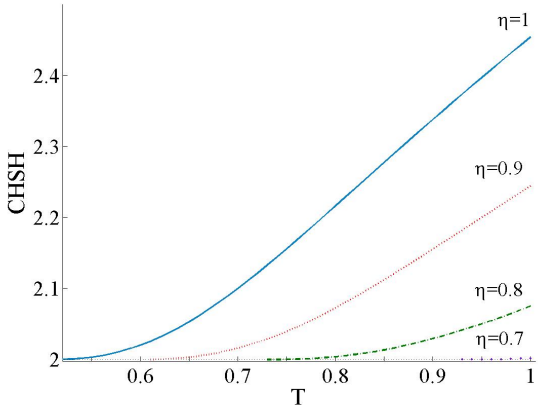

Figure 3.2: CHSH violation as a function of the mapping efficiency T for different values of the photonic efficiency η.

with the equation

$$\begin{aligned} &p(+1+1|\alpha_1\alpha_2) = \\ &(1-p)e^{-\frac{\eta|\alpha_1|^2(\eta' n_{\rm th}+(\eta'-1)p+1)+\eta' T|\alpha_2|^2(p(\eta+\eta n_{\rm th}-1)+1)}{\eta' n_{\rm th}-(\eta'-1)p(\eta+\eta n_{\rm th}-1)+1}}\frac{e^{\frac{\sqrt{p}\eta\eta'(n_{\rm th}+1)\sqrt{T}(\alpha_1^*\alpha_2^*+\alpha_1\alpha_2)}{\eta' n_{\rm th}-(\eta'-1)p(\eta+\eta n_{\rm th}-1)+1}}}{\eta' n_{\rm th}-(\eta'-1)p(\eta+\eta n_{\rm th}-1)+1}. \end{aligned} \tag{3.7}$$

Similarly we can derive the marginals

$$p(+1|\alpha_1) = (1-p)\frac{e^{-\frac{\eta(1-p)|\alpha_1|^2}{(\eta+\eta n_{\rm th}-1)p+1}}}{p(\eta+\eta n_{\rm th}-1)+1}, \tag{3.8}$$

and

$$p(+1|\alpha_2) = (1-p)\frac{e^{-\frac{\eta'(1-p)T|\alpha_2|^2}{(\eta' n_{\rm th}+\eta'-1)p+1}}}{(\eta' n_{\rm th}+\eta'-1)p+1}. \tag{3.9}$$

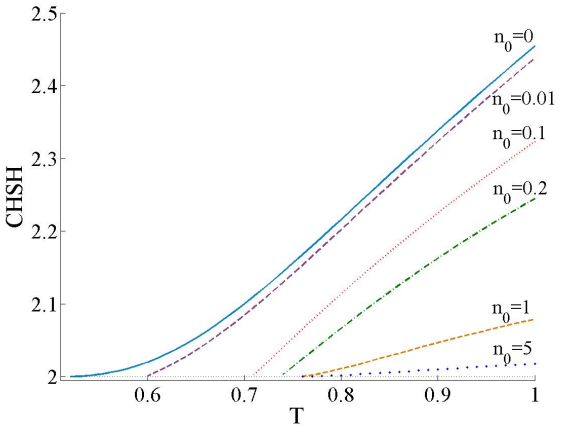

Figure 3.3: CHSH violation for $\eta = 1$ as a function of the mapping efficiency T for different values of the mean occupation number n_{th}.

The results of the optimization of the CHSH value as a function of T for various η and $n_{\text{th}} = 0$ are shown in Fig. 3.2. In Fig. 3.3, on the contrary, the results of the optimization as a function of T for $\eta = 1$ and various values of n_{th} are reported.

3.5 Results and Conclusion

We can summarize the results of this study analysing Fig. 3.2 and 3.3. We see that:

- When the initial mean occupation number of the mechanical mode is 0 for $T = 1$ and $\eta = 1$ we recover the maximal violation of 2.4. Always in this configuration the minimal T is 0.52, for $\eta = 1$. The minimal efficiency in order to have a violation is $\eta = 0.668$.
- When the initial occupation number is higher than 0 it is still possible to detect non-local correlations.

We can, then, conclude that with our proposal it is possible to detect non-local photon-phonon correlations in optomechanical systems. In the next chapter I am going to discuss how one can detect genuine optical-path entanglement in quantum networks using DB measurements.

4 Witnessing optical-path entanglement

4.1 Introduction

There are several prescribed methods to detect optical-path entanglement in a distributed scenario, i.e. using only local measurements. Between them the most important are described by Duan et al. 2001 and Babichev et al. 2004 . In the first case, several copies of an optical-path entangled state are used, while in the second tomography is applied. Both methods are highly demanding in terms of resources and number of measurements respectively. There is another method that doesn't present the drawbacks of the previous methods and it's based on the concept of a "entanglement witness" (Guhne and Toth 2009).
Each observer performs at least two measurements and computes the value of a entanglement witness W. If the value is bigger than a certain threshold value, then we can establish that the state is entangled, otherwise the result is non conclusive. An example of an entanglement witness are Bell inequalities. The CHSH inequality (**Clauser74**) has already been used to build up an entanglement witness in the case of optical-path entanglement with homodyne measurements (Ho et al. 2014; Morin et al. 2013). Nevertheless an issue may arise in using a Bell inequality, i.e. it is not easy to extend the witness to the case of multipartite entanglement. Given a Bell inequality that detects entanglement between N modes, one cannot simply extend it in the case of $(N+1)$ modes for two reasons. First, it doesn't exist a clear way for passing from a Bell inequality that works for N modes to another for $(N+1)$ modes. The only feasible approach consists in testing all the inequalities for $(N+1)$ modes. Second, we do not have any knowledge of three-party Bell inequalities that are violated with measurements relying only on the equator of the Bloch sphere.
It is, then, necessary to find another strategy to work in a N-partite optical-path entangled system. Instead of homodyne detection it is interesting to use the DB measurement as, in this case, we have access to all the Bloch sphere and I have already shown in chapters 2 and 3 that one can violate the CHSH inequality for different implementations using this measurement. Here, I propose a simple approach to implement an entanglement witness suitable for N-partite path entanglement extendable to an arbitrary high number of spatial modes.

4.2 Proposed entanglement witness for two modes

We wish to define a witness suited to detect entanglement in $|W\rangle = \frac{1}{\sqrt{2}}(|01\rangle + |10\rangle)$-type states defined in the Hilbert space composed by two spatial modes A and B. We start from the decomposition of the state $|W\rangle$ in the Pauli representation, i.e. we write the corresponding density matrix $\rho_W = |W\rangle\langle W|$ as:

$$\rho_W = \frac{1}{4}(\mathbb{1} \otimes \mathbb{1} + \sigma_x \otimes \sigma_x + \sigma_y \otimes \sigma_y - \sigma_z \otimes \sigma_z). \tag{4.1}$$

The intuitive idea behind fidelity-based witnesses is that if there is a physical state $\tilde{\rho}$ s.t.

$$\mathrm{Tr}\left(\overline{\mathbb{Z}}\tilde{\rho}\right) \approx 1 \tag{4.2}$$

where $\overline{\mathbb{Z}} = \rho_W$, i.e. the overlap between ρ_W and $\tilde{\rho}$ is close to 1, we can conclude that $\tilde{\rho}$ is necessarily entangled. Given that the term proportional to the identity does not give any information about the correlations between the two modes, we neglect it. We thus define a witness $\mathbb{Z}_2$ s.t.

$$\mathbb{Z}_2 = \sigma_x \otimes \sigma_x + \sigma_y \otimes \sigma_y - \sigma_z \otimes \sigma_z. \tag{4.3}$$

4.3 Bounding the Hilbert space dimension

Since we aim to implement a state-independent protocol, I here explain how to

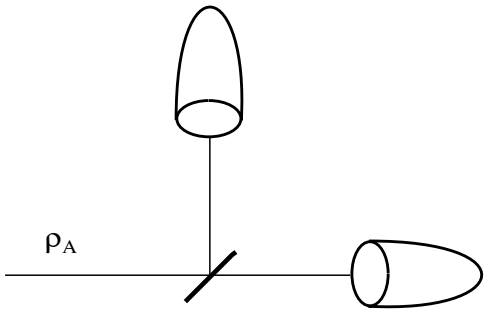

Figure 4.1: Setup for upper-bounding the probability p^* of having more than one photon in mode a (b). The reduced density matrix ρ_a is sent to a 50:50 beam splitter. Each mode is then analysed by two NPNR detectors. The probability of having a detection in both arms in taken in account.

bound the probability of having at least two photons in each arm. We use the setup presented in Fig. 4.1. Let ρ_A be the reduced state of Alice ($\rho_A = \mathrm{Tr}_B\,\rho_{\mathrm{AB}}$). Let us

further consider this state after a beam splitter $U_{BS}^{\dagger}\rho_A U_{BS} = \sum_{n=0,m=0}^{+\infty} c_{nm} |n\rangle \langle m|$, where U_{BS} corresponds to the BS interaction, and $|n\rangle$ is a Fock state with n photons. The probability of having a twofold coincidence after a $50-50$ beam splitter is given by

$$\overline{p} = \mathrm{Tr}\left(U_{BS}^{\dagger}\rho_A U_{BS} P_{\text{click}}^{\eta=1} \otimes P_{\text{click}}^{\eta=1}\right) = \sum_{n=2}^{+\infty} \frac{n}{2^n}(2^{n-1}-1)|c_n|^2 \geq \frac{p\left(n_a \geq 2\right)}{2}, \quad (4.4)$$

where n_a (n_b) is the number of photons in mode a (b). We have, then

$$p\left(n_a \geq 2 \cup n_b \geq 2\right) = p\left(n_a \geq 2\right) + p\left(n_b \geq 2\right) - p\left(n_a \geq 2 \cap n_b \geq 2\right)$$

$$\leq p\left(n_a \geq 2\right) + p\left(n_b \geq 2\right) \leq 2(\overline{p}_A + \overline{p}_B) = p^*. \quad (4.5)$$

We can use this bound to apply our witness to qudit states as shown below.

4.4 Entanglement witness for 2 qudit states

Let's work for the moment under the assumption $\eta = 1$, i.e. unit efficiency NPNR detectors, in the $\{|0\rangle, |1\rangle\}$. As discussed before in paragraph 2.2, in this subspace ϖ_0^1 corresponds to a qubit measurement along the $\mathbf{z}$ direction. Similarly, ϖ_1^1 and ϖ_i^1 approximate pretty well qubit measurements along $\mathbf{x}$ and $\mathbf{y}$ respectively. This encourages us to introduce the observable $\tilde{Z}_2$

$$\tilde{Z}_2 = \varpi_\alpha^1 \otimes \varpi_\alpha^1 + \varpi_{i\alpha}^1 \otimes \varpi_{i\alpha}^1 - \varpi_0^1 \otimes \varpi_0^1. \quad (4.6)$$

Furthermore, we focus on the case where the relative phase of αs is zero but their local value is random. We redefine our witness as

$$Z_2 = \langle \tilde{Z}_2 \rangle = \frac{1}{2\pi}\int_0^{2\pi} d\phi U_p^{\dagger}\tilde{Z}_2 U_p \quad (4.7)$$

where $U_p = U_A \otimes U_B = e^{i\left(a^{\dagger}a + b^{\dagger}b\right)\varphi}$ (which together with the integration over φ gives the random phase), a and b being bosonic operators in modes A and B respectively. Since we have that

$$\langle \varpi_\alpha^\eta \otimes \varpi_\alpha^\eta \rangle = \langle \varpi_{i\alpha}^\eta \otimes \varpi_{i\alpha}^\eta \rangle, \quad (4.8)$$

our witness takes the following form

$$Z_2 = 2\langle \varpi_\alpha^1 \otimes \varpi_\alpha^1 \rangle - \varpi_0^1 \otimes \varpi_0^1. \quad (4.9)$$

The question at issue is what is the maximal value $Z_{\text{PPT}} = \max_{\rho} \mathrm{Tr}(Z_2\rho)$ for any separable state ρ.

In order to find a separable threshold for entangled states we apply the PPT criterion that states that all separable states stay positive under partial transpose (PPT).
Let us consider to work in a Hilbert space of infinite dimension.
In the aim of upperbounding this observable for separable states, we rewrite our state ρ in the following form as

$$\rho = \begin{pmatrix} \rho_{n_a \leq 1 \cap n_b \leq 1} & \rho_{\text{coh}} \\ \rho_{\text{coh}}^{\dagger} & \rho_{n_a \geq 2 \cup n_b \geq 2} \end{pmatrix}. \tag{4.10}$$

Since the maximal (algebraic) value for our witness is 3 and since we know that $p\left(n_a \geq 2 \cup n_b \geq 2\right) \leq p^*$, we have

$$\text{Tr}(Z_2 \rho) \leq \text{Tr}\left(Z_2 \rho_{n_a \leq 2 \cap n_b \leq 2}\right) + 3p^*, \tag{4.11}$$

where $\rho_{n_a \leq 2 \cap n_b \leq 2}$ is the projection of the measured state restricted to the subspace $\{|0\rangle, |1\rangle, |2\rangle\}$. In the term $\text{Tr}\left(Z \rho_{n_a \leq 2 \cap n_b \leq 2}\right)$ there are contributions to the witness that come from $\rho_{n_a \leq 1 \cap n_b \leq 1}$, a part of $\rho_{n_a \geq 2 \cup n_b \geq 2}$ and all the coherence terms between them. All the other contributions to the witness from ρ_{coh} are null because of the phase average procedure. We look for
$Z_{\text{PPT}} = \max_{\rho_{n_a \leq 2 \cap n_b \leq 2}} \text{Tr}\left(Z \rho_{n_a \leq 2 \cap n_b \leq 2}\right) + 3p^*$ s.t.

1. $\rho_{n_a \leq 2 \cap n_b \leq 2} \geq 0$,
2. $\text{Tr}\left(\rho_{n_a \leq 2 \cap n_b \leq 2}\right) \leq 1$,
3. $\text{Tr}\left(\rho_{n_a \leq 1 \cap n_b \leq 1}\right) \geq 1 - p^*$,
4. $\rho_{n_a \leq 1 \cap n_b \leq 1}^{T_B} \geq 0$.

Let us restrict for the moment to the Fock subspace for which $n_A \leq 1 \cap n_B \leq 1$. Consider density matrices of the following form in the Fock basis

$$\rho_{n_A \leq 1 \cap n_B \leq 1} = \begin{pmatrix} p_{00} & 0 & 0 & 0 \\ 0 & p_{01} & d & 0 \\ 0 & d^* & p_{10} & 0 \\ 0 & 0 & 0 & p_{11} \end{pmatrix}. \tag{4.12}$$

Then the previous conditions 1. and 3. lead respectively to $|d|^2 \leq p_{01} p_{10}$ and $|d|^2 \leq p_{00} p_{11}$. The last condition allows us to upperbound Z_{PPT} for separable states in the

regime $\alpha \geq 0.45$ as

$$\begin{aligned} Z_{\mathrm{PPT}} = & \left(2\left(-1+2e^{-|\alpha|^2}\right)^2 - 1\right) P_{00} \\ & + \left(2\left(-1+2e^{-|\alpha|^2}\right)\left(-1+2e^{-|\alpha|^2}|\alpha|^2\right)+1\right)(P_{0c}+P_{c0}) \\ & + \left(2\left(-1+e^{-|\alpha|^2}|\alpha|^4\right)^2 - 1\right)\bar{p}_A \\ & + \left(2\left(-1+2e^{-|\alpha|^2}\right)\left(-1+e^{-|\alpha|^2}|\alpha|^4\right)+4\right)(\bar{p}_A+\bar{p}_B) \\ & + 8\sqrt{2}|\alpha|^2 e^{-2|\alpha|^2}\left(\sqrt{\bar{p}_A\bar{p}_B}|\alpha|^4 + 2\sqrt{P_{00}P_{cc}}\right. \\ & \left. + \left(\sqrt{\bar{p}_B P_{cc}} + \sqrt{\bar{p}_A P_{cc}} + \sqrt{\bar{p}_A\bar{p}_B}\right)|\alpha|^2\right), \end{aligned} \tag{4.13}$$

where P_{00}, (P_{0c}, P_{c0}, P_{cc}) is the probability of having no detections in both modes (no detection/click, click/no detection, click/click) without any displacement. Since I applied the PPT criterion only in the subspace $\{|0\rangle, |1\rangle\}$, if we detect a value $\langle Z\rangle > Z_{\mathrm{PPT}}$ we can conclude that the entanglement lies in this Fock subspace.

4.5 Change in representation

In real experiments, the NPNR detectors have non unit efficiency ($\eta < 1$). Note

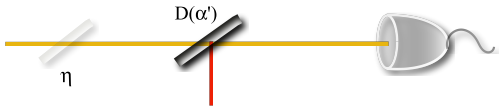

Figure 4.2: Equivalent representation of the DB measurement when the losses are before the displacement.

first that it can be proven that

$$D(\alpha')U_{\mathrm{BS}} = U_{\mathrm{BS}}D(\alpha) \tag{4.14}$$

where U_{BS} is the operator representing a beam splitter with transmission $T = \sqrt{\eta}$ and $\alpha' = \alpha\sqrt{\eta}$. The setup shown in Fig. 5.1 is, thus, equivalent to the setup shown in Fig. 4.2. The optimization performed so far tells whether the state ρ'_{AB} is entangled, while we are interested in the entanglement of ρ_{AB} (Fig. 4.3). We can, nevertheless, show that if ρ_{AB} is separable, then ρ'_{AB} is also separable. If $\rho = \rho_{\mathrm{sep}}$

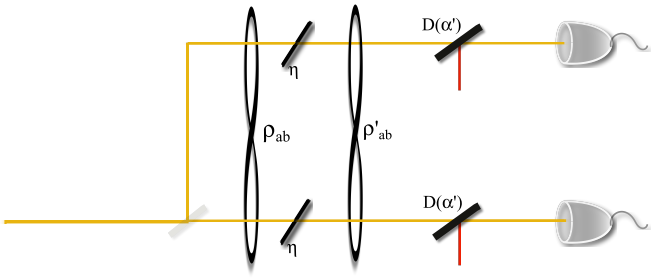

Figure 4.3: Schematic representation of the experimental setup where the losses are considered to be before the displacement. In the picture the entangled density matrices ρ_{AB} and ρ'_{AB} are represented.

is separable, indeed

$$\begin{aligned}\rho' &= U^A_{\mathrm{BS}} \otimes U^B_{\mathrm{BS}}\, \rho_{\mathrm{sep}}\, U^{A\dagger}_{\mathrm{BS}} \otimes U^{B\dagger}_{\mathrm{BS}} \\ &= \sum_i c_i U^A_{\mathrm{BS}} \otimes U^B_{\mathrm{BS}}\, \rho^i_A \otimes \rho^i_B\, U^{A\dagger}_{\mathrm{BS}} \otimes U^{B\dagger}_{\mathrm{BS}} \\ &= \sum_i c_i \rho'^i_A \otimes \rho'^i_B\end{aligned} \tag{4.15}$$

is a separable state as well.
Therefore if ρ' is found to be entangled, ρ is entangled, too. Our entanglement witness thus works even if the NPNR detectors have not unit efficiencies.

4.6 Extension to the N-qubits case

In this paragraph, I show the scalability of the protocol, i.e. I show that it is possible to detect genuine multipartite entanglement for an arbitrary number N of optical paths. Let us restrict to the case of no loss and a maximally entangled single-photon state $|W_N\rangle$. Following the same procedure used for two modes we find the equation of the entanglement witness

$$Z_N = \sum_{m=1}^{N} \sigma_0^{\otimes m} + 4 \sum_{m=0}^{N-2} \sigma_0^{\otimes m} \otimes \langle \sigma_\alpha \sigma_\alpha \rangle + \mathrm{sym.} \tag{4.16}$$

In order to find the genuine multipartite threshold we have first to find the entanglement threshold regarding each possible bipartition of the N optical paths. Let's consider the case where we want to test the entanglement between the first m modes and the other $(N-m)$ and let's call them subgroups A and B. Considering that the $|W_N\rangle$ state lies in the $\{|0\rangle, |1\rangle\}$ space we restrict our study to this subspace. We look for the expression of $Z^m_{\mathrm{PPT}} = \max_\rho \mathrm{Tr}\,(Z_N \rho)$ s.t.

1. $\rho \geq 0$,
2. $\mathrm{Tr}(\rho) = 1$,
3. $\rho^{T_A} \geq 0$,

where ρ^{T_A} is the partial transpose of ρ over subgroup A. The last condition applied on a state ρ that lies in the $\{|0\rangle, |1\rangle\}$ space and has the same probabilities of $|W_N\rangle$ implies

$$|\langle 10...0|\,\rho\,|0...1\rangle|^2 \leq p_{10...1}p_{00...0} = 0. \tag{4.17}$$

Condition $\rho^{T_A} \geq 0$ is symmetric under permutations of the first m (last $(N-m)$) optical modes between them. Thus Equ.(4.17) still stays true for permutations of modes in these two subgroups. The results of the measurement for a $|W_N\rangle$ state and the entanglement threshold Z^m_{PPT} are given by the following expressions

$$\langle Z_N\rangle = \mathrm{Tr}\left(Z_N\,|W_N\rangle\,\langle W_N|\right) = \left(2^N-1\right)N + 2^{N+1}e^{-|\alpha|^2}\left(4|\alpha|^2e^{-|\alpha|^2} - 1 - |\alpha|^2\right)(N-1), \tag{4.18}$$

$$\langle Z_N\rangle - Z^m_{\mathrm{PPT}} = 2^{N+3}\frac{m(N-m)}{N}|\alpha|^2e^{-2|\alpha|^2}. \tag{4.19}$$

The $|W_N\rangle$ state and Z_N are symmetric under permutations of two or more optical paths. Z^m_{PPT} is, then, the threshold for a $m-(N-m)$ bipartite state. The threshold for genuine multipartite entanglement is given by the maximal value of Z^m_{PPT} varying m. Thus the difference between $\langle Z_N\rangle$ and the genuine multipartite entanglement threshold $z^{\mathrm{genuine}}_{\mathrm{PPT}}$ is given by the equation

$$\langle Z_N\rangle - Z^{\mathrm{genuine}}_{\mathrm{PPT}} = 2^{N+3}\frac{N-1}{N}|\alpha|^2e^{-2|\alpha|^2} \geq 0. \tag{4.20}$$

We can conclude that for a state $|W_N\rangle$ in the case of no loss it is always possible to detect genuine multipartite entanglement.

4.7 Experiment

Two experiments in the bipartite and tripartite cases have been realized for showing the goodness of the protocol. The schematics of the setups are shown in Fig. 4.4. A SPDC source generates a squeezed vacuum state. The detection of a photon in the left spatial mode heralds the presence of at least a photon on the right mode. The beam splitters are used to generate the optical-path entangled states. Finally the states are measured locally by mean of the DB measurements.

The results of the measurements for the bipartite case are shown in Fig. 4.5 as a function of the level of entanglement and $\eta \approx 0.3$ (figure on the left) and

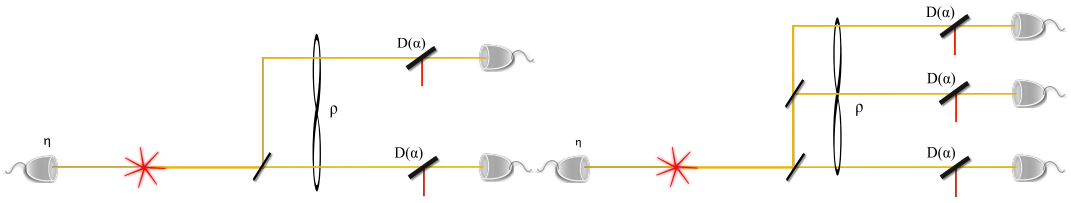

Figure 4.4: Schematics of the experimental setups. The SPDC source generates a two-mode squeezed state. Once that the NPNR detector on the left detects the presence of a photon, one is certain of the presence of at least one photon in the photonic mode on the right of the source. A series of beam splitters generates genuine multipartite entanglement between two or three modes. Finally the modes are analysed through DB measurements.

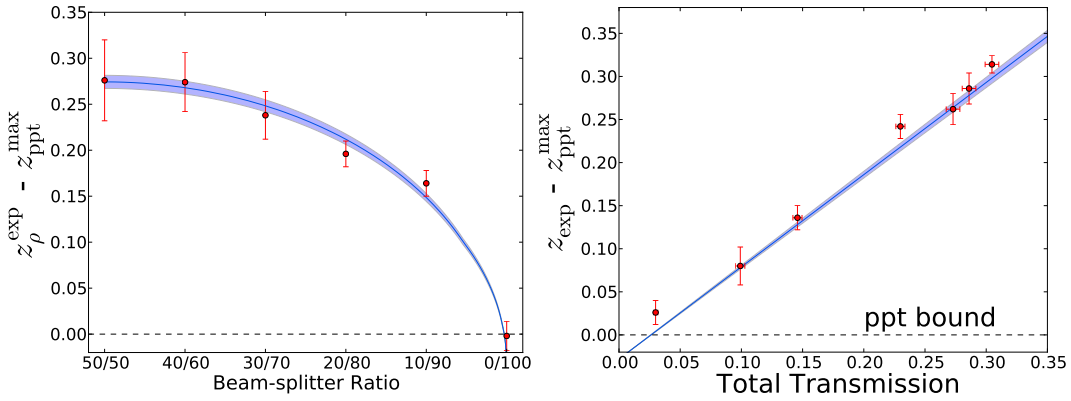

Figure 4.5: Bipartite witness as a function of the level of entanglement (left figure) and overall efficiency (right figure). The red dots represents the experimental results while the blue curve represents a theoretical model obtained through an autonomous analysis.

as a function of the overall transmission for a 50:50 beam splitter (figure on the right). The blue lines represent in both cases a theoretical model obtained using the equations found in paragraph 2.4. In the tripartite experiment only the case with two beam splitters of ratios 30:70 and 50:50, i.e. an almost maximally entangled state, respectively has been studied. The result has been compared with the genuine multipartite threshold obtaining the difference $z_\rho^{\exp} - z_{\text{ppt}}^{\max} = 0.99 \pm 0.10$, in perfect agreement with the theoretical result of 0.99.

4.8 Conclusion

I described a protocol based on an entanglement witness for detecting genuine multipartite entanglement in a quantum network using only local measurements. This method works for an arbitrary high number of modes state-independently with a reasonable number of measurements $\frac{N^2}{2} + \frac{N}{2} + 1$.
The experiments show that the protocol is resistant to loss and it does not depend on the level of entanglement between the modes.
In the following chapter, I discuss how to use these techniques when different detectors are used.

5 Revealing path-entanglement with the human eye

5.1 Introduction

Great improvements have been made in the analysis of the functioning of the human eye as a photon detector. We now know that it can be modelled as a NPNR detector with threshold 7 and efficiency 0.08 (Hecht et al. 1942). One question that may arise is "why are not we able to see quantum features like entanglement with the naked eye?"
In other words, is there any possibility of seeing entanglement, or is there a theoretical reason for which this is not possible?
In the previous chapters, we showed that the DB measurement is very promising in the analysis of optical-path states. Here, I show that the combination between a displacement and a human eye gives access to measures that span the entire Bloch sphere, as for standard DB measurements. After that, I show that it is possible to retrace the procedure of the previous chapter to implement an entanglement witness with the human eye state-independently.

5.2 Proposed experimental setup

The proposed experimental setup is shown in Fig. 5.1. A source (SPDC source+heralding detector) and a beam splitter of transmittivity T generates an optical-path entangled state. The state is then analysed by two different measurements. In mode A, the one on the top of the figure, there is a displacement measurement with a NPNR detector with threshold 1; in mode B, at the bottom of the figure, there is a displacement measurement using the human eye.

5.3 Expression for a detector with threshold θ.

As a first step, we derive here the expression of the operator for a NPNR detector with threshold θ and efficiency η. Such a detector can be modelled as an ideal NPNR detector ($P^{\theta}_{\text{no-click}} = \sum_{m=0}^{\theta-1} |m\rangle \langle m|$) preceded by a beam splitter

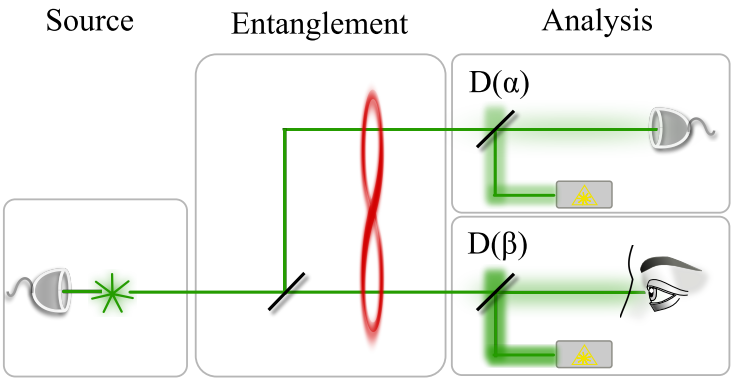

Figure 5.1: Experimental setup. An SPDC source generates a two-mode squeezed state. A detector with a detection heralds the presence of a photon in the mode on the right. The entanglement is generated by mean of a beam splitter whose ratio T can be varied. The two modes are then analysed by two DB measurements. On the top the DB measurement is composed by a displacement of amplitude α and a NPNR detector, while on the bottom it is composed by a displacement of amplitude β and the human eye.

with transmission η. Given the operator U_{BS} representing the beam splitter, i.e. $U_{\text{BS}} = e^{tg\gamma\, ac^\dagger} e^{log(cos\gamma)a^\dagger a} \left|0\right\rangle_C$, the operator for the NPNR detector with threshold θ is

$$P^{\theta,\eta}_{\text{no-click}} = U^\dagger_{\text{BS}} P^{\theta}_{\text{no-click}} U_{\text{BS}} =_C \left\langle 0\right| e^{log(cos\gamma)a^\dagger a} e^{tg\gamma\, a^\dagger c} \sum_{m=0}^{\theta-1} \left|m\right\rangle \left\langle m\right| e^{tg\gamma\, ac^\dagger} e^{log(cos\gamma)a^\dagger a} \left|0\right\rangle_C ,$$

where $\cos^2\gamma = \eta$. Let's consider the mth term of the sum. We have

$$U^\dagger_{\text{BS}} \left|m\right\rangle \left\langle m\right| U_{\text{BS}} = \frac{1}{m!}\eta^m \frac{d^m}{d(1-\eta)^m}(1-\eta)^{a^\dagger a}. \tag{5.1}$$

The final expression for the total operator is

$$\begin{aligned} P^{\theta,\eta}_{\text{no-click}} &= \sum_{m=0}^{\theta-1} \frac{1}{m!}\eta^m \frac{d^m}{d(1-\eta)^m}(1-\eta)^{a^\dagger a} \\ &= \frac{\eta^\theta}{(\theta-1)!}\frac{d^{\theta-1}}{d(1-\eta)^{\theta-1}}\frac{(1-\eta)^{a^\dagger a}}{\eta}. \end{aligned} \tag{5.2}$$

5.4 Displacement-based measurement for a detector with threshold θ

The measurement that we have in mind is shown in Fig. 5.2. It is composed by the detector with threshold θ and efficiency η preceded by a small displacement

of amplitude α. In analogy with the previous measurement, we associate $+1$ to a no-click and -1 to a click. The operator representing the measurement is given by the expression

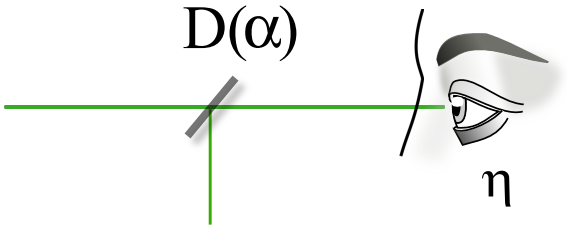

Figure 5.2: Displacement measurement with the human eye.

$$\varpi_{\alpha}^{\theta,\eta} = D^{\dagger}(\alpha)(2P_{\text{no-click}}^{\theta,\eta} - \mathbb{1})D(\alpha), \tag{5.3}$$

where $D(\alpha) = e^{\alpha a^{\dagger} - \alpha^{*} a}$. It follows from this the equation

$$\varpi_{\alpha}^{\theta,\eta} = \frac{\eta^{\theta}}{(\theta-1)!}\frac{d^{\theta-1}}{d(1-\eta)^{\theta-1}}\frac{\mathbb{o}_{\alpha}^{\theta=1,\eta}}{\eta}. \tag{5.4}$$

In Fig. 5.3 the vectors representing the projection of the POVM in the Bloch sphere for different values of η and θ varying α are represented. In all cases it is possible to perform easily a measurement on the x-y plane for $|\alpha| = \sqrt{\frac{\theta}{\eta}}$.
On the other hand, it is not obvious how to perform a measurement in the z direction. Our idea is represented in Fig. 5.4. One has to choose a value α for which $\varpi_{|\alpha|e^{i\varphi}}^{\theta,\eta}$ has a non-null projection with the z direction. The Bloch vector rotates around the z-axis as a function of the phase of α. If one, then, realizes a measurement $\varpi_{\alpha}^{\theta,\eta}$ while the phase of α changes in time the component on the equator of the Bloch sphere averages to 0. It results a final measurement that has only a component on the z-axis, i.e.

$$\frac{1}{2\pi}\int_{0}^{+2\pi}\varpi_{\alpha}^{\theta,\eta}d\varphi = \frac{\eta^{\theta}}{(\theta-1)!}\frac{d^{\theta-1}}{d(1-\eta)^{\theta-1}}\frac{1}{\eta}\begin{pmatrix} 2e^{-\eta|\alpha|^2}-1 & 0 \\ 0 & 2\left(\eta^2|\alpha|^2+1-\eta\right)e^{-\eta|\alpha|^2}-1 \end{pmatrix}, \tag{5.5}$$

where $\alpha = |\alpha|e^{i\varphi}$.

5.5 Entanglement detection in the qubit space

We further assume that all the loss is kept before the displacements. This is possible since a local operation, like displacement, does not create entanglement. In order to detect entanglement we use a fidelity-based entanglement witness, i.e

$$\overline{W} = \frac{\sigma_x\sigma_x + \sigma_y\sigma_y}{2}. \tag{5.6}$$

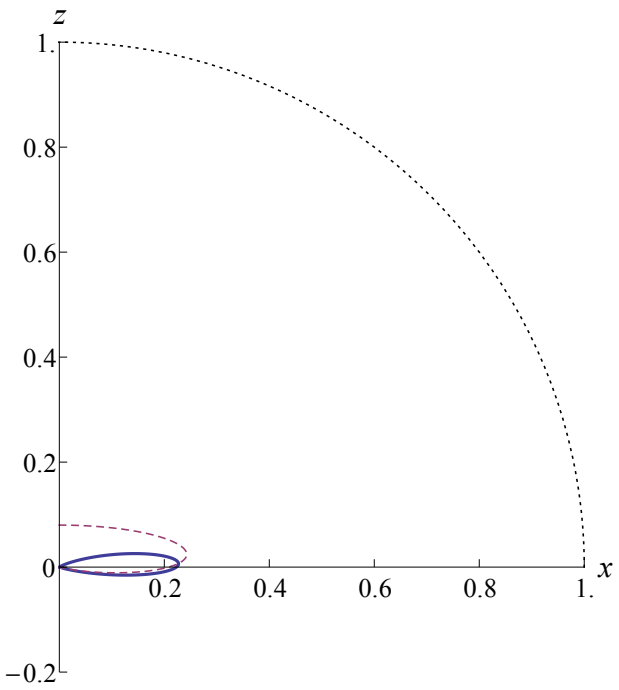

Figure 5.3: Vectors representing $\varpi_\alpha^{\theta,\eta}$ for different values of η and θ. The yellow, violet, and blue curves represent $\eta = 1$ and $\theta = 1$, $\eta = 0.08$ and $\theta = 1$, $\eta = 0.08$ and $\theta = 7$ respectively.

This witness can be implemented up to a proportional factor using the following measurement

$$W =< \varpi_{\sqrt{7}}^{7,\eta} \varpi_1^{1,\eta} >= \frac{1}{2\pi} \int_0^{+2\pi} \varpi_{\sqrt{7}e^{i\varphi}}^{7,\eta} \varpi_{e^{i\varphi}}^{1,\eta} d\varphi, \tag{5.7}$$

where the phase is kept constant between the modes, but changes randomly with time. The phase average allows to perform an average of the measurements on the equator of the Bloch sphere. Let's restrict our work for the moment in the subspace with at most a photon per mode. Let's consider a general density matrix P in the qubit space. To find the entanglement threshold, i.e. the maximal value that the witness can reach for a separable state, we use the PPT criterion. We look for $W_{\mathrm{PPT}} = \max_P \mathrm{Tr}(PW)$ s.t.

1. $P \geq 0$,
2. $\mathrm{Tr}(P) = 1$,
3. $P^{T_b} \geq 0$,

where P^{T_b} is the partial transpose of P regarding mode B. If a state P is such that $\mathrm{Tr}(PW) > W_{\mathrm{PPT}}$, one is forced to conclude that one of the previous conditions does

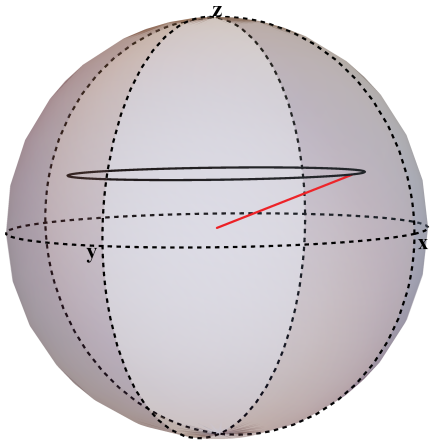

Figure 5.4: Representation of the averaged measurement in the Bloch sphere. The red vector represents the measurement for a real value of the amplitude α of the displacement. When the phase of α varies from 0 to 2π, the arrow of the vector describes a circle around the z-axis.

not apply, i.e. the state is entangled. Let's derive now an analytical expression for W_{PPT}. We have

$$\text{Tr}\,(WP) = \langle ij|\, W\, |ij\rangle + 2|\,\langle 01|\, W\, |10\rangle\,| \min(\sqrt{p_{00}p_{11}}, \sqrt{p_{01}p_{10}}) = W_{\text{PPT}}. \tag{5.8}$$

In the case of a maximally entangled state $|\psi\rangle = \frac{1}{\sqrt{2}}(|01\rangle + |10\rangle)$ and no loss the difference between the measured value $\langle W\rangle$ and the threshold W_{PPT} is

$$\Delta W = \langle W\rangle - W_{\text{PPT}} = \frac{1}{2}|\,\langle 01|\, W\, |10\rangle\,| \geq 0. \tag{5.9}$$

We conclude that in this case it is possible to detect entanglement.

5.6 Detecting entanglement state-independently

We are now going to consider the case when the Hilbert space is not limited to the $\{|0\rangle, |1\rangle\}$ subspace. To this aim we study, first, how to upperbound the probabilities p_{00}, p_{01}, p_{10}, p_{11}, and $p_{n\geq 2B}$ with measurements only relying on $\varpi_0^{1,1}$, and $\varpi_\beta^{7,1}$ on Alice's and Bob's sides respectively.

5.6.1 Upperbounding local and joint probabilities.

In Fig. 5.5 the probabilities $p_{\text{nc}}^n = \langle n|\, D^\dagger(\beta) P_{\text{no-click}}^{7,1} D(\beta)\, |n\rangle$ for $n = 0, 1, 2, 3$ of not having a click when a state $|n\rangle$ is detected by a detector $P_{\text{no-click}}^{7,1}$ with $\eta = 1$.

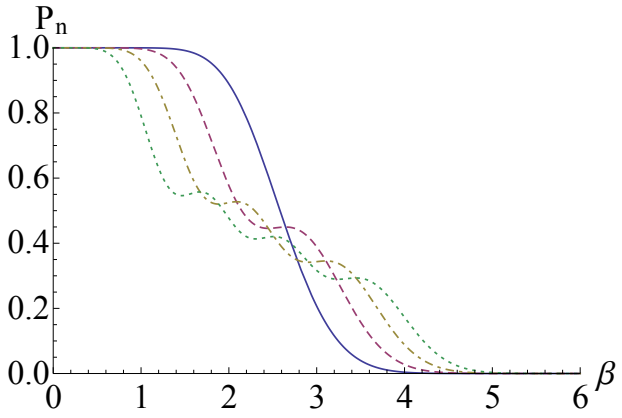

Figure 5.5: Probabilities of no-click $p_{\text{nc}}^n = \langle n| D^\dagger(\beta) P_{\text{no-click}}^{7,1} D(\beta) |n\rangle$ with a DB measurement for a Fock state $|n\rangle$ as a function of the displacement amplitude β.

We upperbound p_{2B}, p_{00}, p_{01}, p_{10}, and p_{11} performing three different measurements. Let's consider the amplitude of the displacement $\beta_1 \approx 2.64$ obtained for $p_{\text{nc}}^0 = p_{\text{nc}}^1$ on Bob's side. Working on the expression of the local measurement $D^\dagger(\beta_1 \approx 2.64) P_{\text{no-click}}^{7,1} D(\beta_1 \approx 2.64)$, we obtain the following series of inequalities

$$\begin{aligned} &\text{Tr}(\rho D^\dagger(\beta_1) P_{\text{no-click}}^{7,1} D(\beta_1)) = p_{0B} p_{\text{nc}}^0 + p_{1B} p_{\text{nc}}^1 + \sum_{n=2} p_{nB} p_{\text{nc}}^n \leq \\ &(p_{0B} + p_{1B}) p_{\text{nc}}^0 + p_{n\geq 2B} p_{\text{nc}}^3 = (p_{\text{nc}}^3 - p_{\text{nc}}^0) p_{n\geq 2B} + p_{\text{nc}}^0, \end{aligned} \tag{5.10}$$

where $p_{nB} =_B \langle n| \rho |n\rangle_B$. We end up with the following inequality

$$p_{n\geq 2B} \leq \frac{\text{Tr}\left(\rho D^\dagger(\beta_1) P_{\text{no-click}}^{7,1} D(\beta_1)\right) - p_{\text{nc}}^0}{p_{\text{nc}}^3 - p_{\text{nc}}^0} = p_B^*. \tag{5.11}$$

The probabilities p_{00} and p_{01} can be upperbounded using the measurement $D^\dagger(\beta_2 \approx 2.713) P_{\text{no-click}}^{1,7} D(\beta_2 \approx 2.713) P_{\text{no-click}}^{1,1}$, where $\beta_2 \approx 2.713$ has been chosen for $p_{\text{nc}}^0 = p_{\text{nc}}^3$, i.e.

$$\begin{aligned} &\text{Tr}\left(\rho D^\dagger(\beta_2) P_{\text{no-click}}^{7,1} D(\beta_2) P_{\text{no-click}}^{1,1}\right) = \\ &p_{00} p_{\text{nc}}^0 + \sum_{n=1} p_{n0} p_{\text{nc}}^n \leq (p_{\text{nc}}^0 - p_{\text{nc}}^1) p_{00} + p_{\text{nc}}^1 p_{0A}. \end{aligned} \tag{5.12}$$

It derives the following upperbound for p_{00},

$$p_{00} \leq \frac{\text{Tr}\left(\rho \left(D^\dagger(\beta_2) P_{\text{no-click}}^{7,1} D(\beta_2) - p_{\text{nc}}^1\right) P_{\text{no-click}}^{1,1}\right)}{p_{\text{nc}}^0 - p_{\text{nc}}^1} = P_{00}. \tag{5.13}$$

Similarly we can upperbound p_{01} as

$$p_{01} \leq \frac{\mathrm{Tr}\left(\rho\left(D^{\dagger}(\beta_2)P^{7,1}_{\text{no-click}}D(\beta_2) - p^1_{\text{nc}}\right)P^{1,1}_{\text{click}}\right)}{p^0_{\text{nc}} - p^1_{\text{nc}}} = P_{01}. \tag{5.14}$$

Following the same line of thoughts for the amplitude $\beta_3 \approx 2.09$ that has the property $p^1_{\text{nc}} = p^2_{\text{nc}}$, we derive the upperbound for p_{10}, and p_{11} as follows

$$p_{10} \leq \frac{\mathrm{Tr}\left(\rho\left(D^{\dagger}(\beta_3)P^{7,1}_{\text{no-click}}D(\beta_3) - p^0_{\text{nc}}\right)P^{1,1}_{\text{no-click}}\right)}{p^1_{\text{nc}} - p^0_{\text{nc}}} = P_{10}, \tag{5.15}$$

$$p_{11} \leq \frac{\mathrm{Tr}\left(\rho\left(D^{\dagger}(\beta_3)P^{7,1}_{\text{no-click}}D(\beta_3) - p^0_{\text{nc}}\right)P^{1,1}_{\text{click}}\right)}{p^1_{\text{nc}} - p^0_{\text{nc}}} = P_{11}. \tag{5.16}$$

5.6.2 PPT criterion

In order to find the threshold of the witness hereafter I follow the method used in the previous chapter for Z_2.
Let us, first, restrict our work in the subspace $n_A \leq 2 \cap n_B \leq 2$.

$$\begin{aligned}
&\mathrm{Tr}\left[\mathfrak{o}^7_{\sqrt{7}} \otimes \mathfrak{o}^1_1 . \rho_{n_A \leq 2 \cap n_B \leq 2}\right] \leq \\
&\frac{(355081 - 360e^7)\left((2e^{-1}-1)\left(P_{00}+P_{01}+P_{10}+P_{11}\right) + 2\left(e^{-1}-1\right)p^*_B\right)}{360e^7} \\
&+ \frac{117649\left(\sqrt{7P_{00}P_{11}} + \frac{\sqrt{7P_{11}p^*_A}}{\sqrt{2}} + \frac{\sqrt{7P_{11}p^*_A}}{2} + 117649\sqrt{\frac{1}{2}}\sqrt{P_{11}p^*_B} + \frac{1}{2}\sqrt{p^*_A p^*_B}\right)}{90e^8} \\
&+ \frac{(3-5e^{-1})\left(720e^7 - 592513\right)p^*_A}{720e^8} = W_{n_A \leq 2 \cap n_B \leq 2},
\end{aligned} \tag{5.17}$$

where $p^*_A = \overline{p}_A$ is founded using the method presented in section 4.3. The final expression of the threshold is $W_{\text{PPT}} = W_{n_A \leq 2 \cap n_B \leq 2} + p^*_A + p^*_B$. In Fig. 5.6 the violation $\Delta W = \langle W \rangle - W_{\text{PPT}}$ optimized over the squeezing parameter g as a function of the transmittivity T is plotted.

5.7 Conclusion

In this chapter, I have focused on the possibility of realising quantum measurements with the human eye.

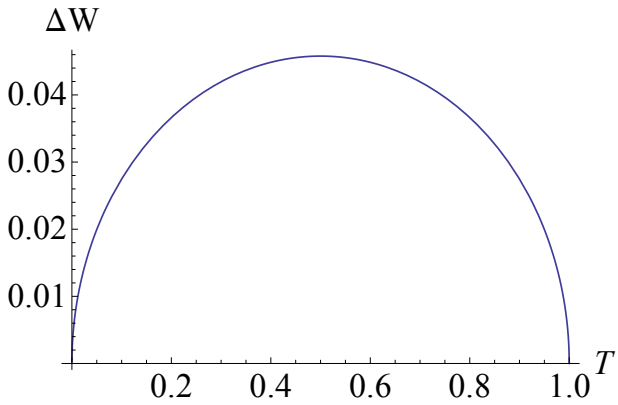

Figure 5.6: Violation ΔW of the witness-like threshold as a function of T.

I have characterized a possible measurement for detection in the $\{|0\rangle - |1\rangle\}$ Fock subspace that consists in a NPNR detector with threshold θ and efficiency η preceded by a small displacement. I have shown that such a measurement is equivalent to the DB measurement with the same efficiency on the equator of the Bloch sphere and that it is possible to realise also a measurement on the z-direction with a small expedient.
This measurement is, then, perfect for the realisation of an entanglement witness that relies only on one measurement in the qubit subspace.
For the purpose of realising a state-independent protocol it is necessary to realise four other measurements that allow one to upperbound the joint probabilities p_{00}, p_{01}, p_{10}, p_{11}, and the local probabilities $p_{n_B \geq 2}$ and $p_{n_A \geq 2}$. Nevertheless with these additional measurements it is possible to detect entanglement between the two modes.

General conclusion and outlook

The goal of this thesis was to investigate different implementations of Bell tests and entanglement witnesses relying on states with few photons.
In the first two chapters, I studied various setups for performing a Bell test with SPDC sources with the aim of comparing them for random number generation.
In chapter 1, I analysed the potentialities of the standard case for photonic systems, i.e. a set of wave-plates, polarizing beam splitters and photon counting techniques. Here, I derived the settings that allow the maximal CHSH violation for photons entangled in polarization. Even though this kind of setups has been studied several times, my work shows that there was still a big gap between theory and experiments. Indeed the production of vacuum and multi-pairs strongly reduces the maximal CHSH violation down to 2.35, compared to the ideal $2\sqrt{2}$. As a consequence, the randomness produced per run is equally reduced.
These results suggested to look for other types of photonic setups relying on optical-path entanglement and two-mode squeezed entanglement respectively, as shown in chapter 2. As a first step I analysed a new measurement scheme relying on small displacements and photon-counting techniques (DB measurements). The DB measurement showed the possibility to realize noisy Pauli measurements in the $\{|0\rangle, |1\rangle\}$ Fock subspace. Nevertheless, the noise does not forbid high violations in the two cases summarized below.
In the first case, I optimized the CHSH violation for optical-path entangled states by means of DB measurements. Here, the state is generated sending a heralded photon through a beam splitter for generating entanglement between two spatial modes. The maximal violation of 2.69 achieved for no loss, is the highest between the three possibilities analysed. At the same time, even if this implies also the highest randomness generation per run, the low rate of generation of the state for some experimental settings suggested to look for other tests.
In the second scenario of the chapter, I treated the case where a two-mode squeezed state is analyzed through DB measurements. The maximal violation shown is 2.4 while the rate of generation is the same of chapter 1. As a consequence this setup is better than the standard setup both in terms of randomness per run and rate of random generation.
The work reported in chapter 1 has already been applied to new research. Indeed, besides providing the instruments for optimizing the maximal violation in a real experiment, the full list of the probabilities for a polarization setup has inspired another group's research about randomness generation (Mattar et al. 2015). They

optimized the maximal randomness generated over all the possible Bell tests. This optimization has shown that binning the so-called non conclusive results reduces the extracted randomness.
The second chapter raises several interesting questions and perspectives. The optical-path setup showed interesting results as, for example, that the minimal detector efficiency for a maximally entangled state is not 0.828, but 0.826. This result is possible since the detector efficiency, i.e. the probability of detecting a photon, does not correspond in such experiment to the detection efficiency. This pushes to further studies in two directions.
First it is interesting to wonder how to redefine the concept of detection efficiency. This point is not interesting only from the theoretical point of view, but also from the experimental one. Indeed, it is my intuition that working with states that do not mandatory rely in a qubit space can in principle show not known correlations, more effective for experiments with other Bell inequalities. This is, for example, the case of Mattar et al. 2015, where the presence of photon multi-pairs gives the possibility to improve the randomness generation. Nevertheless, the entanglement in polarization between photon pairs does not seem to be the most suitable for this task since in this case the measurement setup is conceived for the analysis of only one photon pair entangled in polarization per time. States like optical-path entangled states or two-mode squeezed states are the natural candidates for such task since they rely in the Fock space, i.e. a space of infinite dimension. Furthermore, the probability of detecting a state $|n\rangle$ with a NPNR detector of efficiency η is roughly $\eta^n \leq \eta$. This data explains why our result for the optical-path entanglement setup does not match with previous theoretical works (Eberhard 1993). Consequently, one may wonder whether it is possible to find other states realizable in practice that can be used to lower the minimal required detector efficiency for Bell tests.
Second one other open question about DB measurements is connected to the photon detectors used. Indeed NPNR detectors are nowadays available and are fast becoming highly efficient. Despite that, they may not be the most efficient for optical-path entangled states since it could clearly be important to take into account the number of photons involved in the states. An interesting question is, thereby, what would happen if we were using photon number resolving (PNR) detectors, instead. This could, in principle, lead to two implications. Firstly, focusing on the CHSH inequality, we could perform a different binning and obtain better violations even with the single photon entanglement studied here. Secondly, it could be possible to test other Bell inequalities with more outcomes in terms of randomness generation. In fact this case is in some sense similar to the one studied in Mattar et al. 2015 and it is likely to bring good results.
As a last remark to this part, the introduction of the DB measurement opens the way to other experiments like implementation of steering inequalities and the implementation of CHSH Bell tests.

In chapter 3, I considered the possibility of generating the two-mode squeezed state using an optomechanical cavity and subsequently to test nonlocality through DB measurements. This proposal is the first realistic Bell test suitable for optomechanical cavities. Its interest lies in the possibility of detecting nonlocal correlations in massive systems. Since optomechanical cavities are macroscopic objects, this optomechanical Bell test could be interesting for showing quantum features in macroscopic states.
At the same time, the big mass of a movable mirror could be of great interest for testing explicit collapse models (Pfister et al. 2015), such as GRW (Ghirardi et al. 1986, 1990) or Diosi's and Penrose's theory (Diosi 1989; Penrose 1996), in a theory independent manner. Indeed it has been recently pointed out that a CHSH Bell test can test the nature of decoherence in a specific system and, hence, confirm new physical theories that go beyond quantum physics. This can be applied, for example, to Diosi's theory of gravitational decoherence (Diosi 1989) using optomechanical cavities. What is required for such a test is the presence of two entangled systems on which the Bell test is performed. Furthermore it is important that only one of the systems undergoes decoherence, while the other is a reference system. In this picture the first generated photon is the system of reference, while the phonon undergoes decoherence. The optomechanical Bell test presented in chapter 3 seems, then, suitable for testing Diosi's theory.
Chapters 2 and 3 showed that DB measurements are very promising. Nevertheless, due to the efficiencies of the photon detectors, CHSH tests are still highly challenging. The aim of chapter 4 was to implement a protocol able to detect genuine multipartite optical-path entanglement in a real experiment for an arbitrary high level of losses.
The results of this chapter are, then, highly interesting for two reasons:

1. The possibility of detecting entanglement with high losses and low efficiencies in a distributed scenario,

2. The realization of a protocol that can be generalized also to other appealing scenarios.

Concerning point 1, the procedure relies on the possibility of using the joint probabilities in the analytical expression of the witness of entanglement. Thus, the protocol is not device-independent and it cannot be implemented in Bell tests. At the same time it could be used in steering tests. These test a characteristic, steering, of quantum systems that is something in between entanglement and nonlocality. More explicitly, EPR steering is the ability to nonlocally influence the set of possible quantum states of a given quantum system through the measurements on a second distant system sufficiently entangled with the first one. By choosing which observable to measure on the second system, one can "steer" the first system to be well defined in any of its observables without directly interacting with it.

Consequently, the local probabilities of the second system are accessible and can be used to lower the minimal required efficiency.
Concerning point 2, entanglement lying in the Fock space is more attractive with respect to the entanglement between photon pairs in polarization. In the first case if one wants to generate a $(N+1)$-mode entangled system it is sufficient to add a beam-splitter to an existing N-mode entangled system. As a consequence we can easily generate very complex quantum networks exploiting different kinds of multipartite entanglement. In relation to this, one open question is about the properties of multipartite entanglement that can be used in information theory and how we can detect them. Let's focus on the case of three spatial modes, for example. The most studied kinds of maximally entangled states are the GHZ and W states, i.e.

$$|\mathrm{GHZ}\rangle = \frac{1}{\sqrt{2}}\left(|000\rangle + |111\rangle\right), \tag{1}$$

$$|\mathrm{W}\rangle = \frac{1}{\sqrt{3}}\left(|001\rangle + |010\rangle + |001\rangle\right). \tag{2}$$

GHZ has an interesting property, not present in the bipartite case. More explicitly, consider the density matrix $\rho_{\mathrm{GHZ}} = |\mathrm{GHZ}\rangle\langle\mathrm{GHZ}|$. The partial trace over one mode is a separable state, i.e. $\frac{1}{2}(|00\rangle\langle 00| + |11\rangle\langle 11|)$. This means that each mode is entangled with the whole ensemble of the other two modes, i.e. one needs to analyse the three subsystems together in order to recollect any information about quantum correlations. The W entanglement is more similar to the bipartite one: each mode is entangled with the other two separately. In other words, the partial trace of $\rho_{\mathrm{W}} = |\mathrm{W}\rangle\langle\mathrm{W}|$ over one mode, i.e. $\frac{1}{3}(|00\rangle\langle 00| + |01\rangle\langle 01| + |10\rangle\langle 10| + |01\rangle\langle 10| + |10\rangle\langle 01|)$, is still entangled. Thus tracing over one of the modes is not sufficient to eliminate all entanglement correlations. An interesting article about the difference between the two kinds of entanglement dates 2000 (Coffman et al. 2000). Both states have been defined maximally entangled, but according to two different definitions. The GHZ is maximally entangled in the sense that we do not have any information about how many photons there are in each mode, but once that we obtain this knowledge on one of them, we have maximal knowledge on the other two. W is maximally entangled in the sense that the photon is shared in equal way between the three modes and there is maximal uncertainty about where to find it through measurements.
The issue is, then, how we can exploit these two kind of properties for information applications. One of the most interesting fields for quantum information has always been cryptography.
For the GHZ state I would propose, for example, quantum secret sharing (Hillery et al. 1999). The idea is pretty simple. Consider three players, Alice, Bob, and Charlene. Alice has a message and wants to keep it secret. She decides, then, to give part of the information to Bob and part to Charlene so that both of them are

not able to get any information from their own. At the same time, once that they collect their information together they are able to recover the entire message. Some theoretical studies about the implementation have already been done (Hillery et al. 1999).
For the W state, on the contrary, we have to focus on a different application, that is network coding. Let's imagine that Alice wants to send a message to Dan in a secret way. She, thereby, sends the encrypted message to Bob and Charlene. Since the message has to be kept secret, they both encrypt it in a personal way and they afterwards send it through several other steps to Dan. Dan at his turn knows how to encrypt the two messages and, merging them exploiting the redundancy of the messages, is able to recover the initial one.
The issue at the moment is the way one can quantify and qualify the entanglement for the multimode case only with local measurements. Our witness is not good since it considers only two-mode correlations, i.e. terms with only two σ_x or two σ_y, and as a consequence it investigates only two-mode entanglement like W states. In fact it follows from the decomposition of ρ_{GHZ} in terms of Pauli matrices that all the witnesses suitable for GHZ states must contain products of three σ_x or three σ_y. At the same time, even in the case of W-like states, the use of the joint probabilities and the form of the witness forbid quantifying the amount of entanglement. However, the DB measurement seems to be a promising tool for any kind of protocol in distributed scenarios and is certainly applicable to this subject as well. Likely a correct approach to the problem would be, then, to find a witness suitable for quantifying multipartite entanglement and to adapt it to the DB measurement.
Given the excellent results obtained with DB measurements in photonic systems, I extended in chapter 4 my studies about photon detectors to the human eye. Here I showed that we can use the same procedure used for NPNR detectors also for the eye for realizing a measurement capable of working in the $\{|0\rangle, |1\rangle\}$ Fock subspace and able to detect optical-path entanglement. This is interesting especially from the fundamental point of view since it could be the first step towards the realization of quantum states that can be seen.
The implementation of such an experiment does not seem very challenging, until we consider the optical setup. Indeed the protocol is highly resistant to loss and level of entanglement. The main challenge is, on the contrary, at the level of the eye. Indeed we still do not have a great knowledge of how to couple biological devices with optical ones. Besides this, one could also argue about the way to reveal a detection with the human brain. In other words, unless one does not want to connect the human brain to a computer, there could be the doubt that a detection is the result of a wrong interpretation of the person. An additional problem is represented by the time of reaction of a human brain. In fact, it is surely higher than an electric system. As a consequence the stability of the amplitude of the displacement during all the experiment will be one of the main challenges of the implementation.

An open question is still wether there is a way to finally find a protocol for revealing quantum features with the human eye without the need of a magnifying glass like displacement. In my opinion such possibility is unlikely. Indeed, more than the threshold at 8 photons, the human eye has its biggest challenge in its low efficiency. In fact if we do not want to make use of additional devices, like for example wave-plates, the only possible states suitable for quantum tests rely in the Fock space. At the same time the low efficiency may highly impact the state causing decoherence. Furthermore, it is not easy to imagine a possible implementation that does not imply any additional device and that can reveal quantum features.

Bibliography

Acin, A., Brunner, N., Gisin, N., Massar S. Pironio, S., and Scarani, V. (2007). In: *Phys. Rev. Lett.* 98, p. 230501.

Babichev, S., Appel, J., and Lvovsky, A. (2004). In: *Phys. Rev.Lett.* 92, p. 193601.

Banaszek, K. and Wodkiewicz, K. (1998). In: *Phys. Rev. Lett.* 82, p. 2009.

Bohr Brask, J., Chaves, R., and Brunner, N. (2013). In: *Phys. Rev. A* 88, p. 012111.

Brunner, N., Cavalcanti, D., Pironio, S., Scarani, V., and Wehner, S. (2014). In: *Rev.Mod. Phys.* 86, p. 839.

Chaves, R. and Bohr Brask, J. (2011). In: *Phys. Rev. A* 84, p. 062110.

Christensen, B., McCusker, K. T., Altepeter, J. B., Calkins, B., Gerrits, T., Lita, A. E., Miller, A., Shalm, L. K., Zhang, Y., Nam, S. W., Brunner, N., Lim, C. C. W., Gisin, N., and Kwiat, P. G. (2013). In: *Phys. Rev. Lett.* 111, p. 130406.

Clauser, J., Horne, M., Shimony, A., and Holt, R. (1969). In: *Phys. Rev. Lett.* 23, p. 880.

Coffman, V., Kundu, J., and Wootters, W. K. (2000). In: *Phys. Rev. A* 61.052306.

Colbeck, R. and Kent, A. (2011). In: *J. Phys. A* 44, p. 095305.

D'Ariano, G., Lo Presti, P., and Perinotti, P. (2005). In: *J. Phys. A: Math. Gen.* 38, pp. 5979–5991.

Diosi, L. (1989). In: *Phys. Rev. A* 40, p. 1165.

Duan, L.-M., Lukin, M., Cirac, J., and Zoller, P. (2001). In: *Nature(London)* 414, p. 413.

Eberhard, P. (1993). "Background level and counter efficiencies required for a loophole-free Einstein-Podolsky-Rosen experiment". In: *Phys. Rev. A* 47, R747.

Fukuda, D., Fujii, G., Numata, T., Amemiya, K., Yoshizawa, A., Tsuchida, H., Fujino, H., Ishii, H., Itatani, T., Inoue, S., and Zama, T. (2011). In: *Opt. Express* 19, 870875.

Galland, C., Sangouard, N., Piro, N., Gisin, N., and Kippenberg, T. J. (2014). In: *Phys. Rev. Lett.* 112, p. 143602.

Ghirardi, G. C., Rimini, A., and Weber, T. (1986). In: *Phys. Rev. D* 34, p. 470.

Ghirardi, G. C., Pearle, P., and Rimini, A. (1990). In: *Phys. Rev. A* 42, p. 78.

Gisin, N. (2002). "Quantum cryptography". In: *Rev. Mod. Phys.* 74.1, pp. 145–195. DOI: 10.1103/RevModPhys.74.145.

Gisin, N., Pironio, S., and Sangouard, N. (2010). In: *Phys. Rev. Lett.* 105.7, p. 070501.

Giustina, M., Mech, A., Ramelow, S., Wittmann, B., Kofler, J., Beyer, J., Lita, A., Calkins, B., Gerrits, T., Nam, S. W., Ursin, R., and Zeilinger, A. (2013). In: *Nature* 497.7448, pp. 227–230.

Guhne, O. and Toth, G. (2009). In: *Phys. Rep.* 474, p. 1.
Hecht, S., Shlaer, S., and Pirenne, M. (1942). In: *J.Gen.Physiol.* 25, p. 819.
Hensen, B., Bernien, H., Dréau, A., Reiserer, A., Kalb N. Blok, M., Ruitenberg, J., Vermeulen, R., Schouten, R., Abellán, C., Amaya W. Pruneri, V., Mitchell, M., Markham, M., Twitchen, D., Elkouss, D., Wehner, S., Taminiau, T., and Hanson, R. (2015). In: **arXiv:1508.05949**.
Hessmo, B., Usachev, P., Heydari, H., and Björk, G. (2004). In: *Phys.Rev.Lett.* 92, p. 180401.
Hillery, M., Buek, V., and Berthiaume, A. (1999). In: *Phys. Rev. A* 59, p. 1829.
Ho, M., Morin, O., Bancal, J.-D., Gisin, N., Sangouard, N., and Laurat, J. (2014). In: *arXiv:1406.0381*.
Kimble, H. J. (2008). In: *Nature* 453.7198, pp. 1023–1030.
Kuzmich, A., Walmsley, I. A., and Mandel, L. (2000). In: *Phys. Rev.Lett.* 85, p. 1349.
Lim, C., Portmann, C., Tomamichel, M., Renner, R., and Gisin, N. (2013). In: *Phys. Rev. X* 3, p. 031006.
Lita, A., Miller, A., and Nam, S. (2008). In: *Opt. Express* 16, p. 3032.
Mattar, A., Skrzypczyk, P., Bohr Brask, J., Cavalcanti, D., and Acin, A. (2015). In: *New J. Phys.* 17, p. 022003.
Miller, A. J., Lita, A. E., Calkins, B., Vayshenker, I., Gruber, S. M., and Nam, S. W. (2011). In: *Opt. Express* 19, 91029110.
Morin, O., Bancal, J.-D., Ho, M., Sekatski, P., D'Auria, V., Gisin, N., Laurat, J., and Sangouard, N. (2013). In: *Phys. Rev. Lett.* 110, p. 130401.
Nielsen, M. A. and Chuang, I. L. (2000). *Quantum Computation and Quantum Information*. Cambridge Univ. Press, Cambridge, UK,
Penrose, R. (1996). In: *Gen. Relativ. Gravit.* 28, p. 581.
Pfister, C., Kaniewski, J., Tomamichel, M., Mantri, A., Schmucker, R., McMahon, N., Milburn, G., and Wehner, S. (2015). In: *arXiv:1503.00577*.
Pironio, S., Acín, A., Massar, S., Giroday, A. Boyer de la, Matsukevich, D. N., Maunz, P., Olmschenk, S., Hayes, D., Luo, L., Manning, T. A., and Monroe, C. (2010). In: *Nature* 464, p. 1021.
Sangouard, N., Sanguinetti, B., Curtz, N., Gisin, N., Thew, R., and Zbinden, H. (2011). In: *Phys. Rev. Lett.* 106, p. 120403.
Sekatski, P., Sanguinetti, B., Pomarico, E., Gisin, N., and Simon, C. (2010). In: *Phys. Rev. A* 82, p. 053814.
Verma, V. B., Korzh, B., Bussières, F., Horansky, R. D., Lita, A. E., Marsili, F., Shaw, M. D., Zbinden, H., Mirin, R. P., and Nam, S. W. (2014). In: *Appl. Phys. Lett.* 105, p. 122601.

Appendix

List of publications

[1] V. Caprara Vivoli, Nicolas Sangouard, Mikael Afzelius, Nicolas Gisin, *High-bandwidth quantum memory protocol for storing single photons in rare-earth doped crystals*, New J. Phys. **15**, 095012 (2013). ..... page 51

[2] V. Caprara Vivoli, P. Sekatski, J.-D. Bancal, C.C.W. Lim, B.G. Christensen, A. Martin, R.T. Thew, H. Zbinden, N. Gisin, N. Sangouard, *Challenging preconceptions about Bell tests with photon pairs*, Phys. Rev. A **91**, 012107 (2015). ..... page 57

[3] V. Caprara Vivoli, P. Sekatski, J.-D. Bancal, C.C.W. Lim, A. Martin, R.T. Thew, H. Zbinden, N. Gisin, N. Sangouard, *Comparing different approaches for generating random numbers device-independently using a photon pair source*, New J. Phys. **17**, 023023 (2015). ..... page 63

[4] F. Monteiro, V. Caprara Vivoli, T. Guerreiro, A. Martin, J.-D. Bancal, H. Zbinden, R.T. Thew, N. Sangouard, *Revealing Genuine Optical-Path Entanglement*, Phys. Rev. Lett. **114**, 170504 (2015). ..... page 73

[5] V. Caprara Vivoli, T. Barnea, C. Galland, N. Sangouard, *Proposal for an Optomechanical Bell test*, Phys.Rev.Lett. **116**, 070405 (2016). ..... page 79

[6] V. Caprara Vivoli, P. Sekatski, N. Sangouard, *What does it take to see entanglement?*, arxiv, 1602.01907. (2016). ..... page 85

Publications

1 High-bandwidth quantum memory protocol for storing single photons in rare-earth doped crystals

Challenging preconceptions about Bell tests with photon pairs

V. Caprara Vivoli,[1] P. Sekatski,[2] J.-D. Bancal,[3] C. C. W. Lim,[1] B. G. Christensen,[4] A. Martin,[1] R. T. Thew,[1] H. Zbinden,[1] N. Gisin,[1] and N. Sangouard[1,5]

[1]*Group of Applied Physics, University of Geneva, CH-1211 Geneva 4, Switzerland*
[2]*Institut for Theoretische Physik, Universitat of Innsbruck, Technikerstrasse 25, A-6020 Innsbruck, Austria*
[3]*Centre for Quantum Technologies, National University of Singapore, 3 Science Drive 2, Singapore 117543*
[4]*Department of Physics, University of Illinois at Urbana-Champaign, Urbana, Illinois 61801, USA*
[5]*Department of Physics, University of Basel, CH-4056 Basel, Switzerland*

(Received 8 May 2014; published 14 January 2015)

Motivated by very recent experiments, we consider a scenario "à la Bell" in which two protagonists test the Clauser-Horne-Shimony-Holt (CHSH) inequality using a photon-pair source based on spontaneous parametric down conversion and imperfect photon detectors. The conventional wisdom says that (i) if the detectors have unit efficiency, the CHSH violation can reach its maximum quantum value of $2\sqrt{2}$. To obtain the maximal possible violation, it suffices that the source emits (ii) maximally entangled photon pairs (iii) in two well-defined single modes. Through a nonperturabive calculation of nonlocal correlations, we show that none of these statements are true. By providing the optimal pump parameters, measurement settings and state structure for any detection efficiency and dark count probability, our results give the recipe to close all the loopholes in a Bell test using photon pairs.

DOI: 10.1103/PhysRevA.91.012107 PACS number(s): 03.65.Ud, 42.50.Xa

I. INTRODUCTION

Many physicists are setting up challenging experiments to prove that nonlocality is an element of the physical reality. The game is nonetheless simple. Two players, Alice and Bob, share a pair of entangled particles. Each chooses a measurement, x for Alice and y for Bob, among a set of two projectors represented by $\{x = 0, x = 1\}$ and similarly for y. They get a binary result ± 1, labeled a and b for Alice and Bob, respectively. The game is repeated for as long as it is necessary to accurately estimate the probability distribution $p(ab|xy)$. Alice and Bob then compute the Clauser-Horne-Shimony-Holt (CHSH) [1] value:

$$S = \sum_{x,y=0}^{1} (-1)^{xy} (p(a = b|xy) - p(a \neq b|xy)). \quad (1)$$

If the CHSH inequality is violated, i.e., if $S > 2$, Alice's and Bob's correlations are nonlocal; namely, their correlations cannot be reproduced by a strategy involving local hidden variables only. (Note that the CHSH inequality is the only relevant inequality in a scenario with two parties, two measurement settings, and two results. In particular, the Clauser-Horne (CH) inequality [2] is equivalent under the no-signaling assumption [3].) All the experiments realized so far point out that nature is indeed nonlocal, but they all had loopholes [3].

The realization of a proper Bell test, i.e., without loopholes, would not only demonstrate that nature is nonlocal, it would also open the way towards new applications. A detection-loophole-free Bell test, for example, would allow one to realize device-independent randomness expansion where the size of an initial random bit string is made longer, the resulting randomness being guaranteed without the need to make assumptions about the internal working of the device used to extend the bit string (see Refs. [4,5] for the first proof-of-principle experiments). In the same spirit, it would allow one to make device-independent quantum key distribution (see Ref. [6] for the principle and for example Refs. [7–9] for experimental proposals). Independently of the purpose, the value of S needs to be as close as possible to its maximum quantum value of $2\sqrt{2}$. This makes the corresponding Bell test less demanding in terms of accumulated statistics to prove nonlocality conclusively and more efficient regarding the randomness or the number of secret bits created per experimental run [3].

Although impressive results have been obtained with single atoms [10–12], photons are natural candidates for the applications of Bell tests. Actually, they have already been used to close both the locality loophole [13–15] and the detection loophole [5,16] even though these were in separate experiments. The basic setup exploits a photon-pair source based on spontaneous parametric down conversion and photon detectors, as depicted in Fig. 1. The question that we address in this article is the following: What is the strategy that maximizes the CHSH violation in this specific scenario? We emphasize that we are interested in the raw violation, i.e., the violation obtained without any postselection as we want to quantify properly the nonlocality out of this setup. Instead of using a perturbative approach, assuming, e.g., that the source emits vacuum and from time to time one photon pair with a small probability, we present an exact calculation of correlations. This allows us to answer precisely and definitely the question above. We show, for example, that the maximal value of S is far from $2\sqrt{2}$ even if the detectors have a unit efficiency. This maximum is obtained through a multimode emission (Poissonian statistics) from nonmaximally entangled states. Beyond the fact that these results go against collective intuition, they might significantly facilitate the realization of loophole-free Bell tests and their subsequent applications using photon pairs as they provide the method to follow to maximize the CHSH violation with nonphoton number resolving detectors for any detection efficiency and dark count probability.

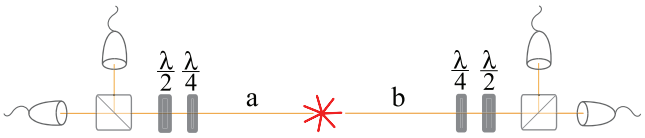

FIG. 1. (Color online) A source (star) based on spontaneous parametric down conversion is excited, e.g., by a pulsed pump and produced photon pairs entangled, e.g., in polarization. The photons are emitted in correlated spatial modes a (b). Each of them includes several temporal, frequency, and spatial modes $a_k - b_k$, the number of temporal modes in the pulsed regime being given by the ratio between the pump duration and the photon coherence time for example. The photons emitted in a (b) are sent to Alice's (Bob's) location where they are projected along an arbitrary direction of the Bloch sphere using a set of wave plates, a polarization beam splitter, and two detectors. Each pump pulse triggers the choice of a measurement setting. The detectors are assumed to be nonphoton number resolving with nonunit efficiency and dark counts.

II. MODELING THE PAIR SOURCE

We first focus on the state produced by a photon-pair source based on spontaneous parametric down conversion. Such a source produces photons in coupled modes, labeled by the bosonic operators a_k and b_k; the former is given to Alice, the latter to Bob. The subscript k (which runs from 1 to N), means that Alice and Bob each receives several temporal, frequency, and spatial modes. Furthermore, the photons are created in entangled states, e.g., in polarization, meaning that each mode splits into two orthogonal polarizations $a_k - a_{k,\perp}$ and $b_k - b_{k,\perp}$. The Hamiltonian of the corresponding down-conversion process is $\mathcal{H} = i\sum_{k=1}^{N}(\chi a_k^\dagger b_{k,\perp}^\dagger - \bar{\chi} a_{k,\perp}^\dagger b_k^\dagger + \text{H.c.})$, where χ and $\bar{\chi}$ are proportional to the nonlinear susceptibility of the crystal and to the power of the pump [17]. Their ratio determines whether maximally or nonmaximally entangled states are produced. The exact expression of the state produced by such a source $|\psi\rangle$ is obtained by applying the corresponding propagator $e^{-i\mathcal{H}t}$ on the vacuum $|\underline{0}\rangle$, as we are focusing on spontaneous emissions (0 is underlined to indicate that all modes are in the vacuum). As each mode k is independent, i.e., two bosonic operators with different subscripts k commute, $e^{-i\mathcal{H}t} = \Pi_{k=1}^{N} e^{g a_k^\dagger b_{k,\perp}^\dagger - \bar{g} a_{k,\perp}^\dagger b_k^\dagger + \text{H.c.}}$, where $g = \chi t$ and $\bar{g} = \bar{\chi} t$ are the squeezing parameters for the coupled modes $a_k b_{k,\perp}$ and $a_{k,\perp} b_k$, respectively. Similarly, since $a_k b_{k,\perp}$ commutes with $a_{k,\perp} b_k$, $e^{-i\mathcal{H}t} = \Pi_{k=1}^{N} U_k \bar{U}_k$, where $U_k = e^{g a_k^\dagger b_{k,\perp}^\dagger + \text{H.c.}}$, $\bar{U}_k = e^{-\bar{g} a_{k,\perp}^\dagger b_k^\dagger + \text{H.c.}}$ are squeezing operators. Finally, as the set $\{a_k^\dagger b_{k,\perp}^\dagger, a_k b_{k,\perp}, a_k^\dagger a_k, b_{k,\perp}^\dagger b_{k,\perp}\}$ is closed with respect to the commutator, $U_k = e^{T_g a_k^\dagger b_{k,\perp}^\dagger} C_g^{-(1+a_k^\dagger a_{k,\perp} + b_k^\dagger b_{k,\perp})} e^{-T_g a_k b_{k,\perp}}$ [18]. T_g (C_g) stands for $\tanh(g)$ [$\cosh(g)$]. Using a similar formula for $\bar{U}_k$, it is easy to show that

$$|\psi\rangle = \left(1 - T_g^2\right)^{\frac{N}{2}} \left(1 - T_{\bar{g}}^2\right)^{\frac{N}{2}} \Pi_{k=1}^{N} e^{T_g a_k^\dagger b_{k,\perp}^\dagger - T_{\bar{g}} a_{k,\perp}^\dagger b_k^\dagger} |\underline{0}\rangle.$$

Note that the number of modes N is a tunable parameter. For $N = 1$, the photon statistic in each mode a_k, $a_{k,\perp}$, b_k, and $b_{k,\perp}$ corresponds to a thermal distribution, whereas in the limit $N \to +\infty$, it follows a Poissonian distribution. Moreover, the pair production in the modes $a_k^\dagger b_{k,\perp}^\dagger$ and $a_{k,\perp}^\dagger b_k^\dagger$ can be seen as two separate parametric processes that one pumps coherently, e.g., by the same laser. The squeezing parameters g and $\bar{g}$, and thus the amount of entanglement, can be tuned by controlling the pump power of each parametric process.

III. MODELING THE PHOTON DETECTORS

Let us now focus on the detectors. We consider photon detectors which do not resolve the photon number, do not distinguish the different modes k, and have nonunit efficiency η. Formally, the event no-click corresponds to a positive operator $D_{\text{nc}}^a = \Pi_{k=1}^{N} C_L^{k\dagger} T_{\text{nc}}^k C_L^k$, where $T_{\text{nc}}^k = |0\rangle_k\langle 0|$ is the projection operator on the vacuum for the mode k and corresponds to an ideal nonphoton-number-resolving detector and $C_L^k = e^{\gamma(a_k^\dagger \ell_k - a_k \ell_k^\dagger)}|0_{\ell_k}\rangle$ is the loss channel with $\eta = \cos^2\gamma$. ℓ_k is the initially empty mode whose coupling to a_k is responsible for the loss. As $C_L^{k\dagger} f(a_k) C_L^k = \langle 0_{\ell_k}| f(\sqrt{\eta} a_k + \sqrt{1-\eta}\ell_k)|0_{\ell_k}\rangle$, and $|0\rangle_k\langle 0| =: e^{-a_k^\dagger a_k} :$, where $: :$ is the normal order, we have $C_L^{k\dagger} T_{\text{nc}}^k C_L^k = : e^{-\eta a_k^\dagger a_k} :$. Furthermore, since $: e^{(e^k-1)a_k^\dagger a_k} := e^{k a_k^\dagger a_k}$ [19], D_{nc}^a can be written in a simple form as $D_{\text{nc}}^a = \Pi_{k=1}^{N}(1-\eta)^{a_k^\dagger a_k}$. Note here that the detector dark counts (with the dark count probability p_{dc}) can be added by hand, as the probability for having no click requires all the k modes to be empty and the absence of dark count, i.e.,

$$D_{\text{nc}}^a = (1 - p_{\text{dc}})\Pi_{k=1}^{N}(1-\eta)^{a_k^\dagger a_k}. \tag{2}$$

Analogously, the operator for a click D_{c}^a is given by $\mathbf{1} - D_{\text{nc}}^a$ so that the detector is fully characterized by the positive-operator-valued measure $\{D_{\text{c}}^a, D_{\text{nc}}^a\}$.

IV. DERIVATION OF THE PROBABILITY DISTRIBUTION

Now we use the above models of the source and detectors to calculate the probability distribution $p(ab|xy)$ needed in the CHSH inequality. If the readers do not want to see the details on how they are derived, we invite them to go directly to the next section where the results are described. At each experimental run, Alice and Bob choose a measurement setting; i.e., they rotate the polarization of their modes,

$$\begin{aligned} a_k &= \cos\alpha A_k + e^{i\phi_\alpha}\sin\alpha A_{k,\perp}, \\ a_{k,\perp} &= e^{-i\phi_\alpha}\sin\alpha A_k - \cos\alpha A_{k,\perp}, \end{aligned} \tag{3}$$

(similarly for Bob with angles $\beta - \phi_\beta$ and the modes $B_k - B_{k,\perp}$) before they detect the modes A_k, $A_{k,\perp}$, B_k, and $B_{k,\perp}$ (see Fig. 1). They then look at their outcomes; i.e., they record which of their two detectors click. Locally, they can observe four different outcomes: no click, one click in one of the two detectors, or two clicks. We emphasize that none of these events can be ignored to properly quantify the CHSH violation in this setup. Before we discuss the way to postprocess the results, let us calculate for example the probability $p(\text{nc}_A)$ that Alice gets no click in A. It is obtained from $\text{tr}(D_{\text{nc}}^A|\psi_{\alpha,\beta}\rangle\langle\psi_{\alpha,\beta}|)$, where tr stands for the trace over A_k, $A_{k,\perp}$, B_k, and $B_{k,\perp}$, and $|\psi_{\alpha,\beta}\rangle$ is obtained by introducing the expressions of $A_k - A_{k,\perp}$ and $B_k - B_{k,\perp}$ given in Eq. (3) in $|\psi\rangle$. Note that $p(\text{nc}_A) = (1 - p_{\text{dc}})(\text{tr} R^{A_k^\dagger A_k}|\psi_{\alpha,\beta}^k\rangle\langle\psi_{\alpha,\beta}^k|)^N$, with $|\psi_{\alpha,\beta}\rangle = \Pi_{k=1}^{N}|\psi_{\alpha,\beta}^k\rangle$, $R = (1-\eta)$, and since the trace is cyclic $p(\text{nc}_A) = (1 - p_{\text{dc}})(\text{tr} R^{\frac{A_k^\dagger A_k}{2}}|\psi_{\alpha,\beta}^k\rangle\langle\psi_{\alpha,\beta}^k| R^{\frac{A_k^\dagger A_k}{2}})^N$.

Furthermore, from $x^{a^\dagger a} f(a^\dagger) = f(xa^\dagger)x^{a^\dagger a}$ [18], we have $R^{\frac{A_k^\dagger A_k}{2}}|\psi_{\alpha,\beta}^k\rangle = (1-T_g^2)^{\frac{1}{2}}(1-T_{\bar{g}}^2)^{\frac{1}{2}} e^{(A_k^\dagger, A_{k,\perp}^\dagger) M \binom{B_k^\dagger}{B_{k,\perp}^\dagger}}|\underline{0}\rangle$, with $M = \begin{pmatrix} R^{\frac{1}{2}}(T_g C_\alpha S_\beta^\star - T_{\bar{g}} S_\alpha^\star C_\beta) & R^{\frac{1}{2}}(-T_g C_\alpha C_\beta - T_{\bar{g}} S_\alpha^\star S_\beta) \\ T_g S_\alpha S_\beta^\star + T_{\bar{g}} C_\alpha C_\beta & -T_g S_\alpha C_\beta + T_{\bar{g}} C_\alpha S_\beta \end{pmatrix}$, C_α and S_α (C_β and S_β) meaning $\cos\alpha$ and $e^{i\phi_\alpha}\sin\alpha$ ($\cos\beta$ and $e^{i\phi_\beta}\sin\beta$), respectively. From the singular value decomposition of $M = U\begin{pmatrix}\lambda_1 & 0 \\ 0 & \lambda_2\end{pmatrix}V^\star$, $R^{\frac{A_k^\dagger A_k}{2}}|\psi_k(\alpha,\beta)\rangle$ reduces to $(1-T_g^2)^{\frac{1}{2}}(1-T_{\bar{g}}^2)^{\frac{1}{2}} e^{\lambda_1 U A_k^\dagger V B_k^\dagger + \lambda_2 U A_{k,\perp}^\dagger V B_{k,\perp}^\dagger}|\underline{0}\rangle$, and we end up with the simple formula

$$p(\mathrm{nc}_A) = (1-p_{\mathrm{dc}})\left(\frac{(1-T_g^2)(1-T_{\bar{g}}^2)}{(1-\lambda_1^2)(1-\lambda_2^2)}\right)^N = (1-p_{\mathrm{dc}})\left(\frac{2}{2-\eta+\eta\left(C_{2g}C_\alpha^2 + C_{2\bar{g}}|S_\alpha|^2\right)}\right)^N. \quad (4)$$

Following the same line of thought, we can derive all the no-detection probabilities $p(\mathrm{nc}_A \,\&\, \mathrm{nc}_{A_\perp})$, etc.

To compute the CHSH value, Alice and Bob need to bin their results; i.e., they have to choose a local strategy to assign the values ±1 to their four possible events. Among the 256 possible strategies to deal with the nonconclusive events, a simple strategy consists in assigning the value -1 to one of the results corresponding to one click locally [the detector A (B) clicks whereas $A_\perp$ ($B_\perp$) does not] and $+1$ to the other events. Hence, $p(-1-1|xy) = \mathrm{tr}[(\mathbf{1}-D_{\mathrm{nc}}^A)D_{\mathrm{nc}}^{A_\perp}(\mathbf{1}-D_{\mathrm{nc}}^B)D_{\mathrm{nc}}^{B_\perp}|\psi_{\alpha,\beta}\rangle\langle\psi_{\alpha,\beta}|]$ and can be related to the no-detection probabilities derived previously through $p(\mathrm{nc}_{A_\perp} \,\&\, \mathrm{nc}_{B_\perp}) - p(\mathrm{nc}_A \,\&\, \mathrm{nc}_{A_\perp} \,\&\, \mathrm{nc}_{B_\perp}) - p(\mathrm{nc}_{A_\perp} \,\&\, \mathrm{nc}_B \,\&\, \mathrm{nc}_{B_\perp}) + p(\mathrm{nc}_A \,\&\, \mathrm{nc}_{A_\perp} \,\&\, \mathrm{nc}_B \,\&\, \mathrm{nc}_{B_\perp})$. (See the Appendix for the complete expressions.) Processing $p(+1-1|xy)$, $p(-1+1|xy)$, and $p(+1+1|xy)$ in a similar way makes it possible to optimize the CHSH value over the squeezing parameters ($g-\bar{g}$), the number of modes N, and the measurement settings for any detection efficiency and dark count probability.

V. RESULTS

The results are shown in Fig. 2. They have been obtained under the assumption that there is no dark count. Furthermore, we have checked that the strategy described before for binning the four possible results locally is optimal. Therefore, the solid curve of Fig. 2 gives the maximal violation of the CHSH inequality that can be obtained in the scheme represented in Fig. 1. Several results deserve to be elaborated.

(i) The maximum CHSH value obtained with unit efficiency detectors is $\sim$2.35. This is very far from the maximal quantum value of $2\sqrt{2}$ that can be obtained with any two-qubit states that are maximally entangled. The reason is that the photon-pair source under consideration inevitably produces vacuum and multiple pairs. The vacuum leads to no detections and the corresponding CHSH value is 2. Similarly, when many pairs are produced, the four detectors click. This also results in a CHSH value of 2. One might think that the vacuum and the multiphoton events can be safely discarded as the postselected data would violate the CHSH inequality only if the raw data lead to a CHSH value larger than 2. However,

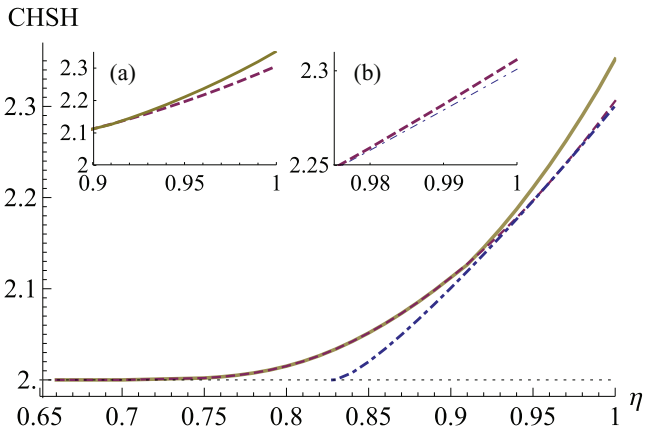

FIG. 2. (Color online) CHSH values as a function of the detection efficiency η. The solid curve is optimized over the structure of the states produced by a spontaneous parametric down-conversion source (the squeezing parameters and the number of modes), the measurement settings, and the local strategy with which the outcomes are assigned to results ±1. The dark count probability is set to zero. The optimal violation (solid curve) is compared to the CHSH value obtained by restricting the emission to a single mode, i.e., thermal photon number statistics (dashed line). A zoom on the region of high efficiencies is given in the inset (a). The CHSH value is also compared to the one obtained by focusing on the single mode case with maximally entangled states ($g=\bar{g}$, see dash-dotted line). A zoom on the region of high efficiencies is given in the inset (b) where the monomode case is compared to the monomode case restricted to maximally entangled states. Note that the CH value can be deduced from the here shown CHSH value through $\frac{S-2}{4}$.

the nonlocal correlations characterizing the experiment are obviously the ones obtained without postselection. This is well illustrated when one considers applications of the Bell test, e.g., for randomness expansion as there is no way to get more randomness from a subset of the raw data. Clearly, removing "unfavorable" events is not an option to properly quantify the Bell violation of a given setup. None of these events prevent the violation of the CHSH inequality but they reduce the observed violation.

(ii) The maximal violation is obtained when the number of modes tends to infinity (Poissonian statistics). For comparison, we can restrict the emission to be monomode ($N=1$) and still optimize the CHSH value over the squeezing parameters and the measurement settings. The corresponding results are given by the dashed line in the inset (a) of Fig. 2. The maximal CHSH value is unchanged for efficiencies smaller than $\sim$91%, but for higher efficiencies, the many-mode configuration favors larger violations. The intuition in the ideal case $\eta=1$ is that the relative probability for having a single pair is greater for the Poissonian distribution compared to the thermal distribution for a mean photon number around 1. However, for inefficient detectors, it becomes more difficult to have an intuition as, in addition to the photon statistics, we have to take into account the detrimental effect of multiphoton events underlying losses.

(iii) In the case $\eta=1$, the maximum violation is reached for the ratio $g/\bar{g}\sim0.92$, i.e., for nonmaximally entangled states [20]. For comparison, the dotted thin curve of the inset (b) in Fig. 2 gives the optimal value when forcing the squeezing

parameters to be the same (still in the monomode case). This shows that, even in the monomode case, it is never optimal to use maximally entangled states, even when dealing with unit efficiency detectors. The intuition is that the two nonconclusive events (no click and two clicks locally) both have an effect analogous to loss and we know from Eberhard [21] that nonmaximally entangled states have a greater resistance to loss.

(iv) The minimum efficiency required to observe nonlocal correlations is 2/3. This is surprising at least at first sight, as this corresponds exactly to the minimum efficiency that is required to violate the CHSH inequality when dealing with two-qubit states. The intuition is that neither the vacuum nor the multiphoton events prevent the violation as each leads to $S = 2$. Hence, the CHSH inequality is violated as long as the two-qubit component (one photon pair exactly) leads to $S > 2$. To further decrease the required efficiency, we could investigate other Bell inequalities with more outputs and/or inputs. This provides work for the future.

VI. CONCLUSION AND PERSPECTIVES

We have presented an exact derivation of correlations in a scenario with two parties testing the CHSH inequality with a source based on spontaneous parametric down conversion. In particular, we have shown that the maximal CHSH value is $\sim$2.35. This limits substantially the efficiency of the scenario drawn in Fig. 1 for device-independent quantum key distribution [6] or device-independent quantum random number generation [4]. Note that a higher violation can be obtained through amplification [7] or nonlinear filtering [8] at the price of increasing complexity.

As our results give the strategy that optimizes the observed violation, we expect that they will have a significant impact on ongoing experiments. Focusing on the experiment reported in Ref. [5] for example, in which photon pairs distributed over $N = 25$ modes and detectors with an (overall) efficiency of 75% have been used for a Bell test while closing the detection loophole, we find the maximum S value of 2.0018 optimizing the state structure $(g, \bar{g})$ and measurement settings while the observed value was 2.0002. (The measurement settings used in Ref. [5] were obtained numerically assuming qubits, i.e., the state of the form $(r a_1^\dagger b_{1,\perp}^\dagger + a_{1,\perp}^\dagger b_1^\dagger)|\underline{0}\rangle$ with appropriate normalization and where the value of r was measured.) This translates into a speeding up of randomness expansion by 1 order of magnitude. Even if the dark count probability ($p_{\mathrm{dc}} = 8 \times 10^{-6}$) and the fluorescence background (between 0.15% and 0.25% of the mean singles) are taken into account, we envision a speeding up by a factor of $\sim$3 in the most conservative case (background noise 0.25% of the mean singles). Note that in practice, one is tempted to use a single detector locally, as in Ref. [5]. In this case, the strategy with which the nonconclusive results are treated is different from the one presented here but we have found that it is also one that is optimal.

ACKNOWLEDGMENTS

We warmly thank V. Scarani for helpful discussions and comments. This work was supported by the Swiss NCCR QSIT, the Swiss National Science Foundation SNSF (Grant No. PP00P2_150579 and "Early PostDoc.Mobility"), the European Commission (IP SIQS, Chist-era DIQIP), the Singapore Ministry of Education (partly through the Academic Research Fund Tier 3, Grant No. MOE2012-T3-1-009), and the National Research Foundation of Singapore.

APPENDIX

We here present a list of all the no-detection probabilities. They provide all the information that is necessary to compute the optimal CHSH value. As far as the notation is concerned, we have maintained the one presented in the main text for T_g, C_g ($T_{\bar{g}}$ and $C_{\bar{g}}$), and C_α (C_β), while S_α (S_β) now means $\sin\alpha$ ($\sin\beta$). Furthermore, $C_{\phi_A-\phi_B}$ means $\cos(\phi_A - \phi_B)$.

The probability to detect no photon in mode A is given by

$$p(\mathrm{nc}_A) = (1 - p_{\mathrm{dc}})\left(\frac{2}{2 - \eta + \eta\left(C_\alpha^2 C_{2g} + C_{2\bar{g}} S_\alpha^2\right)}\right)^N. \tag{A1}$$

The expressions for $p(\mathrm{nc}_{A_\perp})$, $p(\mathrm{nc}_{B_\perp})$, and $p(\mathrm{nc}_B)$ can be obtained from Eq. (A1) by inverting g and $\bar{g}$, replacing α with β, and inverting g and $\bar{g}$ and replacing α with β, respectively. The probability for no detection in modes A and $A_\perp$ (B and $B_\perp$) is given by the following expression:

$$p(\mathrm{nc}_A \,\&\, \mathrm{nc}_{A_\perp}) = p(\mathrm{nc}_B \,\&\, \mathrm{nc}_{B_\perp}) = (1 - p_{\mathrm{dc}})^2 \times \left(\frac{4}{(2 - \eta + \eta C_{2g})(2 - \eta + \eta C_{2\bar{g}})}\right)^N. \tag{A2}$$

The probability for no detection in modes A and B is given by

$$\begin{aligned} p(\mathrm{nc}_A \,\&\, \mathrm{nc}_B) = (1 - p_{\mathrm{dc}})^2 4^N \left(C_g^2 C_{\bar{g}}^2\right)^{-N} \\ \times (4 + 2\eta^2 T_g T_{\bar{g}} C_{\phi_A-\phi_B} S_{2\alpha} S_{2\beta} \\ - T_{\bar{g}}^2 (2 - \eta + \eta C_{2\alpha})(2 - \eta - \eta C_{2\beta}) \\ + T_g^2 \big[(2 - \eta - \eta C_{2\alpha})(\eta - 2 - \eta C_{2\beta}) \\ + 4(1 - \eta)^2 T_{\bar{g}}^2\big]^{-N}. \end{aligned} \tag{A3}$$

Similarly, $p(\mathrm{nc}_{A_\perp} \,\&\, \mathrm{nc}_B)$, $p(\mathrm{nc}_A \,\&\, \mathrm{nc}_{B_\perp})$, and $p(\mathrm{nc}_{A_\perp} \,\&\, \mathrm{nc}_{B_\perp})$ can be derived from Eq. (A3) by substituting α with $\alpha + \frac{\pi}{2}$, β with $\beta + \frac{\pi}{2}$, and α with $\alpha + \frac{\pi}{2}$ and β with $\beta + \frac{\pi}{2}$, respectively. The probability $p(\mathrm{nc}_A \,\&\, \mathrm{nc}_{A_\perp} \,\&\, \mathrm{nc}_B)$ of no detection in modes A, $A_\perp$, and B is given by

$$p(\mathrm{nc}_A \,\&\, \mathrm{nc}_{A_\perp} \,\&\, \mathrm{nc}_B) = \frac{(1 - p_{\mathrm{dc}})^3}{\left(C_g^2 C_{\bar{g}}^2 \left\{1 - \frac{1}{2}(1 - \eta) T_{\bar{g}}^2 (2 - \eta - \eta C_{2\beta}) - (1 - \eta) T_g^2 \left[1 - \eta S_\beta^2 - (1 - \eta)^2 T_{\bar{g}}^2\right]\right\}\right)^N}. \tag{A4}$$

Similarly the expressions for $p(\mathrm{nc}_A \,\&\, \mathrm{nc}_{A_\perp} \,\&\, \mathrm{nc}_{B_\perp})$, $p(\mathrm{nc}_{A_\perp} \,\&\, \mathrm{nc}_B \,\&\, \mathrm{nc}_{B_\perp})$, and $p(\mathrm{nc}_A \,\&\, \mathrm{nc}_B \,\&\, \mathrm{nc}_{B_\perp})$ can be obtained from Eq. (A4) by inverting g and $\bar{g}$, inverting α and β, and inverting g and $\bar{g}$ and α and β, respectively. Finally,

$$p(\mathrm{nc}_A \,\&\, \mathrm{nc}_{A_\perp} \,\&\, \mathrm{nc}_B \,\&\, \mathrm{nc}_{B_\perp}) = (1 - p_{\mathrm{dc}})^4 \left(\frac{4}{\{1 + (1-\eta)^2 + [1-(1-\eta)^2]C_{2g}\}\{1 + (1-\eta)^2 + [1-(1-\eta)^2]C_{2\bar{g}}\}} \right)^N . \quad \text{(A5)}$$

[1] J. F. Clauser, M. Horne, A. Shimony, and R. A. Holt, Phys. Rev. Lett. **23**, 880 (1969).
[2] J. Clauser and M. Horne, Phys. Rev. D **10**, 526 (1974).
[3] N. Brunner, D. Cavalcanti, S. Pironio, V. Scarani, and S. Wehner, Rev. Mod. Phys. **86**, 419 (2014).
[4] S. Pironio *et al.*, Nature (London) **464**, 1021 (2010).
[5] B. G. Christensen *et al.*, Phys. Rev. Lett. **111**, 130406 (2013).
[6] A. Acin, N. Brunner, N. Gisin, S. Massar, S. Pironio, and V. Scarani, Phys. Rev. Lett. **98**, 230501 (2007).
[7] N. Gisin, S. Pironio, and N. Sangouard, Phys. Rev. Lett. **105**, 070501 (2010).
[8] N. Sangouard, B. Sanguinetti, N. Curtz, N. Gisin, R. Thew, and H. Zbinden, Phys. Rev. Lett. **106**, 120403 (2011).
[9] C. C. W. Lim, C. Portmann, M. Tomamichel, R. Renner, and N. Gisin, Phys. Rev. X **3**, 031006 (2013).
[10] M. A. Rowe *et al.*, Nature (London) **409**, 791 (2001).
[11] D. N. Matsukevich *et al.*, Phys. Rev. Lett. **100**, 150404 (2008).
[12] J. Hofmann *et al.*, Science **337**, 72 (2012).
[13] A. Aspect, J. Dalibard, and G. Roger, Phys. Rev. Lett. **49**, 1804 (1982).
[14] W. Tittel, J. Brendel, H. Zbinden, and N. Gisin, Phys. Rev. Lett. **81**, 3563 (1998).
[15] G. Weihs, T. Jennewein, C. Simon, H. Weinfurter, and A. Zeilinger, Phys. Rev. Lett. **81**, 5039 (1998).
[16] M. Giustina *et al.*, Nature (London) **497**, 227 (2013).
[17] We assumed that χ and $\bar{\chi}$ are independent of k; i.e., the distribution of spatial/frequency modes is flat.
[18] P. Sekatski, B. Sanguinetti, E. Pomarico, N. Gisin, and C. Simon, Phys. Rev. A **82**, 053814 (2010).
[19] M. J. Collett, Phys. Rev. A **38**, 2233 (1988).
[20] Note that we found the following optimal parameters for unit efficiencies: $g \sim 0.106$, $\bar{g} \sim 0.115$, $\alpha_1 \sim -0.163$, $\alpha_2 \sim 0.491$, $\phi_{\alpha 1} \sim -0.635$, $\phi_{\alpha 2} \sim -0.635$, $\beta_1 \sim 1.733$, $\beta_2 \sim 1.079$, $\phi_{\beta 1} \sim -0.635$, and $\phi_{\beta 2} \sim -0.635$. Furthermore, if one adds dark counts, say, with $p_{\mathrm{dc}} = 10^{-6}$, this reduces the violation obtained with unit efficiencies by $\sim 10^{-6}$.
[21] P. H. Eberhard, Phys. Rev. A **47**, R747 (1993).

2 Challenging preconceptions about Bell tests with photon pairs

Challenging preconceptions about Bell tests with photon pairs

V. Caprara Vivoli,[1] P. Sekatski,[2] J.-D. Bancal,[3] C. C. W. Lim,[1] B. G. Christensen,[4] A. Martin,[1] R. T. Thew,[1] H. Zbinden,[1] N. Gisin,[1] and N. Sangouard[1,5]

[1]*Group of Applied Physics, University of Geneva, CH-1211 Geneva 4, Switzerland*
[2]*Institut for Theoretische Physik, Universitat of Innsbruck, Technikerstrasse 25, A-6020 Innsbruck, Austria*
[3]*Centre for Quantum Technologies, National University of Singapore, 3 Science Drive 2, Singapore 117543*
[4]*Department of Physics, University of Illinois at Urbana-Champaign, Urbana, Illinois 61801, USA*
[5]*Department of Physics, University of Basel, CH-4056 Basel, Switzerland*

(Received 8 May 2014; published 14 January 2015)

Motivated by very recent experiments, we consider a scenario "à la Bell" in which two protagonists test the Clauser-Horne-Shimony-Holt (CHSH) inequality using a photon-pair source based on spontaneous parametric down conversion and imperfect photon detectors. The conventional wisdom says that (i) if the detectors have unit efficiency, the CHSH violation can reach its maximum quantum value of $2\sqrt{2}$. To obtain the maximal possible violation, it suffices that the source emits (ii) maximally entangled photon pairs (iii) in two well-defined single modes. Through a nonperturabive calculation of nonlocal correlations, we show that none of these statements are true. By providing the optimal pump parameters, measurement settings and state structure for any detection efficiency and dark count probability, our results give the recipe to close all the loopholes in a Bell test using photon pairs.

DOI: 10.1103/PhysRevA.91.012107 PACS number(s): 03.65.Ud, 42.50.Xa

I. INTRODUCTION

Many physicists are setting up challenging experiments to prove that nonlocality is an element of the physical reality. The game is nonetheless simple. Two players, Alice and Bob, share a pair of entangled particles. Each chooses a measurement, x for Alice and y for Bob, among a set of two projectors represented by $\{x = 0, x = 1\}$ and similarly for y. They get a binary result ± 1, labeled a and b for Alice and Bob, respectively. The game is repeated for as long as it is necessary to accurately estimate the probability distribution $p(ab|xy)$. Alice and Bob then compute the Clauser-Horne-Shimony-Holt (CHSH) [1] value:

$$S = \sum_{x,y=0}^{1} (-1)^{xy} (p(a = b|xy) - p(a \neq b|xy)). \quad (1)$$

If the CHSH inequality is violated, i.e., if $S > 2$, Alice's and Bob's correlations are nonlocal; namely, their correlations cannot be reproduced by a strategy involving local hidden variables only. (Note that the CHSH inequality is the only relevant inequality in a scenario with two parties, two measurement settings, and two results. In particular, the Clauser-Horne (CH) inequality [2] is equivalent under the no-signaling assumption [3].) All the experiments realized so far point out that nature is indeed nonlocal, but they all had loopholes [3].

The realization of a proper Bell test, i.e., without loopholes, would not only demonstrate that nature is nonlocal, it would also open the way towards new applications. A detection-loophole-free Bell test, for example, would allow one to realize device-independent randomness expansion where the size of an initial random bit string is made longer, the resulting randomness being guaranteed without the need to make assumptions about the internal working of the device used to extend the bit string (see Refs. [4,5] for the first proof-of-principle experiments). In the same spirit, it would allow one to make device-independent quantum key distribution (see Ref. [6] for the principle and for example Refs. [7–9] for experimental proposals). Independently of the purpose, the value of S needs to be as close as possible to its maximum quantum value of $2\sqrt{2}$. This makes the corresponding Bell test less demanding in terms of accumulated statistics to prove nonlocality conclusively and more efficient regarding the randomness or the number of secret bits created per experimental run [3].

Although impressive results have been obtained with single atoms [10–12], photons are natural candidates for the applications of Bell tests. Actually, they have already been used to close both the locality loophole [13–15] and the detection loophole [5,16] even though these were in separate experiments. The basic setup exploits a photon-pair source based on spontaneous parametric down conversion and photon detectors, as depicted in Fig. 1. The question that we address in this article is the following: What is the strategy that maximizes the CHSH violation in this specific scenario? We emphasize that we are interested in the raw violation, i.e., the violation obtained without any postselection as we want to quantify properly the nonlocality out of this setup. Instead of using a perturbative approach, assuming, e.g., that the source emits vacuum and from time to time one photon pair with a small probability, we present an exact calculation of correlations. This allows us to answer precisely and definitely the question above. We show, for example, that the maximal value of S is far from $2\sqrt{2}$ even if the detectors have a unit efficiency. This maximum is obtained through a multimode emission (Poissonian statistics) from nonmaximally entangled states. Beyond the fact that these results go against collective intuition, they might significantly facilitate the realization of loophole-free Bell tests and their subsequent applications using photon pairs as they provide the method to follow to maximize the CHSH violation with nonphoton number resolving detectors for any detection efficiency and dark count probability.

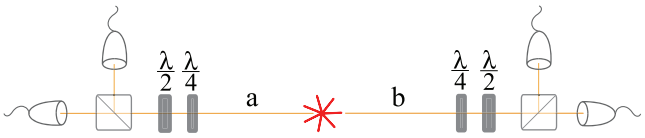

FIG. 1. (Color online) A source (star) based on spontaneous parametric down conversion is excited, e.g., by a pulsed pump and produced photon pairs entangled, e.g., in polarization. The photons are emitted in correlated spatial modes a (b). Each of them includes several temporal, frequency, and spatial modes $a_k - b_k$, the number of temporal modes in the pulsed regime being given by the ratio between the pump duration and the photon coherence time for example. The photons emitted in a (b) are sent to Alice's (Bob's) location where they are projected along an arbitrary direction of the Bloch sphere using a set of wave plates, a polarization beam splitter, and two detectors. Each pump pulse triggers the choice of a measurement setting. The detectors are assumed to be nonphoton number resolving with nonunit efficiency and dark counts.

II. MODELING THE PAIR SOURCE

We first focus on the state produced by a photon-pair source based on spontaneous parametric down conversion. Such a source produces photons in coupled modes, labeled by the bosonic operators a_k and b_k; the former is given to Alice, the latter to Bob. The subscript k (which runs from 1 to N), means that Alice and Bob each receives several temporal, frequency, and spatial modes. Furthermore, the photons are created in entangled states, e.g., in polarization, meaning that each mode splits into two orthogonal polarizations $a_k - a_{k,\perp}$ and $b_k - b_{k,\perp}$. The Hamiltonian of the corresponding down-conversion process is $\mathcal{H} = i\sum_{k=1}^{N}(\chi a_k^\dagger b_{k,\perp}^\dagger - \bar{\chi} a_{k,\perp}^\dagger b_k^\dagger + \text{H.c.})$, where χ and $\bar{\chi}$ are proportional to the nonlinear susceptibility of the crystal and to the power of the pump [17]. Their ratio determines whether maximally or nonmaximally entangled states are produced. The exact expression of the state produced by such a source $|\psi\rangle$ is obtained by applying the corresponding propagator $e^{-i\mathcal{H}t}$ on the vacuum $|\underline{0}\rangle$, as we are focusing on spontaneous emissions (0 is underlined to indicate that all modes are in the vacuum). As each mode k is independent, i.e., two bosonic operators with different subscripts k commute, $e^{-i\mathcal{H}t} = \Pi_{k=1}^{N} e^{g a_k^\dagger b_{k,\perp}^\dagger - \bar{g} a_{k,\perp}^\dagger b_k^\dagger + \text{H.c.}}$, where $g = \chi t$ and $\bar{g} = \bar{\chi} t$ are the squeezing parameters for the coupled modes $a_k b_{k,\perp}$ and $a_{k,\perp} b_k$, respectively. Similarly, since $a_k b_{k,\perp}$ commutes with $a_{k,\perp} b_k$, $e^{-i\mathcal{H}t} = \Pi_{k=1}^{N} U_k \bar{U}_k$, where $U_k = e^{g a_k^\dagger b_{k,\perp}^\dagger + \text{H.c.}}$, $\bar{U}_k = e^{-\bar{g} a_{k,\perp}^\dagger b_k^\dagger + \text{H.c.}}$ are squeezing operators. Finally, as the set $\{a_k^\dagger b_{k,\perp}^\dagger, a_k b_{k,\perp}, a_k^\dagger a_k, b_{k,\perp}^\dagger b_{k,\perp}\}$ is closed with respect to the commutator, $U_k = e^{T_g a_k^\dagger b_{k,\perp}^\dagger} C_g^{-(1+a_k^\dagger a_{k,\perp} + b_k^\dagger b_{k,\perp})} e^{-T_g a_k b_{k,\perp}}$ [18]. T_g (C_g) stands for $\tanh(g)$ [$\cosh(g)$]. Using a similar formula for $\bar{U}_k$, it is easy to show that

$$|\psi\rangle = \left(1 - T_g^2\right)^{\frac{N}{2}} \left(1 - T_{\bar{g}}^2\right)^{\frac{N}{2}} \Pi_{k=1}^{N} e^{T_g a_k^\dagger b_{k,\perp}^\dagger - T_{\bar{g}} a_{k,\perp}^\dagger b_k^\dagger} |\underline{0}\rangle.$$

Note that the number of modes N is a tunable parameter. For $N = 1$, the photon statistic in each mode a_k, $a_{k,\perp}$, b_k, and $b_{k,\perp}$ corresponds to a thermal distribution, whereas in the limit $N \to +\infty$, it follows a Poissonian distribution. Moreover, the pair production in the modes $a_k^\dagger b_{k,\perp}^\dagger$ and $a_{k,\perp}^\dagger b_k^\dagger$ can be seen as two separate parametric processes that one pumps coherently, e.g., by the same laser. The squeezing parameters g and $\bar{g}$, and thus the amount of entanglement, can be tuned by controlling the pump power of each parametric process.

III. MODELING THE PHOTON DETECTORS

Let us now focus on the detectors. We consider photon detectors which do not resolve the photon number, do not distinguish the different modes k, and have nonunit efficiency η. Formally, the event no-click corresponds to a positive operator $D_{\text{nc}}^a = \Pi_{k=1}^{N} C_L^{k\dagger} T_{\text{nc}}^k C_L^k$, where $T_{\text{nc}}^k = |0\rangle_k\langle 0|$ is the projection operator on the vacuum for the mode k and corresponds to an ideal nonphoton-number-resolving detector and $C_L^k = e^{\gamma(a_k^\dagger \ell_k - a_k \ell_k^\dagger)}|0_{\ell_k}\rangle$ is the loss channel with $\eta = \cos^2\gamma$. ℓ_k is the initially empty mode whose coupling to a_k is responsible for the loss. As $C_L^{k\dagger} f(a_k) C_L^k = \langle 0_{\ell_k}| f(\sqrt{\eta} a_k + \sqrt{1-\eta}\ell_k)|0_{\ell_k}\rangle$, and $|0\rangle_k\langle 0| =: e^{-a_k^\dagger a_k} :$, where $: :$ is the normal order, we have $C_L^{k\dagger} T_{\text{nc}}^k C_L^k = : e^{-\eta a_k^\dagger a_k} :$. Furthermore, since $: e^{(e^k-1)a_k^\dagger a_k} := e^{k a_k^\dagger a_k}$ [19], D_{nc}^a can be written in a simple form as $D_{\text{nc}}^a = \Pi_{k=1}^{N}(1-\eta)^{a_k^\dagger a_k}$. Note here that the detector dark counts (with the dark count probability p_{dc}) can be added by hand, as the probability for having no click requires all the k modes to be empty and the absence of dark count, i.e.,

$$D_{\text{nc}}^a = (1 - p_{\text{dc}})\Pi_{k=1}^{N}(1-\eta)^{a_k^\dagger a_k}. \tag{2}$$

Analogously, the operator for a click D_{c}^a is given by $\mathbf{1} - D_{\text{nc}}^a$ so that the detector is fully characterized by the positive-operator-valued measure $\{D_{\text{c}}^a, D_{\text{nc}}^a\}$.

IV. DERIVATION OF THE PROBABILITY DISTRIBUTION

Now we use the above models of the source and detectors to calculate the probability distribution $p(ab|xy)$ needed in the CHSH inequality. If the readers do not want to see the details on how they are derived, we invite them to go directly to the next section where the results are described. At each experimental run, Alice and Bob choose a measurement setting; i.e., they rotate the polarization of their modes,

$$\begin{aligned} a_k &= \cos\alpha A_k + e^{i\phi_\alpha}\sin\alpha A_{k,\perp}, \\ a_{k,\perp} &= e^{-i\phi_\alpha}\sin\alpha A_k - \cos\alpha A_{k,\perp}, \end{aligned} \tag{3}$$

(similarly for Bob with angles $\beta - \phi_\beta$ and the modes $B_k - B_{k,\perp}$) before they detect the modes A_k, $A_{k,\perp}$, B_k, and $B_{k,\perp}$ (see Fig. 1). They then look at their outcomes; i.e., they record which of their two detectors click. Locally, they can observe four different outcomes: no click, one click in one of the two detectors, or two clicks. We emphasize that none of these events can be ignored to properly quantify the CHSH violation in this setup. Before we discuss the way to postprocess the results, let us calculate for example the probability $p(\text{nc}_A)$ that Alice gets no click in A. It is obtained from $\text{tr}(D_{\text{nc}}^A|\psi_{\alpha,\beta}\rangle\langle\psi_{\alpha,\beta}|)$, where tr stands for the trace over A_k, $A_{k,\perp}$, B_k, and $B_{k,\perp}$, and $|\psi_{\alpha,\beta}\rangle$ is obtained by introducing the expressions of $A_k - A_{k,\perp}$ and $B_k - B_{k,\perp}$ given in Eq. (3) in $|\psi\rangle$. Note that $p(\text{nc}_A) = (1 - p_{\text{dc}})(\text{tr} R^{A_k^\dagger A_k}|\psi_{\alpha,\beta}^k\rangle\langle\psi_{\alpha,\beta}^k|)^N$, with $|\psi_{\alpha,\beta}\rangle = \Pi_{k=1}^{N}|\psi_{\alpha,\beta}^k\rangle$, $R = (1-\eta)$, and since the trace is cyclic $p(\text{nc}_A) = (1 - p_{\text{dc}})(\text{tr} R^{\frac{A_k^\dagger A_k}{2}}|\psi_{\alpha,\beta}^k\rangle\langle\psi_{\alpha,\beta}^k| R^{\frac{A_k^\dagger A_k}{2}})^N$.

Furthermore, from $x^{a^\dagger a} f(a^\dagger) = f(xa^\dagger)x^{a^\dagger a}$ [18], we have $R^{\frac{A_k^\dagger A_k}{2}}|\psi_{\alpha,\beta}^k\rangle = (1-T_g^2)^{\frac{1}{2}}(1-T_{\bar{g}}^2)^{\frac{1}{2}} e^{(A_k^\dagger, A_{k,\perp}^\dagger) M \binom{B_k^\dagger}{B_{k,\perp}^\dagger}}|\underline{0}\rangle$, with $M = \begin{pmatrix} R^{\frac{1}{2}}(T_g C_\alpha S_\beta^\star - T_{\bar{g}} S_\alpha^\star C_\beta) & R^{\frac{1}{2}}(-T_g C_\alpha C_\beta - T_{\bar{g}} S_\alpha^\star S_\beta) \\ T_g S_\alpha S_\beta^\star + T_{\bar{g}} C_\alpha C_\beta & -T_g S_\alpha C_\beta + T_{\bar{g}} C_\alpha S_\beta \end{pmatrix}$, C_α and S_α (C_β and S_β) meaning $\cos\alpha$ and $e^{i\phi_\alpha}\sin\alpha$ ($\cos\beta$ and $e^{i\phi_\beta}\sin\beta$), respectively. From the singular value decomposition of $M = U\begin{pmatrix}\lambda_1 & 0 \\ 0 & \lambda_2\end{pmatrix}V^\star$, $R^{\frac{A_k^\dagger A_k}{2}}|\psi_k(\alpha,\beta)\rangle$ reduces to $(1-T_g^2)^{\frac{1}{2}}(1-T_{\bar{g}}^2)^{\frac{1}{2}} e^{\lambda_1 U A_k^\dagger V B_k^\dagger + \lambda_2 U A_{k,\perp}^\dagger V B_{k,\perp}^\dagger}|\underline{0}\rangle$, and we end up with the simple formula

$$p(\mathrm{nc}_A) = (1-p_{\mathrm{dc}})\left(\frac{(1-T_g^2)(1-T_{\bar{g}}^2)}{(1-\lambda_1^2)(1-\lambda_2^2)}\right)^N = (1-p_{\mathrm{dc}})\left(\frac{2}{2-\eta+\eta\left(C_{2g}C_\alpha^2 + C_{2\bar{g}}|S_\alpha|^2\right)}\right)^N. \quad (4)$$

Following the same line of thought, we can derive all the no-detection probabilities $p(\mathrm{nc}_A \,\&\, \mathrm{nc}_{A_\perp})$, etc.

To compute the CHSH value, Alice and Bob need to bin their results; i.e., they have to choose a local strategy to assign the values ±1 to their four possible events. Among the 256 possible strategies to deal with the nonconclusive events, a simple strategy consists in assigning the value -1 to one of the results corresponding to one click locally [the detector A (B) clicks whereas $A_\perp$ ($B_\perp$) does not] and $+1$ to the other events. Hence, $p(-1-1|xy) = \mathrm{tr}[(\mathbf{1}-D_{\mathrm{nc}}^A)D_{\mathrm{nc}}^{A_\perp}(\mathbf{1}-D_{\mathrm{nc}}^B)D_{\mathrm{nc}}^{B_\perp}|\psi_{\alpha,\beta}\rangle\langle\psi_{\alpha,\beta}|]$ and can be related to the no-detection probabilities derived previously through $p(\mathrm{nc}_{A_\perp} \,\&\, \mathrm{nc}_{B_\perp}) - p(\mathrm{nc}_A \,\&\, \mathrm{nc}_{A_\perp} \,\&\, \mathrm{nc}_{B_\perp}) - p(\mathrm{nc}_{A_\perp} \,\&\, \mathrm{nc}_B \,\&\, \mathrm{nc}_{B_\perp}) + p(\mathrm{nc}_A \,\&\, \mathrm{nc}_{A_\perp} \,\&\, \mathrm{nc}_B \,\&\, \mathrm{nc}_{B_\perp})$. (See the Appendix for the complete expressions.) Processing $p(+1-1|xy)$, $p(-1+1|xy)$, and $p(+1+1|xy)$ in a similar way makes it possible to optimize the CHSH value over the squeezing parameters ($g-\bar{g}$), the number of modes N, and the measurement settings for any detection efficiency and dark count probability.

V. RESULTS

The results are shown in Fig. 2. They have been obtained under the assumption that there is no dark count. Furthermore, we have checked that the strategy described before for binning the four possible results locally is optimal. Therefore, the solid curve of Fig. 2 gives the maximal violation of the CHSH inequality that can be obtained in the scheme represented in Fig. 1. Several results deserve to be elaborated.

(i) The maximum CHSH value obtained with unit efficiency detectors is $\sim$2.35. This is very far from the maximal quantum value of $2\sqrt{2}$ that can be obtained with any two-qubit states that are maximally entangled. The reason is that the photon-pair source under consideration inevitably produces vacuum and multiple pairs. The vacuum leads to no detections and the corresponding CHSH value is 2. Similarly, when many pairs are produced, the four detectors click. This also results in a CHSH value of 2. One might think that the vacuum and the multiphoton events can be safely discarded as the postselected data would violate the CHSH inequality only if the raw data lead to a CHSH value larger than 2. However,

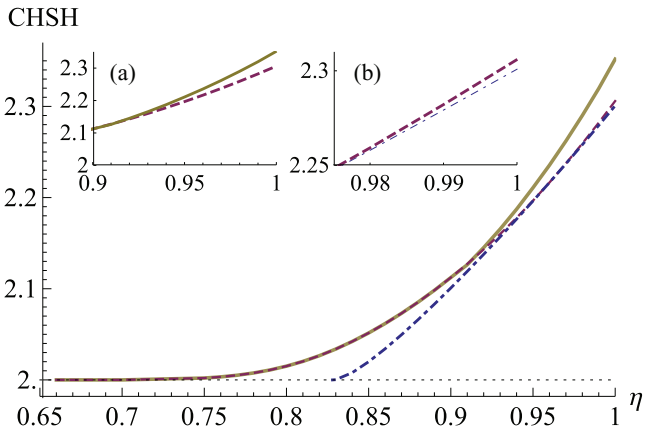

FIG. 2. (Color online) CHSH values as a function of the detection efficiency η. The solid curve is optimized over the structure of the states produced by a spontaneous parametric down-conversion source (the squeezing parameters and the number of modes), the measurement settings, and the local strategy with which the outcomes are assigned to results ±1. The dark count probability is set to zero. The optimal violation (solid curve) is compared to the CHSH value obtained by restricting the emission to a single mode, i.e., thermal photon number statistics (dashed line). A zoom on the region of high efficiencies is given in the inset (a). The CHSH value is also compared to the one obtained by focusing on the single mode case with maximally entangled states ($g=\bar{g}$, see dash-dotted line). A zoom on the region of high efficiencies is given in the inset (b) where the monomode case is compared to the monomode case restricted to maximally entangled states. Note that the CH value can be deduced from the here shown CHSH value through $\frac{S-2}{4}$.

the nonlocal correlations characterizing the experiment are obviously the ones obtained without postselection. This is well illustrated when one considers applications of the Bell test, e.g., for randomness expansion as there is no way to get more randomness from a subset of the raw data. Clearly, removing "unfavorable" events is not an option to properly quantify the Bell violation of a given setup. None of these events prevent the violation of the CHSH inequality but they reduce the observed violation.

(ii) The maximal violation is obtained when the number of modes tends to infinity (Poissonian statistics). For comparison, we can restrict the emission to be monomode ($N=1$) and still optimize the CHSH value over the squeezing parameters and the measurement settings. The corresponding results are given by the dashed line in the inset (a) of Fig. 2. The maximal CHSH value is unchanged for efficiencies smaller than $\sim$91%, but for higher efficiencies, the many-mode configuration favors larger violations. The intuition in the ideal case $\eta=1$ is that the relative probability for having a single pair is greater for the Poissonian distribution compared to the thermal distribution for a mean photon number around 1. However, for inefficient detectors, it becomes more difficult to have an intuition as, in addition to the photon statistics, we have to take into account the detrimental effect of multiphoton events underlying losses.

(iii) In the case $\eta=1$, the maximum violation is reached for the ratio $g/\bar{g}\sim0.92$, i.e., for nonmaximally entangled states [20]. For comparison, the dotted thin curve of the inset (b) in Fig. 2 gives the optimal value when forcing the squeezing

parameters to be the same (still in the monomode case). This shows that, even in the monomode case, it is never optimal to use maximally entangled states, even when dealing with unit efficiency detectors. The intuition is that the two nonconclusive events (no click and two clicks locally) both have an effect analogous to loss and we know from Eberhard [21] that nonmaximally entangled states have a greater resistance to loss.

(iv) The minimum efficiency required to observe nonlocal correlations is 2/3. This is surprising at least at first sight, as this corresponds exactly to the minimum efficiency that is required to violate the CHSH inequality when dealing with two-qubit states. The intuition is that neither the vacuum nor the multiphoton events prevent the violation as each leads to $S = 2$. Hence, the CHSH inequality is violated as long as the two-qubit component (one photon pair exactly) leads to $S > 2$. To further decrease the required efficiency, we could investigate other Bell inequalities with more outputs and/or inputs. This provides work for the future.

VI. CONCLUSION AND PERSPECTIVES

We have presented an exact derivation of correlations in a scenario with two parties testing the CHSH inequality with a source based on spontaneous parametric down conversion. In particular, we have shown that the maximal CHSH value is $\sim$2.35. This limits substantially the efficiency of the scenario drawn in Fig. 1 for device-independent quantum key distribution [6] or device-independent quantum random number generation [4]. Note that a higher violation can be obtained through amplification [7] or nonlinear filtering [8] at the price of increasing complexity.

As our results give the strategy that optimizes the observed violation, we expect that they will have a significant impact on ongoing experiments. Focusing on the experiment reported in Ref. [5] for example, in which photon pairs distributed over $N = 25$ modes and detectors with an (overall) efficiency of 75% have been used for a Bell test while closing the detection loophole, we find the maximum S value of 2.0018 optimizing the state structure $(g, \bar{g})$ and measurement settings while the observed value was 2.0002. (The measurement settings used in Ref. [5] were obtained numerically assuming qubits, i.e., the state of the form $(r a_1^\dagger b_{1,\perp}^\dagger + a_{1,\perp}^\dagger b_1^\dagger)|\underline{0}\rangle$ with appropriate normalization and where the value of r was measured.) This translates into a speeding up of randomness expansion by 1 order of magnitude. Even if the dark count probability ($p_{\mathrm{dc}} = 8 \times 10^{-6}$) and the fluorescence background (between 0.15% and 0.25% of the mean singles) are taken into account, we envision a speeding up by a factor of $\sim$3 in the most conservative case (background noise 0.25% of the mean singles). Note that in practice, one is tempted to use a single detector locally, as in Ref. [5]. In this case, the strategy with which the nonconclusive results are treated is different from the one presented here but we have found that it is also one that is optimal.

ACKNOWLEDGMENTS

We warmly thank V. Scarani for helpful discussions and comments. This work was supported by the Swiss NCCR QSIT, the Swiss National Science Foundation SNSF (Grant No. PP00P2_150579 and "Early PostDoc.Mobility"), the European Commission (IP SIQS, Chist-era DIQIP), the Singapore Ministry of Education (partly through the Academic Research Fund Tier 3, Grant No. MOE2012-T3-1-009), and the National Research Foundation of Singapore.

APPENDIX

We here present a list of all the no-detection probabilities. They provide all the information that is necessary to compute the optimal CHSH value. As far as the notation is concerned, we have maintained the one presented in the main text for T_g, C_g ($T_{\bar{g}}$ and $C_{\bar{g}}$), and C_α (C_β), while S_α (S_β) now means $\sin\alpha$ ($\sin\beta$). Furthermore, $C_{\phi_A-\phi_B}$ means $\cos(\phi_A - \phi_B)$.

The probability to detect no photon in mode A is given by

$$p(\mathrm{nc}_A) = (1 - p_{\mathrm{dc}})\left(\frac{2}{2 - \eta + \eta\left(C_\alpha^2 C_{2g} + C_{2\bar{g}} S_\alpha^2\right)}\right)^N. \tag{A1}$$

The expressions for $p(\mathrm{nc}_{A_\perp})$, $p(\mathrm{nc}_{B_\perp})$, and $p(\mathrm{nc}_B)$ can be obtained from Eq. (A1) by inverting g and $\bar{g}$, replacing α with β, and inverting g and $\bar{g}$ and replacing α with β, respectively. The probability for no detection in modes A and $A_\perp$ (B and $B_\perp$) is given by the following expression:

$$p(\mathrm{nc}_A \,\&\, \mathrm{nc}_{A_\perp}) = p(\mathrm{nc}_B \,\&\, \mathrm{nc}_{B_\perp}) = (1 - p_{\mathrm{dc}})^2 \times \left(\frac{4}{(2 - \eta + \eta C_{2g})(2 - \eta + \eta C_{2\bar{g}})}\right)^N. \tag{A2}$$

The probability for no detection in modes A and B is given by

$$\begin{aligned} p(\mathrm{nc}_A \,\&\, \mathrm{nc}_B) = (1 - p_{\mathrm{dc}})^2 4^N \left(C_g^2 C_{\bar{g}}^2\right)^{-N} \\ \times (4 + 2\eta^2 T_g T_{\bar{g}} C_{\phi_A-\phi_B} S_{2\alpha} S_{2\beta} \\ - T_{\bar{g}}^2 (2 - \eta + \eta C_{2\alpha})(2 - \eta - \eta C_{2\beta}) \\ + T_g^2 \big[(2 - \eta - \eta C_{2\alpha})(\eta - 2 - \eta C_{2\beta}) \\ + 4(1 - \eta)^2 T_{\bar{g}}^2\big]^{-N}. \end{aligned} \tag{A3}$$

Similarly, $p(\mathrm{nc}_{A_\perp} \,\&\, \mathrm{nc}_B)$, $p(\mathrm{nc}_A \,\&\, \mathrm{nc}_{B_\perp})$, and $p(\mathrm{nc}_{A_\perp} \,\&\, \mathrm{nc}_{B_\perp})$ can be derived from Eq. (A3) by substituting α with $\alpha + \frac{\pi}{2}$, β with $\beta + \frac{\pi}{2}$, and α with $\alpha + \frac{\pi}{2}$ and β with $\beta + \frac{\pi}{2}$, respectively. The probability $p(\mathrm{nc}_A \,\&\, \mathrm{nc}_{A_\perp} \,\&\, \mathrm{nc}_B)$ of no detection in modes A, $A_\perp$, and B is given by

$$p(\mathrm{nc}_A \,\&\, \mathrm{nc}_{A_\perp} \,\&\, \mathrm{nc}_B) = \frac{(1 - p_{\mathrm{dc}})^3}{\left(C_g^2 C_{\bar{g}}^2 \left\{1 - \frac{1}{2}(1 - \eta) T_{\bar{g}}^2 (2 - \eta - \eta C_{2\beta}) - (1 - \eta) T_g^2 \left[1 - \eta S_\beta^2 - (1 - \eta)^2 T_{\bar{g}}^2\right]\right\}\right)^N}. \tag{A4}$$

Similarly the expressions for $p(\mathrm{nc}_A \,\&\, \mathrm{nc}_{A_\perp} \,\&\, \mathrm{nc}_{B_\perp})$, $p(\mathrm{nc}_{A_\perp} \,\&\, \mathrm{nc}_B \,\&\, \mathrm{nc}_{B_\perp})$, and $p(\mathrm{nc}_A \,\&\, \mathrm{nc}_B \,\&\, \mathrm{nc}_{B_\perp})$ can be obtained from Eq. (A4) by inverting g and $\bar{g}$, inverting α and β, and inverting g and $\bar{g}$ and α and β, respectively. Finally,

$$p(\mathrm{nc}_A \,\&\, \mathrm{nc}_{A_\perp} \,\&\, \mathrm{nc}_B \,\&\, \mathrm{nc}_{B_\perp}) = (1 - p_{\mathrm{dc}})^4 \left(\frac{4}{\{1 + (1-\eta)^2 + [1-(1-\eta)^2]C_{2g}\}\{1 + (1-\eta)^2 + [1-(1-\eta)^2]C_{2\bar{g}}\}} \right)^N . \quad \text{(A5)}$$

[1] J. F. Clauser, M. Horne, A. Shimony, and R. A. Holt, Phys. Rev. Lett. **23**, 880 (1969).
[2] J. Clauser and M. Horne, Phys. Rev. D **10**, 526 (1974).
[3] N. Brunner, D. Cavalcanti, S. Pironio, V. Scarani, and S. Wehner, Rev. Mod. Phys. **86**, 419 (2014).
[4] S. Pironio *et al.*, Nature (London) **464**, 1021 (2010).
[5] B. G. Christensen *et al.*, Phys. Rev. Lett. **111**, 130406 (2013).
[6] A. Acin, N. Brunner, N. Gisin, S. Massar, S. Pironio, and V. Scarani, Phys. Rev. Lett. **98**, 230501 (2007).
[7] N. Gisin, S. Pironio, and N. Sangouard, Phys. Rev. Lett. **105**, 070501 (2010).
[8] N. Sangouard, B. Sanguinetti, N. Curtz, N. Gisin, R. Thew, and H. Zbinden, Phys. Rev. Lett. **106**, 120403 (2011).
[9] C. C. W. Lim, C. Portmann, M. Tomamichel, R. Renner, and N. Gisin, Phys. Rev. X **3**, 031006 (2013).
[10] M. A. Rowe *et al.*, Nature (London) **409**, 791 (2001).
[11] D. N. Matsukevich *et al.*, Phys. Rev. Lett. **100**, 150404 (2008).
[12] J. Hofmann *et al.*, Science **337**, 72 (2012).
[13] A. Aspect, J. Dalibard, and G. Roger, Phys. Rev. Lett. **49**, 1804 (1982).
[14] W. Tittel, J. Brendel, H. Zbinden, and N. Gisin, Phys. Rev. Lett. **81**, 3563 (1998).
[15] G. Weihs, T. Jennewein, C. Simon, H. Weinfurter, and A. Zeilinger, Phys. Rev. Lett. **81**, 5039 (1998).
[16] M. Giustina *et al.*, Nature (London) **497**, 227 (2013).
[17] We assumed that χ and $\bar{\chi}$ are independent of k; i.e., the distribution of spatial/frequency modes is flat.
[18] P. Sekatski, B. Sanguinetti, E. Pomarico, N. Gisin, and C. Simon, Phys. Rev. A **82**, 053814 (2010).
[19] M. J. Collett, Phys. Rev. A **38**, 2233 (1988).
[20] Note that we found the following optimal parameters for unit efficiencies: $g \sim 0.106$, $\bar{g} \sim 0.115$, $\alpha_1 \sim -0.163$, $\alpha_2 \sim 0.491$, $\phi_{\alpha 1} \sim -0.635$, $\phi_{\alpha 2} \sim -0.635$, $\beta_1 \sim 1.733$, $\beta_2 \sim 1.079$, $\phi_{\beta 1} \sim -0.635$, and $\phi_{\beta 2} \sim -0.635$. Furthermore, if one adds dark counts, say, with $p_{\mathrm{dc}} = 10^{-6}$, this reduces the violation obtained with unit efficiencies by $\sim 10^{-6}$.
[21] P. H. Eberhard, Phys. Rev. A **47**, R747 (1993).

3 Comparing different approaches for generating random numbers device-independently using a photon pair source

Comparing different approaches for generating random numbers device-independently using a photon pair source

2015 New J. Phys. 17 023023

(http://iopscience.iop.org/1367-2630/17/2/023023)

New Journal of Physics
The open access journal at the forefront of physics

Deutsche Physikalische Gesellschaft DPG
IOP Institute of Physics

Published in partnership with: Deutsche Physikalische Gesellschaft and the Institute of Physics

OPEN ACCESS

RECEIVED
17 September 2014

REVISED
15 December 2014

ACCEPTED FOR PUBLICATION
15 January 2015

PUBLISHED
10 February 2015

PAPER

Comparing different approaches for generating random numbers device-independently using a photon pair source

V Caprara Vivoli[1], P Sekatski[2], J-D Bancal[3], C C W Lim[1], A Martin[1], R T Thew[1], H Zbinden[1], N Gisin[1] and N Sangouard[4]

[1] Group of Applied Physics, University of Geneva, CH-1211 Geneva 4, Switzerland
[2] Institut for Theoretische Physik, Universitat of Innsbruck, Technikerstr. 25, A-6020 Innsbruck, Austria
[3] Centre for Quantum Technologies, National University of Singapore, 3 Science Drive 2, Singapore 117543, Singapore
[4] Department of Physics, University of Basel, CH-4056 Basel, Switzerland

E-mail: valentina.caprara@unige.ch

Keywords: non-locality, random numbers, photon pair source

Abstract

What is the most efficient way to generate random numbers device-independently using a photon pair source based on spontaneous parametric down conversion? We consider this question by comparing two implementations of a detection-loophole-free Bell test. In particular, we study in detail a scenario where a source is used to herald path-entangled states, i.e. entanglement between two spatial modes sharing a single photon and where non-locality is revealed using photon counting preceded by small displacement operations. We start by giving a theoretical description of such a measurement. We then show how to optimize the Bell–CHSH violation through a non-perturbative calculation, taking the main experimental imperfections into account. We finally bound the amount of randomness that can be extracted and compare it to the one obtained with the conventional scenario using photon pairs entangled e.g. in polarization and analyzed through photon counting. While the former requires higher overall detection efficiencies, it is far more efficient in terms of the entropy per experimental run and under reasonable assumptions, it provides higher random bit rates.

1. Introduction

In the last decades, the idea of using the randomness present in quantum phenomena to create random number strings has been pushed forward [1–3]. Among the quantum techniques that are envisaged to expand a given random bit string, those based on a Bell test [4–6], the so-called device-independent quantum random number generators (DI-QRNG), are very attractive because they are based on a few assumptions that are relatively easy to check in real time. The price to pay is to realize a Bell test without the detection loophole. The detection loophole has been addressed in several experiments including single ions [7, 8] and single atoms [9] and very recently, using photon pair sources [10, 11]. The latter has several advantages in practice in that it is much less restrictive in terms of wavelength and bandwidth than atoms. It further has the advantage of simple implementation since $\chi^{(2)}$ nonlinear crystals are well integrated devices, commercially available and operating at room temperature. The bottleneck of photonic experiments is the detector inefficiency, but given recent improvements [12–15], setups based on spontaneous parametric down conversion (SPDC) sources are attracting more and more attention, including for their commercial perspectives.

The conventional setup, used e.g. in the experiments [10, 11], is shown in figure 1(A). A SPDC source produces photon pairs entangled e.g. in polarization. The photons are then analyzed by a set of wave plates and non-photon number resolving (NPNR) detectors[5]. Importantly, it has been realized recently [16] that the maximal CHSH–Bell violation [17] that can be reached in this scenario is intrinsically limited by the characteristics of the source, i.e. by the presence of vacuum and multiple photon pairs. As shown in [4], the

[5] Note that TES detectors are capable of number resolution. Nevertheless, this capability was not used in [10, 11].

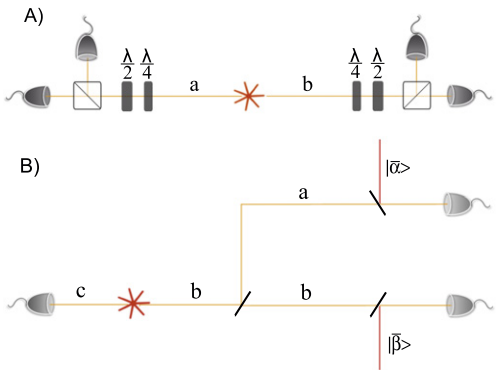

Figure 1. Scheme of two possible implementations of a Bell test using a photon pair source. (A) A source (star) based on SPDC is excited e.g. by a pulsed pump and produce photon pairs entangled e.g. in polarization. The photons are emitted in correlated spatial modes a (b). Each of them might include several temporal/frequency/spatial modes a_k–b_k. The photons emitted in a (b) are sent to Alice's (Bob's) location where they are projected along an arbitrary direction of the Bloch sphere using a set of wave-plates, a polarization beam splitter and two detectors. (B) A source (star) based on SPDC produces photon pairs. We assume that in this scenario the emission is mono-mode. The detection of one photon thus heralds the creation of its twin in a pure state. The latter is sent through a beam splitter. This leads to an entangled state between the two paths a and b. The state of each path is displaced in the phase space using an unbalanced beamsplitter and a coherent state, before being detected though photon counting techniques. The detectors are assumed to be non-photon number resolving with non-unit efficiency.

observed CHSH violation can be used to quantify the amount of extractable randomness in the experimental data. That is, the min-entropy of the data is lower bounded by a function monotonically increasing in the observed CHSH violation. A reduction in the violation thus implies a reduction in the amount of extractable randomness. This raises the question of whether other scenarios involving similar resources could provide larger Bell violations and hence would be more suited for DI-QRNG.

An alternative scenario for Bell test with photons has been proposed by Banaszek and Wodkiewicz in 1998 [18] (see also related theoretical investigations [19–23]) leading to a proof of principle experiment in 2004 [24]. The corresponding implementation using a SPDC source is shown in figure 1(B). A nonlinear crystal is pumped by a pulsed laser with an intensity carefully tuned to create a pair of photons with a small probability in modes b and c. A detection in c, even with an inefficient NPNR detector, heralds the creation of its twin photon in b. The latter is subsequently sent through a beam splitter, entangling the two output spatial modes a and b. Each of these modes is then analyzed through photon counting preceded by small displacements in phase space. Such a displacement is easily implemented in practice, using an unbalanced beamsplitter and a coherent state. In the subspace with at most one photon $\{|0\rangle, |1\rangle\}$, this measurement corresponds to a noisy qubit measurement whose direction in the Bloch sphere depends on the size of the displacement, as detailed below. By choosing the appropriate settings and by taking the events 'click' and 'no-click' as binary outputs of a Bell test, a CHSH–Bell value of $\approx$2.69 can be obtained with a state of the form $\frac{1}{\sqrt{2}}(|01\rangle + |10\rangle)$ [20, 21]. However, it was not previously clear what the maximum violation could be in a realistic scenario involving a SPDC source, non-unit efficiency and noisy detectors. Here we present such an analysis with the aim of establishing the best experimental setup for DI-QRNG. More precisely, we start by providing a detailed theoretical analysis of this measurement involving photon counting preceded by a small displacement operation. We then show how to calculate the Bell correlations in a non-perturbative way in the scenario presented in figure 1(B) that we call 'spatial entanglement' in the rest of the paper. We then optimize the CHSH violation for a given detection efficiency η over the squeezing parameter, the displacement amplitudes, and the splitting ratio of the beam splitter. Lastly we calculate the min entropy and the rate of random bits that can be extracted in this setup. We compare them to the conventional case where entangled pairs are detected by photon counting (see figure 1(A)). We show that while the scenario based on spatial entanglement requires higher overall detection efficiencies, it is preferable to the two photon case regarding the min entropy and, under reasonable assumptions, regarding the rate of random bits as well.

2. Measurement analysis

In this section, we provide a detailed analysis of the measurement device used in the scenario based on spatial entanglement. We consider a NPNR detector of efficiency η preceded by a displacement $\alpha = |\alpha|e^{i\delta}$. The no click/click events are associated to two elements of a POVM $\{P_0, P_c\}$ which satisfy $P_0 + P_c = \mathbb{1}$. The no-click event of our NPNR detector is described by the operator $(1-\eta)^{a^\dagger a}$. Taking the displacement into account, one gets

$P_0 = \mathcal{D}^\dagger(\alpha)(1-\eta)^{a^\dagger a}\mathcal{D}(\alpha)$. To gain insight on this measurement, let us restrict P_0 to the Hilbert space spanned by $|0\rangle = \begin{pmatrix}1\\0\end{pmatrix}$ and $|1\rangle = \begin{pmatrix}0\\1\end{pmatrix}$ where it takes the following matrix form

$$P_0 = \begin{pmatrix} e^{-\eta|\alpha|^2} & -\eta\,\alpha^* e^{-\eta|\alpha|^2} \\ -\eta\,\alpha e^{-\eta|\alpha|^2} & \left(1-\eta+\eta^2|\alpha|^2\right)e^{-\eta|\alpha|^2} \end{pmatrix}. \tag{1}$$

Let us recall that $P_c = \mathbb{1} - P_0$. For non-unit efficiency $\eta < 1$, the POVM $\{P_0,\ P_c\}$ is not extremal [25]

$$\left\{P_0,\ P_c\right\} = \mu\left\{\Pi_{\vec{n}},\ \Pi_{-\vec{n}}\right\} + \left(1-\mu\right)\left\{r_0\mathbb{1},\ r_c\mathbb{1}\right\}. \tag{2}$$

This means that this measurement corresponds to a projective measurement in the direction

$$\vec{n} \propto \begin{pmatrix} -e^{-\eta|\alpha|^2}\,|\alpha|\,\eta\cos\left(\delta\right) \\ e^{-\eta|\alpha|^2}\,|\alpha|\,\eta\sin\left(\delta\right) \\ \frac{1}{2}e^{-\eta|\alpha|^2}\eta\left(1-|\alpha|^2\eta\right) \end{pmatrix}$$

on the Bloch sphere with probability

$$\mu = \sqrt{\eta^2 e^{-2|\alpha|^2\eta}\left(|\alpha|^2\left(|\alpha|^2\eta^2 - 2\eta + 4\right) + 1\right)}.$$

With the remaining probability $(1-\mu)$, the output of the measurement is given randomly (regardless of the input state) accordingly to the distribution $\{r_0,\ r_c\}$ where

$$r_0 = \frac{1}{2} \times \frac{\frac{\eta\left(|\alpha|^2\eta - 1\right) + 2}{\sqrt{\eta^2\left(|\alpha|^2\left(\eta\left(|\alpha|^2\eta - 2\right) + 4\right) + 1\right)}} - 1}{\frac{e^{|\alpha|^2\eta}}{\sqrt{\eta^2\left(|\alpha|^2\left(\eta\left(|\alpha|^2\eta - 2\right) + 4\right) + 1\right)}} - 1} \tag{3}$$

and $r_c = 1 - r_0$. As an example, consider the case without displacement $\alpha = 0$. The previous POVM reduces to

$$\left\{P_0,\ P_c\right\} = \eta\left\{\Pi_0,\ \Pi_1\right\} + \left(1-\eta\right)\left\{\mathbb{1},\ 0\right\} \tag{4}$$

i.e. it corresponds to a projective measurement in the direction z with the probability η and with the remaining probability $(1-\eta)$, a no-click event occurs regardless of the input state.

Note that the phase term of the displacement $e^{i\delta}$ affects the polar angle of $\vec{n}$ only. For simplicity, we consider the case $\alpha = |\alpha|$, where the direction of the measurement lays in the x–z plane of the Bloch sphere. We further focus on the projective part of the POVM $\mu\ \{\Pi_{\vec{n}},\ \Pi_{-\vec{n}}\}$ and we look at the direction and length of the corresponding vector $\mu\vec{n}$ on the Bloch sphere. The result is shown in figure 2. For $\eta = 1$ and $\alpha = 0$, this vector is directed in the z direction and has a unit length. The measurement device thus performs a projection along z. When α increases, the vector starts to rotate toward x while its length reduces. For non-unit efficiencies, the vector is shorter and it also rotates toward x when α increases. Surprisingly, we remark that the vector length increases with α (before it drops to zero), i.e. the 'effective detection efficiency' of the measurement setup μ gets larger than the intrinsic efficiency of the detector itself η.

3. Exact derivation of Bell–CHSH correlators

The purpose of this section is to derive the exact expression of the CHSH–Bell correlators in the case of spatial entanglement (see figure 1(B)). We first focus on the density matrix ρ_h of b resulting from a detection in c. The state created by the SPDC source is given by $|\psi\rangle = \sqrt{1-T_g^2}\sum_n \frac{T_g^n}{n!}b^{\dagger n}c^{\dagger n}|00\rangle$, where $T_g = \tanh(g)$, g being the squeezing parameter. To obtain ρ_h, we have to calculate $\mathrm{tr}_c\left(|\psi\rangle\langle\psi|\left(\mathbb{1} - (1-\eta_h)^{c^\dagger c}\right)\right)$. η_h stands for the efficiency of the heralding detector and tr_c is the trace on c. This can be expressed as the difference of two terms. The first one is simply the trace over $|\psi\rangle$ while the second one can be written as $\mathrm{tr}_c\left(R_h^{c^\dagger c}|\psi\rangle\langle\psi|R_h^{c^\dagger c}\right)$, with $R_h = \sqrt{1-\eta_h}$. Using the formula $R_h^{c^\dagger c}e^{T_g a^\dagger c^\dagger} = e^{R_h T_g a^\dagger c^\dagger}R_h^{c^\dagger c}$ [26], and re-normalizing the obtained state, the resulting density matrix ρ_h can be written as

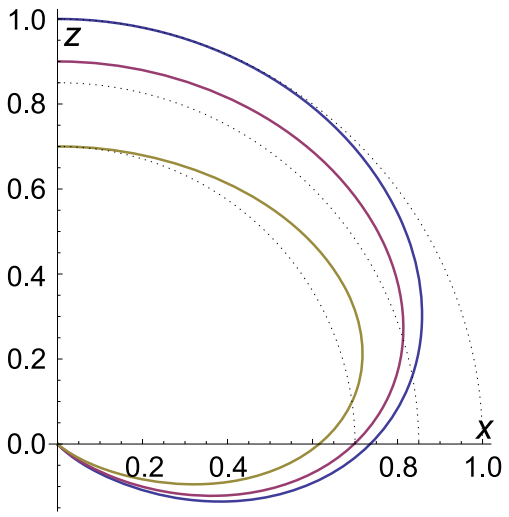

Figure 2. Focusing on the projective part $\mu\ \{\Pi_{\vec{n}},\ \Pi_{-\vec{n}}\}$ of the studied POVM, we here represent the length μ and the direction of the corresponding vector in the Bloch sphere. As we consider real α, this vector lies in the x–z plane. For unit detection efficiency ($\eta = 1$, outermost curve) and $\alpha = 0$, this vector has a unit length and is directed to the z direction. When α increases (α spans the interval $[0,\ 4]$), the vector starts to rotate (the polar angle gives the azimuthal angle of $\vec{n}$ on the Bloch sphere) and its length decreases (the radius decreases). In the limit of large α, the vector length tends to zero. The two inner curves corresponds to non-unit efficiency ($\eta = 90\%$ and $\eta = 70\%$, respectively).

$$\rho_h = \frac{1 - R_h^2\ T_g^2}{T_g^2\left(1 - R_h^2\right)}\left[\rho_{\rm th}\left(\bar{n} = \frac{T_g^2}{1 - T_g^2}\right) - \frac{1 - T_g^2}{1 - R_h^2 T_g^2}\rho_{\rm th}\left(\bar{n} = \frac{R_h^2 T_g^2}{1 - R_h^2 T_g^2}\right)\right], \tag{5}$$

i.e. a difference between two thermal states $\rho_{\rm th}(\bar{n}) = \frac{1}{1+\bar{n}}\sum_k \left(\frac{\bar{n}}{1+\bar{n}}\right)^k |k\rangle\langle k|$, where $\bar{n}$ is the mean photon number. Let us first calculate the correlators that would be obtained from a thermal state. We recall that a thermal state is classical with respect to the P representation. Therefore, it can be written as a mixture of coherent states $|\gamma\rangle$. Concretely, $\rho_{\rm th}\left(\bar{n}\right) = \int {\rm d}^2\gamma P^{\bar{n}}(\gamma)|\gamma\rangle\langle\gamma|$ with $P^{\bar{n}}(\gamma) = \frac{1}{\pi\bar{n}}{\rm e}^{-\frac{|\gamma|^2}{\bar{n}}}$. The correlators associated to a thermal state can thus be obtained by looking at the behavior of a coherent state. A beam splitter splits a coherent state into two coherent states, i.e. $|\gamma\rangle \rightarrow |\sqrt{R}\gamma\rangle_a|\sqrt{T}\gamma\rangle_b$, where T and R are, respectively, the transmittivity and the reflectivity. A displacement $D(\alpha)$ on a coherent state $|\gamma\rangle$ gives another coherent state with mean photon number $|\gamma + \alpha|^2$, i.e. $D(\alpha)|\gamma\rangle = |\gamma + \alpha\rangle$. From

$$(1 - \eta)^{\frac{a^\dagger a}{2}}\ |\bar{\gamma}\rangle = {\rm e}^{-\frac{\eta|\gamma|^2}{2}}\left|\sqrt{1 - \eta}\,\bar{\gamma}\right\rangle, \tag{6}$$

we easily obtain the probability to get no click in both sides from a thermal state $\rho_{\rm th}(\bar{n})$ knowing the amplitudes of the local displacements α and β

$$p_{\alpha,\beta}^{\rm nc,nc} = \frac{{\rm e}^{-\eta\left(|\alpha|^2+|\beta|^2\right)+\frac{\bar{n}\eta^2}{1+\bar{n}\eta}|\sqrt{R}\alpha+\sqrt{T}\beta|^2}}{1 + \eta\bar{n}}. \tag{7}$$

Attributing the value $+1$ (-1) to a 'no-click' event ('click' event), we then obtain an explicit expression for the correlator $E_{\alpha,\beta}^{\rm th} = p_{\alpha,\beta}^{\rm nc,nc} + p_{\alpha,\beta}^{\rm c,c} - p_{\alpha,\beta}^{\rm nc,c} - p_{\alpha,\beta}^{\rm c,nc}$ associated to a thermal state $\rho_{\rm th}(\bar{n})$

$$E_{\alpha,\beta}^{\rm th} = 1 + 4\frac{{\rm e}^{-\eta\left(|\alpha|^2+|\beta|^2\right)+\frac{\bar{n}\eta^2}{1+\bar{n}\eta}|\sqrt{R}\alpha+\sqrt{T}\beta|^2}}{1 + \eta\bar{n}} - 2\frac{{\rm e}^{-\frac{\eta|\alpha|^2}{1+\eta\bar{n}R}}}{1 + \eta\bar{n}R} - 2\frac{{\rm e}^{-\frac{\eta|\beta|^2}{1+\eta\bar{n}T}}}{1 + \eta\bar{n}T}.$$

From this last expression, we deduce the correlator $E_{\alpha_i\beta_j}$ for the state (5)

$$E_{\alpha_i\beta_j} = \frac{1 - R_h^2\ T_g^2}{T_g^2\left(1 - R_h^2\right)}\left[E_{\alpha_i\beta_j}^{\rm th}\left(\bar{n} = \frac{T_g^2}{1 - T_g^2}\right) - \frac{1 - T_g^2}{1 - R_h^2 T_g^2}E_{\alpha_i\beta_j}^{\rm th}\left(\bar{n} = \frac{R_h^2 T_g^2}{1 - R_h^2 T_g^2}\right)\right]. \tag{8}$$

This explicit expression of $E_{\alpha_i\beta_j}$ allows one to optimize the CHSH–Bell value, i.e. the value of $S = |E_{\alpha_1\beta_1} + E_{\alpha_1\beta_2} + E_{\alpha_2\beta_1} - E_{\alpha_2\beta_2}|$, for given efficiencies (η, η_h) over the tunable parameters of the system, i.e. the squeezing parameter g, the amplitude of the local displacements α_i and β_j (measurement settings), and the transmittivity T of the beam splitter. Note that the CH [31] and CHSH inequalities are equivalent for all

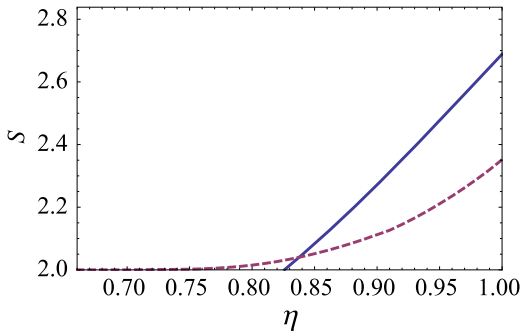

Figure 3. Optimal CHSH value as a function of the efficiency η. The full (dashed) curve is obtained in the case of spatial entanglement, see figure 1(B) (polarization-entanglement, see figure 1(A)) (see the text for detail).

probability distributions satisfying the no-signaling condition, i.e. for all quantum correlations [6]. Namely, they are related by the affine relation $4CH = S - 2$.

4. Optimization of the CHSH value

In this section, we present the result of the optimization of the CHSH–Bell value in the case of spatial entanglement (figure 1(B)). Figure 3 shows S as a function of the efficiency η and compares it to the case of polarization entanglement for which the optimization of the CHSH–Bell value has been reported in [16]. We emphasize that η is the overall detection efficiency including the transmission efficiency from the source to the detector. We assume that the efficiencies for modes a and b are the same. They are equal to the heralding efficiency $\eta_h = \eta$. Three results deserve to be highlighted.

(i) In the ideal case where $\eta = 1$, the maximal violation is around 2.69. This value is obtained in the limit $g \to 0$, i.e. when the production of multiple photon pairs is negligible. Since the heralding signal eliminates the vacuum component, we end up with a single photon Fock state in b to a very good approximation. We thus retrieve the maximal violation that can be obtained in the scenario presented in figure 1(B) with a single photon [20, 21]. Note that in practice, the value of g is limited by the probability $p_{\rm dc}$ of having a dark count in the heralding detector which is negligible if $p_{\rm dc} \ll \eta T_g^2$ only. More concretely, if one assumes that the probability of having a dark count is $p_{\rm dc} \approx 10^{-5}$ for example, we found the optimal violation $S \sim 2.67$ which is obtained for $g \sim 0.07$ and still $\eta = 1$.

(ii) We observe that the optimal state is always obtained from a 50–50 beam splitter ($R = T = \frac{1}{2}$) in the limit $g \to 0$, i.e. it is a two-qubit maximally entangled state. This is unexpected as in the case of a two-qubit state entangled in polarization, lower efficiencies can be tolerated from non-maximally entangled states [27].

(iii) The minimal required detection efficiency is $\eta_{\rm min} = 0.826$. This is counterintuitive, at least at first sight, since there is a local model reproducing the correlation of the singlet state as soon as the detection efficiency is lower or equal to $\frac{2}{\sqrt{2}+1} \approx 0.828$ [28–30]. Nevertheless, this model assumes that the probability of having a conclusive event is η whereas the probability for having a non-conclusive event is $1-\eta$. This does not hold in the case of spatial entanglement. Let us also recall that in the scenario of spatial entanglement, the effective efficiency of the overall measurement device can be higher than the detection efficiency of the NPNR detector.

Note that the CHSH–Bell values given in figure 3 are optimized over the local strategies that are used to assign binary results ± 1 to physical events (click and no-click). We found that they are all equivalent, i.e. they all lead to the same value of S. The sum $E_{\alpha_1\beta_1} + E_{\alpha_1\beta_2} + E_{\alpha_2\beta_1} - E_{\alpha_2\beta_2}$ simply needs to be minimized or maximized depending on the strategy.

5. Rate of random bit generation

In this section, we estimate the amount of randomness created in both setups that are presented in figure 1. We present two quantities, (i) the randomness per run, i.e. the min entropy $H_{\rm min}(S)$, and (ii) the rate of randomness generation. Let us first focus on the min entropy $H_{\rm min}(S)$. As mentioned earlier in the introduction, the min-

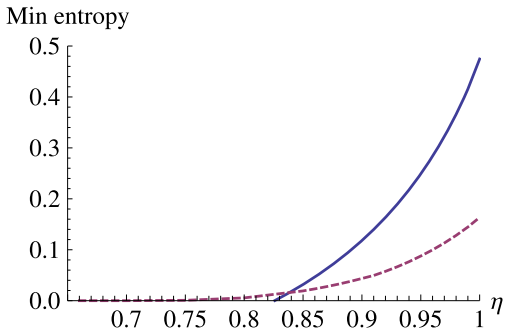

Figure 4. Min entropy per experimental run as a function of the efficiency η. The full (dashed) curve corresponds to the case of spatial entanglement (figure 1(B)) (polarization-entanglement, see figure 1(A)).

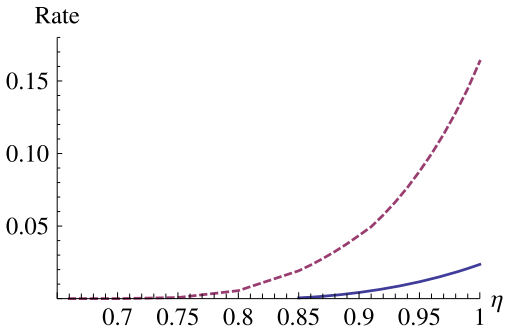

Figure 5. Rates of random bits (in unit of the pump-laser rate) as a function of the efficiency η. The full (dashed) curve corresponds to the case of spatial-entanglement (polarization-entanglement).

entropy rate (amount of randomness per bit) can be lower bounded in terms of the observed CHSH violation S [4]. The lower bound is given by

$$H_{\min}(S) = 1 - \log_2\left(1 + \sqrt{2 - \frac{S^2}{4}}\right). \tag{9}$$

$H_{\min}(S)$ is equal to 0 when S is 2 and it reaches its maximum value 1 when S is maximal, i.e. $S = 2\sqrt{2}$.[6] Since the min entropy is a monotonic function of S, large S favors large min entropy. The optimal value of $H_{\min}(S)$ computed from [4] for the two different implementations of figure 1 is shown in figure 4. Since a larger violation can be obtained in the scenario involving spatial entanglement, the scheme of figure 1(B) provides higher min entropy than the scheme of figure 1(A) for large enough efficiencies. On the other hand, the scenario involving the spatial-entanglement requires efficiencies higher than 0.826 while the scenario with polarization-entangled states allows one to get small but non-zero min entropy for efficiencies in between ≈0.67 and 0.826.

Let us now focus on the rate of randomness generation. It is given by

$$R(S) = rH_{\min}(S), \tag{10}$$

where r is the rate at which the states are analyzed. Consider first the case where the repetition rate is set by the pump laser. For the conventional setup (figure 1(A)) $R(S) = r_{\text{pump}} H_{\min}(S)$ whereas in the case of spatial entanglement, the rate at which the states are analyzed is intrinsically limited by the heralding rate, i.e. $R(S) = r_{\text{pump}} \frac{\eta_h T_g^2}{1-(1-\eta_h)T_g^2} H_{\min}(S)$. Assuming $\eta_h = \eta$, we have optimized $R(S)$ over the squeezing parameter g, the values of α_i and β_j, and the transmittivity T. The result is shown in figure 5 and is compared to the conventional scenario (see figure 1(A)). One sees that the high violations that are obtained in the scenario involving the spatial entanglement do not compensate the reduction of the repetition rate.

Consider now the situation where the rate is not limited by the pump laser but by the speed at which the measurement settings are chosen, as in [10], or by the deadtime of the detectors so that the heralding rate (r_{d}) in

[6] Note that higher bounds can *a priori* be obtained by considering the outcomes observed by two parties, or by evaluating the min entropy based on all observed statistics (rather than just the value of CHSH), see [32].

the scenario given in figure 1(A) is the same that the detection rate of the scenario of figure 1(B). In this case, the rate of random bits is given by $R(S) = r_d H(S)$ and can thus be deduced from figure 4. It is clear that the rate of randomness in the scenario involving spatial entanglement is substantially higher than the conventional one (figure 1(A)) for efficiencies larger than 0.84 as its Bell violation is higher. Furthermore, in practice, randomness extraction is normally carried out on a fixed input bit string and the size of the output string is approximately given by the min-entropy of the input bit string. Seen from this point of view, it is clear that our spatial entanglement setup allows a larger number of extractable secret bits for a fixed input bit string.

6. Conclusion and discussions

Motivated by very recent experiments reporting on the first-detection-loophole-free Bell tests with photon pairs, we have studied two different scenarios, both of them based on SPDC sources and photon counting techniques, for the generation of random bits. In particular, we have shown how to calculate the correlators in the scenario involving spatial entanglement (represented in figure 1(B)) in a non-perturbative way. This allowed us to optimize the CHSH–Bell value, that we have compared to the one obtained in the more conventional scenario of figure 1(A). While the detection technique of the scenario given in figure 1(B) involves small displacement operations, i.e. requires a noise free local oscillator indistinguishable from the photons to be detected, and overall detection efficiencies larger than in the conventional scenario, the scenario involving spatial entanglement has several interesting features:

(i) First, only one mode needs to be detected efficiently. Therefore one can use filtering techniques on the heralding mode to prepare it in a mode having high coupling and detection efficiency [33, 34].

(ii) For efficiencies higher than 84%, the scenario based on spatial entanglement leads to substantial improvements over the conventional setup in terms of min entropy.

(iii) Assuming that the number of experimental runs is large enough so that the Bell violation is accurately estimated in both setups, we have shown that in the realistic regime where the repetition rate is limited e.g. by the detector dead time in both scenarios, the higher CHSH–Bell violation of the scenario with spatial entanglement leads to higher bit rates than the one of the conventional scenario.

We believe that these advantages could provide motivations for several experimental research groups to realize detection-loophole free Bell tests following the idea that Banaszek and Wodkiewicz [18] have initiated more than 15 years ago.

Acknowledgments

We thank V Scarani, T Barnea, and G Pütz for discussions and comments. This work was supported by the Swiss NCCR QSIT, the Swiss National Science Foundation SNSF (grant PP00P2 – 150579 and 'Early PostDoc. Mobility'), the European Commission (IP SIQS, Chist-era DIQIP), the Singapore Ministry of Education (partly through the Academic Research Fund Tier 3 MOE2012-T3-1-009) and the Singapore National Research Foundation.

References

[1] Jennewein T, Achleitner U, Weihs G, Weinfurter H and Zeilinger A 2000 *Rev. Sci. Instrum.* **71** 1675–80
[2] Stefanov A, Gisin N, Guinnard O, Guinnard L and Zbinden H 2000 *J. Mod. Opt.* **47** 4
[3] Dynes J F, Yuan Z L, Sharpe A W and Shields A J 2008 *Appl. Phys. Lett.* **93** 031109
[4] Pironio S *et al* 2010 *Nature* **464** 1021
[5] Colbeck R and Kent A 2011 *J. Phys. A: Math. Theor.* **44** 095305
[6] Brunner N, Cavalcanti D, Pironio S, Scarani V and Wehner S 2014 *Rev. Mod. Phys.* **86** 839
[7] Rowe M A, Kielpinski D, Meyer V, Sackett C A, Itano W M, Monroe C and Wineland D J 2001 *Nature* **409** 791
[8] Matsukevich D N, Maunz P, Moehring D L, Olmschenk S and Monroe C 2008 *Phys. Rev. Lett.* **100** 150404
[9] Hofmann J, Krug M, Ortegel N, Gérard L, Weber M, Rosenfeld W and Weinfurter H 2012 *Science* **337** 72
[10] Christensen B G *et al* 2013 *Phys. Rev. Lett.* **111** 130406
[11] Giustina M *et al* 2013 *Nature* **497** 227
[12] Lita A E, Miller A J and Nam S W 2008 *Opt. Express* **16** 3032
[13] Miller A J, Lita A E, Calkins B, Vayshenker I, Gruber S M and Nam S W 2011 *Opt. Express* **19** 9102–10
[14] Fukuda D *et al* 2011 *Opt. Express* **19** 870–5
[15] Verma V B, Korzh B, Bussières F, Horansky R D, Lita A E, Marsili F, Shaw M D, Zbinden H, Mirin R P and Nam S W 2014 *Appl. Phys. Lett.* **105** 122601

[16] Caprara Vivoli V, Sekatski P, Bancal J D, Lim C C W, Christensen B G, Martin A, Thew R T, Zbinden H, Gisin N and Sangouard N 2015 *Phys. Rev.* A **91** 012107
[17] Clauser J F, Horne M A, Shimony A and Holt R A 1969 *Phys. Rev. Lett.* **23** 880
[18] Banaszek K and Wodkiewicz K 1998 *Phys. Rev. Lett.* **82** 2009
[19] Tan S M, Walls D F and Collett M J 1991 *Phys. Rev. Lett.* **66** 252
[20] Chaves R and Brask J Bohr 2011 *Phys. Rev.* A **84** 062110
[21] Bohr Brask J, Chaves R and Brunner N 2013 *Phys. Rev.* A **88** 012111
[22] Torlai G, McKeown G, Marek P, Filip R, Jeong H, Paternostro M and De Chiara G 2013 *Phys. Rev.* A **87** 052112
[23] Seshadreesan K P, Wildfeuer C, Kim M B, Lee H and Dowling J P 2013 arXiv:1310.1410
[24] Hessmo B, Usachev P, Heydari H and Björk G 2004 *Phys. Rev. Lett.* **92** 180401
[25] D'Ariano G M, Lo Presti P and Perinotti P 2005 *J. Phys. A: Math. Gen.* **38** 5979–91
[26] Sekatski P, Sanguinetti B, Pomarico E, Gisin N and Simon C 2010 *Phys. Rev.* A **82** 053814
[27] Eberhard P H 1993 *Phys. Rev.* A **47** R747
[28] Garg A and Mermin N D 1987 *Phys. Rev.* D **35** 3831
[29] Larsson J-Å 1998 *Phys. Rev.* A **57** R3145
[30] Massar S and Pironio S 2003 *Phys. Rev.* A **68** 062109
[31] Clauser J and Horne M 1974 *Phys. Rev.* D **10** 526535
[32] Nieto-Silleras O, Pironio S and Silman J 2014 *New J. Phys.* **16** 013035
Bancal J-D, Sheridan L and Scarani V 2014 *New J. Phys.* **16** 033011
[33] Pomarico E, Sanguinetti B, Guerreiro T, Thew R and Zbinden H 2012 *Opt. Express* **20** 23846
[34] Guerreiro T, Martin A, Sanguinetti B, Bruno N, Zbinden H and Thew R T 2013 *Opt. Express* **21** 27641

4 Revealing Genuine Optical-Path Entanglement

Revealing Genuine Optical-Path Entanglement

F. Monteiro,[1] V. Caprara Vivoli,[1] T. Guerreiro,[1] A. Martin,[1] J.-D. Bancal,[2] H. Zbinden,[1] R. T. Thew,[1,*] and N. Sangouard[3,†]
[1]Group of Applied Physics, University of Geneva, CH-1211 Geneva 4, Switzerland
[2]Centre for Quantum Technologies, National University of Singapore, 3 Science Drive 2, Singapore 117543, Singapore
[3]Department of Physics, University of Basel, CH-4056 Basel, Switzerland
(Received 10 February 2015; published 1 May 2015)

How can one detect entanglement between multiple optical paths sharing a single photon? We address this question by proposing a scalable protocol, which only uses local measurements where single photon detection is combined with small displacement operations. The resulting entanglement witness does not require postselection, nor assumptions about the photon number in each path. Furthermore, it guarantees that entanglement lies in a subspace with at most one photon per optical path and reveals genuinely multipartite entanglement. We demonstrate its scalability and resistance to loss by performing various experiments with two and three optical paths. We anticipate applications of our results for quantum network certification.

DOI: 10.1103/PhysRevLett.114.170504 PACS numbers: 03.67.Mn, 03.65.Ud, 42.50.Dv

Optical path entanglement—entanglement between several optical paths sharing a single photon—is one of the simplest forms of entanglement to produce. It is also a promising resource for long-distance quantum communication where the direct transmission of photons through an optical fiber is limited by loss. In this context, loss can be overcome by using quantum repeaters, which require the creation and storage of entanglement in small-distance links and subsequent entanglement swapping operations between the links. Among the different quantum repeater schemes, those using path-entangled states $|1\rangle_A|0\rangle_B + |0\rangle_A|1\rangle_B$, where a single photon is delocalized into two nodes A and B are appealing—they require fewer resources and are less sensitive to memory and detector efficiencies compared to repeater architectures based, e.g., on polarization entanglement [1]. Many ingredients composing these networks have been experimentally demonstrated, including path entanglement based teleportation [2], entanglement swapping [3], purification [4], quantum storage [5,6], and an elementary network link [7].

A natural question is how this body of work could serve to extend known point-to-point quantum repeaters to richer geometries for quantum networks? Figure 1 presents a possible solution: A single photon incident on a multiport coupler generates entanglement over N output paths [see Fig. 1(a)], due to its nonclassical nature [8]. The small network created in this way can be entangled with other, potentially distant, networks via entanglement swapping operations using 50/50 beam splitters and single photon detectors—a single detection is then enough to entangle the remaining $2N$-2 nodes [see Fig. 1(b)]. Such 2D networks could open up new perspectives for multiuser quantum information processing including secret sharing [9] or secure multiparty quantum computation [10] as well as for experiments simulating quantum many-body system dynamics [11].

A central challenge, however, is to find an efficient, yet trustworthy, way to certify the functioning of these networks, i.e., how to characterize path entanglement in a distributed scenario using only local measurements. One might do this by using several copies of path-entangled states, as is the case for standard quantum repeater schemes [12]; however, doing so is resource demanding and addresses a restrictive class of applications—those accepting postselection. State tomography has also been realized [13] to characterize two-path entangled states but the exponential increase in measurements with the number of subsystems makes the tomographic approach impractical for detecting entanglement in large multipartite systems like quantum networks. Recently, an entanglement witness for bipartite path entangled states has been proposed and demonstrated; it is based on a Bell inequality combined with local homodyne detections [14,15]. However, it is not clear how this approach can be extended to more than two paths as even for three parties we know of no Bell inequality that can be violated for W-like states with measurements lying on the equator of the Bloch sphere (plane defined by eigenstates of Pauli matrices σ_x and σ_y).

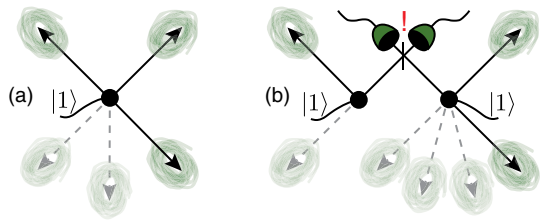

FIG. 1 (color online). Proposal to build up 2D networks over long distances. (a) Networks made with neighboring nodes are made with N-path entangled states. (b) These local networks can be connected remotely by means of entanglement swapping operations resulting in a large scale network.

In this Letter we propose an entanglement witness specifically developed to reveal path entanglement in distributed systems. It relies on an accurate description of measurement operators and assumes that each path is described by a single mode. However, it does not require postselection, nor assumptions about the photon number of the measured state; hence, it reveals entanglement in a trustworthy manner. Moreover, it only makes use of local measurements and easily scales to multipartite systems.

The principle of the witness is the following: N distant observers share a state ρ describing N optical paths. Assuming that each path is completely described by a single mode of the electromagnetic field, the aim is not only to say whether the overall state is entangled, but also to check that entanglement lies in a subspace with at most one photon in each mode and to check that entanglement is genuine. To do this, each observer uses a measurement combining a small displacement operation and a single photon detector, a measurement initially proposed in Refs. [16–18] and demonstrated in Ref. [19]. In the qubit subspace $\{|0\rangle, |1\rangle\}$, the POVM elements corresponding to click and no-click events of such a measurement can be seen as nonextremal projective measurements on the Bloch sphere whose direction depends on the amplitude and phase of the displacement [20]. In other words, if one considers nonphoton-number-resolving (NPNR) detectors with a quantum efficiency η and a small displacement $D(\alpha) = e^{\alpha a_i^\dagger - \alpha^\star a_i}$ operating on the mode i, the corresponding observable is given by

$$\sigma_\alpha^\eta = D^\dagger(\alpha)(2(1-\eta)^{a_i^\dagger a_i} - \mathbb{1})D(\alpha) \tag{1}$$

if one assigns the outcome $+1$ when the detector does not click and -1 when it clicks. If the measured state belongs to the subspace with at most one photon and with $\eta = 1$, σ_0 (the superscript is omitted when $\eta = 1$) corresponds to the Pauli matrix σ_z, i.e., a qubit measurement along the $\mathbf{z}$ direction. Similarly, for $\alpha = 1$ and $\alpha = i$, σ_1 and σ_i are a good approximation to qubit measurements along $\mathbf{x}$ and $\mathbf{y}$, respectively. We use this analogy to build up a fidelity-based entanglement witness of the form $\mathcal{Z}_N = N(2^N|W_N\rangle\langle W_N| - \mathbb{1})$, where $W_N = (1/\sqrt{N})\sum_{i=1}^N |0_1, \ldots, 1_i, \ldots 0_N\rangle$ refers to the state involving N modes sharing a single photon. We approximate this expression by the operator

$$\begin{aligned}\tilde{Z}_N = &\sum_{m=1}^{N}(N-2m)\sigma_0^{\otimes m} \otimes \mathbb{1}^{\otimes N-m} \\ &+ 2\sum_{m=0}^{N-2}\sigma_0^{\otimes m} \otimes \mathbb{1}^{\otimes N-2-m} \otimes (\sigma_\alpha \otimes \sigma_\alpha + \sigma_{i\alpha} \otimes \sigma_{i\alpha}) \\ &+ \text{sym},\end{aligned} \tag{2}$$

which only involves measurements of the form (1). $\sigma_0^{\otimes m} \otimes \mathbb{1}^{\otimes N-m}$ stand for a measurement in which the first m paths are measured with the observable σ_0 and the $N-m$ remaining ones are traced out. "sym" indicates that we add terms corresponding to permutations over all paths.

To make our witness suitable for experiments, we focus on the case where the displacements are phase averaged so that the relative phase of displacements is random but the phase of each displacement with respect to the state on which it operates is well controlled. Under this assumption, the statistics on outcomes obtained by measuring m paths with $\sigma_{|\alpha|e^{i\phi}}$ is the same for any ϕ. (α is decomposed into an absolute value times a phase factor. As the phase factor is irrelevant, we leave the absolute value in the rest of the Letter.) Hence, our witness reduces to

$$\begin{aligned}Z_N = (\Pi_{i=1}^N e^{i a_i^\dagger a_i \phi})\Big(&\sum_{m=1}^{N}(N-2m)\sigma_0^{\otimes m} \otimes \mathbb{1}^{\otimes N-m} \\ &+ 4\sum_{m=0}^{N-2}\sigma_0^{\otimes m} \otimes \mathbb{1}^{\otimes N-2-m} \otimes \sigma_\alpha \otimes \sigma_\alpha \\ &+ \text{sym}\Big)(\Pi_{i=1}^N e^{-i a_i^\dagger a_i \phi}),\end{aligned} \tag{3}$$

where ϕ is averaged out. In order to detect entanglement with Z_N, it is sufficient to compare its value to the maximum value $z_{\text{ppt},1}^{\max} = (1/2\pi)\int_0^{2\pi} d\phi \text{Tr}[Z_N\rho]$ that it can take if the projection of the state ρ in the $\{0,1\}$ subspace has a positive partial transposition (PPT) with respect to a single party. Indeed, the observation of a value of Z_N larger than $z_{\text{ppt},1}^{\max}$ implies by the Peres criterion [21,22] that the measured state is entangled and that the entanglement lies in the qubit subspace. Since finding $z_{\text{ppt},1}^{\max}$ constitutes a linear optimization problem with semidefinite positive constraints, it can be computed efficiently (see Supplemental Material [23]). Similarly, comparing the value of Z_N to $z_{\text{ppt}}^{\max}$, the maximum value of $z_{\text{ppt},s}^{\max}$ further optimized over all possible PPTs, reveals genuine multipartite entanglement.

As an example, consider the value that the witness would take, z_W, in a scenario without loss and involving a state W_N in which N optical paths share a single photon. We can compare this to the value $z_{\text{ppt}}^{\max}$ that would be achieved without genuine entanglement in the $\{|0\rangle, |1\rangle\}$ subspace. We show in the Supplemental Material [23] that

$$z_W - z_{\text{ppt}}^{\max} = 2^{N+3}\frac{N-1}{N}|\alpha|^2 e^{-2|\alpha|^2}, \tag{4}$$

which is positive for all N. The proposed witness thus has the capability to reveal genuine entanglement of W_N states for any path number. Note that $z_W - z_{\text{ppt}}^{\max}$ is maximized for $|\alpha|^2 = 1/2$. In practice, i.e., in the presence of loss, the value of α is reoptimized to make the difference $z_W - z_{\text{ppt}}^{\max}$ as large as possible.

When the measured state is not entirely contained in the $\{|0\rangle, |1\rangle\}$ subspace, contributions from higher photon numbers can increase the value $z_{\text{ppt}}^{\max}$. To get a valid bound in

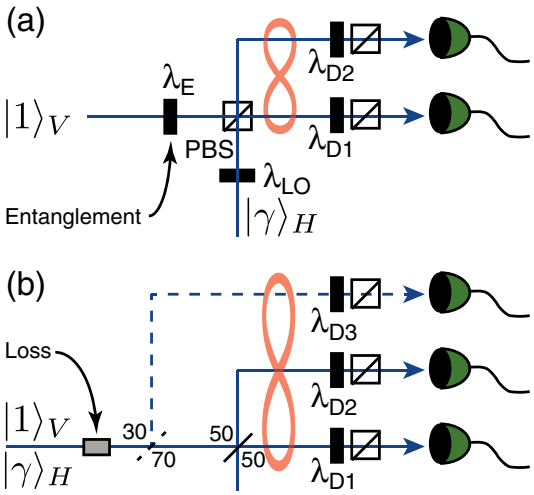

FIG. 2 (color online). Three different setups used to test the proposed entanglement witness for two and three parties: (a) The heralded state can be tuned from maximally entangled to separable by the half-wave plate (HWP) λ_E before the first polarizing beam splitter (PBS). The local oscillator is introduced at the other port of the PBS such that in each arm, the coherent state and the single photon have orthogonal polarization. The displacement operation is performed by rotating the HWPs at λ_{D1} and λ_{D2}. (b) The single photon and coherent state are input earlier in the setup with orthogonal polarizations. The input loss can be varied to study the robustness of the witness. This setup can be easily modified, by adding a 30/70 beam splitter and another (dashed) arm, allowing us to herald and probe a tripartite W state.

this regime, we used autocorrelation measurements in each mode. They give a bound on the probability of having more than one photon in each path ($p_c^{(i)}$ denotes this bound for mode i) and avoid making assumptions about the photon number. The computation of $z_{\mathrm{ppt}}^{\max}$ is then slightly modified to take the value of $p_c^{(i)}$ into account (see Supplemental Material [23]). Importantly, the autocorrelation measurements are performed locally with a beam splitter and two photon detectors. Overall, the number of measurements required to reveal genuine entanglement between N paths scales quadratically $(N^2/2 + N/2 + 1)$, which shows a much more favorable scaling compared to the exponential scaling of tomographic approaches.

We now report on a series of experiments demonstrating the feasibility of our witness. We prepare entangled networks made with 2 or 3 paths by sending single photons onto beam splitters; see Fig. 2. The photons are prepared using a heralded single photon source (HSPS) based on a bulk Periodically poled Lithium Niobate nonlinear crystal [24]. The crystal is pumped by a pulsed laser at 532 nm in the ps regime with a repetition rate of 430 MHz producing nondegenerate photons at 1550 and 810 nm via spontaneous parametric down conversion. The telecom photon is filtered down to 200 pm and subsequently detected by InGaAs single photon avalanche diodes (SPAD), producing pure heralded single photons at 810 nm—the purity is verified by measuring the second order autocorrelation function $g^2(0)$ [25]. To ensure a high fidelity entangled state, the pair creation probability per pulse is limited to 10^{-3}, to minimize the effect of double pairs, the photons are coupled with 90% efficiency [26] and the overall system transmission is optimized. We herald single-photon states at a rate of ~8 kHz.

The measurements are performed by combining displacement operations and single photon detection. The local oscillator for the displacements is generated in a similar PPLN nonlinear crystal pumped by the same 532 nm pulsed laser as well as a 1550 nm telecom cw laser—this ensures a high degree of indistinguishability between the HSPS and the local oscillator, which is confirmed by measuring a Hong-Ou-Mandel interference dip between the two sources, where the visibility is only limited by the statistics of the two sources [25]. Custom gated silicon SPADs are then used to detect the photons at 810 nm [27]. The detectors operate at 50% efficiency and have a dark-count probability of 10^{-2} per gate, for a gate width of approximately 2.3 ns.

To determine the value of the witness, which reduces to

$$Z_2 = \Pi_{i=1}^{2} e^{i a_i^\dagger a_i \phi} (2\sigma_\alpha \otimes \sigma_\alpha - \sigma_0 \otimes \sigma_0) e^{-i a_i^\dagger a_i \phi} \qquad (5)$$

in the bipartite case, we measure click (c) or no-click (0) events in the two paths and calculate the corresponding probabilities, $P_{00}, P_{0c}, P_{c0}, P_{cc}$, as well as the bounds on the probabilities for having more than one photon in each path, $p_c^{(1)}$ and $p_c^{(2)}$. The correlators of the form $\{\sigma_{\alpha'} \otimes \sigma_{\alpha'}\}$ in Eq. (5) then correspond to $P_{00} + P_{cc} - P_{0c} - P_{c0}$, for $\alpha' = \alpha$ or 0. We first block the single photon from going to the setup and apply the displacement operators in both arms, validating that $|\alpha|$ corresponds to the desired value. Experimentally, $|\alpha|$ is such that $P_c \sim P_0$ locally; see the Supplemental Material [23] Second, we allow the single photon to go to the setup and record the correlators with, and without, the displacement operations. An automated series of measurements is performed, integrating over 1 s for each setting, and is repeated as many times as needed to have good statistics. The values for $p_c^{(1)}$ and $p_c^{(2)}$ are dominated by detector noise due to operating the detectors at such high efficiencies so as to maximize the global efficiency of the measurements. These values are used to determine the observed value of Z_N labeled z_ρ^{exp} and the maximum value $z_{\mathrm{ppt}}^{\max}$ that would be obtained if the projection of the measured state in the $\{|0\rangle, |1\rangle\}$ subspace has a positive partial transpose (see Supplemental Material [23]).

To test the bipartite witness as a function of the amount of entanglement, the single photon and local oscillator are combined at different ports of a polarizing beam splitter ensuring that they leave in the same spatial mode with orthogonal polarizations; see Fig. 2(a). A half-wave plate λ_E placed in the single photon input arm is used to adjust the splitting ratio in the two output modes and the subsequent amplitudes for the entangled state. σ_α are

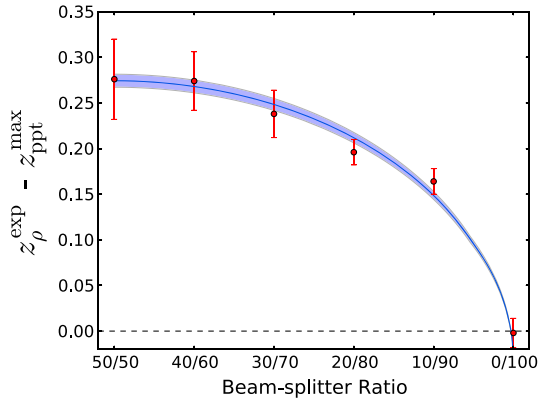

FIG. 3 (color online). Observed value for the bipartite entanglement witness (relatively to the PPT bound) as a function of the beam splitter ratio. Concretely, the half-wave plate λ_E in Fig. 2(a) is rotated which changes the state from a maximally entangled to a separable state (50/50–0/100 splitting ratio, respectively). The blue band is obtained from a theoretical model, taking into account the setup's global transmission, the characteristics of sources and gated detectors and the value for $|\alpha| \sim 0.83$ in the displacement operations.

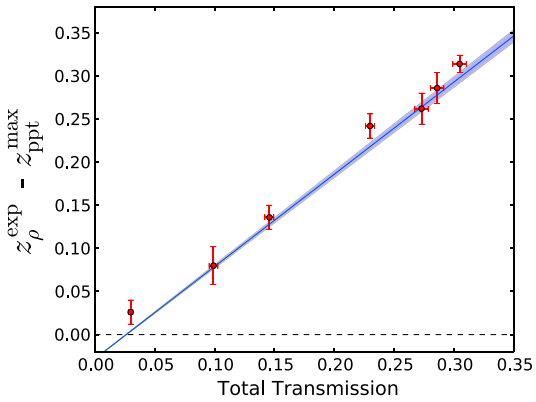

FIG. 4 (color online). Observed value for the bipartite entanglement witness (relatively to the PPT bound) as a function of loss. The total transmission consists of the photon coupling, transmission through the system, and detector efficiencies.

performed via a rotation of the wave plates λ_{D1}, λ_{D2} (< 1 degree) before the final PBSs. The amplitude of the displacement $|\alpha| \sim 0.83$ is set to maximize $z_\rho^{\exp} - z_{\text{ppt}}^{\max}$. Figure 3 shows the result as a function of the beam-splitter ratio, from maximally entangled (50/50) to a separable state (0/100). The shaded line is obtained from a theoretical model with independently measured system parameters, with the associated uncertainty (see Supplemental Material [23]). The theory and experimental results are in excellent agreement and prove that the proposed witness can reveal even very small amounts of entanglement.

To prove the robustness of this witness against loss, and demonstrate the scalability, we introduce a different experimental configuration, Fig. 2(b), with only a 50/50 beam splitter, to generate maximally entangled states, and the single photon and local oscillator are combined earlier in the setup. We can then introduce loss to the input state, thus increasing the mixedness of the state. Figure 4 shows the value of our witness of entanglement as we increase loss. The starting point has a slightly larger value than in Fig. 3, due to a slightly better transmission. Note that the maximum transmission of $\gtrsim$30% includes photon coupling, transmission, and detection efficiency. Here we see that the witness is capable of revealing entanglement even in the case of high loss, or similarly, for low detection efficiency.

Finally, by adding a 30/70 beam splitter and another arm, dashed line in Fig. 2(b), we herald tripartite states. If we assume perfect transmission and detectors with unit efficiency, we expect a maximum value for $z_\rho^{\exp} - z_{\text{ppt}}^{\max} \sim 7.63$, where a value greater than zero indicates the presence of genuine entanglement. By applying our model, similarly to the bipartite case, again with $|\alpha| \sim 0.83$, but with total transmissions in each arm of 0.19 ± 0.002, we expect to find a theoretical value of 0.99 (see Supplemental Material [23]). We found a value of 0.99 ± 0.10 that agrees with our model and shows a clear violation, thus revealing genuine tripartite path entanglement.

In conclusion, we have shown an entanglement witness suited for path entangled states that is robust and scalable, providing the means for the characterization of genuine multipartite entanglement distributed over complex quantum networks. The copropagation of the local oscillator with the path entangled state overcomes the potential problem of distributing a phase reference, which also has the added advantage that it could be exploited for stabilization and synchronization of distributed networks. Interestingly, our witness provides a trustworthy means to reveal entanglement, without the need to make assumptions about the number of photons in each path. A possible extension would be to make it fully device independent through the violation of a Bell inequality, which would require higher overall efficiencies [20,28].

The authors would like to thank M. Ho, P. Sekatski, and F. Fröwis for stimulating discussions. This work was supported by the Swiss NCCR QSIT, the Swiss National Science Foundation SNSF (Grant No. PP00P2-150579), the EU project SIQS and Chist-Era: DIQIP and Qscale, as well as the Singapore Ministry of Education (partly through the Academic Research Fund Tier 3 MOE2012-T3-1-009) and the Singapore National Research Foundation. F. M. and V. C. V. contributed equally to this work.

*robert.thew@unige.ch
†nicolas.sangouard@unibas.ch

[1] N. Sangouard, C. Simon, H. de Riedmatten, and N. Gisin, Rev. Mod. Phys. **83**, 33 (2011).
[2] E. Lombardi, F. Sciarrino, S. Popescu, and F. Martini, Phys. Rev. Lett. **88**, 070402 (2002).

[3] F. Sciarrino, E. Lombardi, G. Milani, and F. Martini, Phys. Rev. A **66**, 024309 (2002).
[4] D. Salart, O. Landry, N. Sangouard, N. Gisin, H. Herrmann, B. Sanguinetti, C. Simon, W. Sohler, R. T. Thew, A. Thomas *et al.*, Phys. Rev. Lett. **104**, 180504 (2010).
[5] C. W. Chou, H. de Riedmatten, D. Felinto, S. V. Polyakov, S. J. van Enk, and H. J. Kimble, Nature (London) **438**, 828 (2005).
[6] K. S. Choi, H. Deng, J. Laurat, and H. J. Kimble, Nature (London) **452**, 67 (2008).
[7] C.-W. Chou, J. Laurat, H. Deng, K. S. Choi, H. de Riedmatten, D. Felinto, and H. J. Kimble, Science **316**, 1316 (2007).
[8] J. K. Asbóth, J. Calsamiglia, and H. Ritsch, Phys. Rev. Lett. **94**, 173602 (2005).
[9] M. Hillery, V. Bužek, and A. Berthiaume, Phys. Rev. A **59**, 1829 (1999).
[10] C. Crépeau, D. Gottesman, and A. Smith, in Proceedings of the Thirty-Fourth Annual ACM Symposium on Theory of Computing (2002), STOC '02, (Wiley, New York, 2002), p. 643.
[11] H. J. Kimble, Nature (London) **453**, 1023 (2008).
[12] L. M. Duan, M. D. Lukin, J. I. Cirac, and P. Zoller, Nature (London) **414**, 413 (2001).
[13] S. A. Babichev, J. Appel, and A. I. Lvovsky, Phys. Rev. Lett. **92**, 193601 (2004).
[14] O. Morin, J.-D. Bancal, M. Ho, P. Sekatski, V. D'Auria, N. Gisin, J. Laurat, and N. Sangouard, Phys. Rev. Lett. **110**, 130401 (2013).
[15] M. Ho, O. Morin, J.-D. Bancal, N. Gisin, N. Sangouard, and J. Laurat, New J. Phys. **16**, 103035 (2014).
[16] S. M. Tan, D. F. Walls, and M. J. Collett, Phys. Rev. Lett. **66**, 252 (1991).
[17] L. Hardy, Phys. Rev. Lett. **73**, 2279 (1994).
[18] K. Banaszek and K. Wodkiewicz, Phys. Rev. Lett. **82**, 2009 (1999).
[19] B. Hessmo, P. Usachev, H. Heydari, and G. Björk, Phys. Rev. Lett. **92**, 180401 (2004).
[20] V. Caprara Vivoli, P. Sekatski, J.-D. Bancal, C. C. W. Lim, A. Martin, R. T. Thew, H. Zbinden, N. Gisin, and N. Sangouard, New J. Phys. **17**, 023023 (2015).
[21] A. Peres, Phys. Rev. Lett. **77**, 1413 (1996).
[22] M. Horodecki, P. Horodecki, and R. Horodecki, Phys. Lett. A **223**, 1 (1996).
[23] See Supplemental Material at http://link.aps.org/supplemental/10.1103/PhysRevLett.114.170504 for description of the theoretical details.
[24] E. Pomarico, B. Sanguinetti, T. Guerreiro, R. T. Thew, and H. Zbinden, Opt. Express **20**, 23846 (2012).
[25] N. Bruno, A. Martin, and R. T. Thew, Opt. Commun. **327**, 17 (2014).
[26] T. Guerreiro, A. Martin, B. Sanguinetti, N. Bruno, H. Zbinden, and R. T. Thew, Opt. Express **21**, 27641 (2013).
[27] T. Lunghi, E. Pomarico, C. Barreiro, D. Stucki, B. Sanguinetti, and H. Zbinden, Appl. Opt. **51**, 8455 (2012).
[28] J. B. Brask, R. Chaves, and N. Brunner, Phys. Rev. A **88**, 012111 (2013).

5 Proposal for an Optomechanical Bell test

Proposal for an Optomechanical Bell Test

V. Caprara Vivoli,[1] T. Barnea,[1] C. Galland,[2] and N. Sangouard[3]
[1]Group of Applied Physics, University of Geneva, CH-1211 Geneva 4, Switzerland
[2]Ecole Polytechnique Federale de Lausanne (EPFL), CH-1015 Lausanne, Switzerland
[3]Department of Physics, University of Basel, CH-4056 Basel, Switzerland
(Received 26 June 2015; revised manuscript received 9 October 2015; published 18 February 2016)

Photons of a laser beam driving the upper motional sideband of an optomechanical cavity can decay into photon-phonon pairs by means of an optomechanical parametric process. The phononic state can subsequently be mapped to a photonic state by exciting the lower sideband, hence creating photon-photon pairs out of an optomechanical system. Here we show that these pairs can violate a Bell inequality when they are measured with photon counting techniques preceded by small displacement operations in phase space. The consequence of such a violation as well as the experimental requirements are intensively discussed.

DOI: 10.1103/PhysRevLett.116.070405

Introduction.—Cavity optomechanics, which describes a mechanical oscillator controlled by an electromagnetic cavity mode via a generalized radiation pressure force, is the subject of intense research [1–3]. Most recent progress includes the cooling of mechanical oscillators down to the ground state [4–6], the readout of the mechanical position with a readout imprecision below the standard quantum limit [7] as well as optomechanical squeezing [8,9] and entanglement [10]. Reciprocally, the mechanical degrees of freedom can be used to control the cavity light, e.g., for fast and slow light [11,12], frequency conversions [13,14], squeezing [15], and information storage in long-lived mechanical oscillations [10,16].

Optomechanical systems are also envisioned as test benches for physical theories [17–23]. As a step in this direction, quantum correlations between light and mechanics have been observed recently [10]. In this experiment, quantum features have been detected through an entanglement witness where one assumes that the measurement devices are well characterized and where quantum theory is used to predict the results of these measurements on separable states. It is interesting to wonder whether the nonclassical behavior of optomechanical systems can be certified outside of the quantum formalism, i.e., from a Bell test [24]. This is particularly relevant to test postquantum theories including explicit collapse models [25–28], where the assumption that the system behaves quantum mechanically may be questionable [29].

In this Letter, we show how to perform such a Bell test in the experimentally relevant weak-optomechanical coupling and sideband-resolved regime. Our proposal, which starts with a mechanical oscillator close to its ground state, consists of two steps. First, the optomechanical system is excited by a laser tuned to the upper motional sideband of the cavity to create photon-phonon pairs via optomechanical parametric conversion. Second, a laser resonant with the lower sideband is used to map the phononic state to the cavity field. The correlations between the photons generated at the cavity frequency during the first and second steps are then analyzed by photon counting preceded by small displacement operations in phase space. We show that they violate the Bell-CHSH (Clauser-Horne-Shimony-Holt) inequality [30], revealing that the optomechanical state is nonlocal, i.e., provides stronger correlations than entanglement [31]. This claim is device independent, i.e., holds without assumptions on the dimension of the underlying Hilbert space or on the precise alignment of the measurement settings [32]. While several requirements are challenging to meet in practice, our proposal can be seen as a natural extension of ongoing experiments [33] performing photon counting in optomechanical cavities.

Principle of the optomechanical Bell test.—The basic principle is inspired by Refs. [34,35] and is represented in Fig. 1. We use two laser pulses driving either the upper or the lower optomechanical sideband, at frequency $\omega_\pm$, which is the sum or the difference of the cavity (ω_c) and the mechanical (Ω_m) frequencies. The optomechanical Hamiltonian includes $H_0 = \hbar\omega_c a^\dagger a + \hbar\Omega_m b^\dagger b$, the uncoupled cavity and mechanical systems with respective bosonic operators a and b, $H_{\mathrm{OM}} = -\hbar g_0 a^\dagger a(b^\dagger + b)$, the optomechanical interaction with g_0 the optomechanical coupling, and $H_l = \hbar(s_\pm^* e^{i\omega_\pm t} a + s_\pm e^{-i\omega_\pm t} a^\dagger)$, the driving laser with $|s_\pm| = \sqrt{\kappa P_\pm/\hbar\omega_\pm}$, $P_\pm$ being the laser power and κ the cavity decay rate (assuming that the intracavity loss is negligible). In the interaction picture, the weak coupling limit $g_0 \ll \kappa$ and the resolved sideband regime $\kappa \ll \Omega_m$, the dynamics are given by a set of Langevin equations,

$$\frac{da}{dt} = \frac{i}{\hbar}[H_\pm, a] - \frac{\kappa}{2}a + \sqrt{\kappa}a_{\mathrm{in}}, \tag{1}$$

$$\frac{db}{dt} = \frac{i}{\hbar}[H_\pm, b] - \frac{\gamma}{2}b + \sqrt{\gamma}b_{\mathrm{in}}, \tag{2}$$

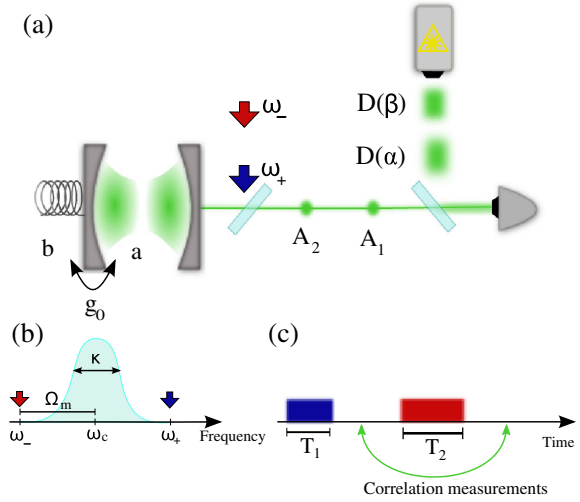

FIG. 1. (a) Principle of the proposed Bell test. Starting with the mechanical system in its motional ground state, a first laser excites the blue detuned sideband to create correlated photon-phonon pairs. A second laser then drives the red detuned sideband to coherently convert the phonons into photons. The resulting photons pairs (mode A_1 and A_2) are analyzed using a photon detector preceded by a displacement in phase space. (b) Cavity linewidth κ and its two sidebands ($\omega_\pm$) detuned from the cavity frequency ω_c by the mechanical frequency (ω_m). (c) Pulse sequence in time. The first laser resonantly excites the blue sideband while the second laser is resonant with the red sideband.

with the linearized Hamiltonians $H_+ = -g_+\hbar a^\dagger b^\dagger + \text{H.c.}$ for a blue detuned drive and $H_- = -g_-\hbar a^\dagger b + \text{H.c.}$ for a red detuned drive. $g_\pm$ are the effective optomechanical coupling rates enhanced by the intracavity photon number $g_\pm = g_0\sqrt{n_\pm} = (\kappa P_\pm/\hbar\omega_c(\Omega_m^2 + \kappa^2/4))$. a_{in} is the vacuum noise entering the cavity. We assume that the laser is shot-noise limited; hence, it does not add contributions to the input noise. b_{in} is the thermal noise from a phonon bath at temperature T_{bath} and mean occupation number $n_{\text{th}} = (k_B T_{\text{bath}}/\hbar\Omega_m)$. In the following treatment, we neglect the mechanical decay which is well justified for time scales smaller than the thermal decoherence time $1/\gamma n_{\text{th}}$, γ being the coupling rate between the mechanical oscillator and the thermal bath.

Consider first the case where the mechanics is driven by a blue detuned laser. In the regime $g_+ \ll \kappa$, the cavity mode can be adiabatically eliminated and Eq. (1) leads to $a_1 = (2/\kappa)(ig_+ b^\dagger + \sqrt{\kappa}a_{1,\text{in}})$ (the subscript on the cavity field operators is used to recall that we are considering the first step). Further, introducing the input-output relation, $a_{1,\text{out}} = -a_{1,\text{in}} + \sqrt{\kappa}a_1$, we obtain

$$a_{1,\text{out}} = a_{1,\text{in}} + i\sqrt{2\bar{g}_+}b^\dagger, \tag{3}$$

$$\frac{db}{dt} = \bar{g}_+ b + i\sqrt{2\bar{g}_+}a_{1,\text{in}}^\dagger, \tag{4}$$

where $\bar{g}_+ = (2g_+^2/\kappa)$. To solve these coupled equations, we follow Hofer *et al.* [35] and introduce the temporal modes $A_{1,\text{in}}(t) = \sqrt{(2\bar{g}_+/1-e^{-2\bar{g}_+ t})}\int_0^t dt' e^{-\bar{g}_+ t'} a_{1,\text{in}}(t')$, $A_{1,\text{out}}(t) = \sqrt{(2\bar{g}_+/e^{2\bar{g}_+ t}-1)}\int_0^t dt' e^{\bar{g}_+ t'} a_{1,\text{out}}(t')$. The solutions of Eqs. (3) and (4) take the following simple forms: $A_{1,\text{out}}(t) = e^{\bar{g}_+ t}A_{1,\text{in}}(t) + i\sqrt{e^{2\bar{g}_+ t}-1}b^\dagger(0)$, $b(t) = e^{\bar{g}_+ t}b(0) + i\sqrt{e^{2\bar{g}_+ t}-1}A_{1,\text{in}}^\dagger(t)$. These solutions can be rewritten as $A_{1,\text{out}} = \tilde{U}_1^\dagger(t)A_{1,\text{in}}\tilde{U}_1(t)$ and $b(t) = \tilde{U}_1^\dagger(t)b(0)\tilde{U}_1(t)$, where the propagator is given by

$$\tilde{U}_1(t) = e^{i\sqrt{1-e^{-2\bar{g}_+ t}}A_{1,\text{in}}^\dagger b^\dagger} \times e^{\bar{g}_+ t(-1-A_{1,\text{in}}^\dagger A_{1,\text{in}} - b^\dagger b)} e^{i\sqrt{1-e^{-2\bar{g}_+ t}}A_{1,\text{in}} b}. \tag{5}$$

When applied on the vacuum, this propagator leads to the creation of photon-phonon pairs where the number of photons equals the number of phonons, each of them following a thermal statistics with mean excitation number $e^{2\bar{g}_+ t} - 1$.

Now consider the case where the mechanics is driven by a red detuned laser; i.e., the dynamics is given by the beam splitter Hamiltonian H_-. Following the same procedure as before, Eqs. (3) and (4) become

$$a_{2,\text{out}} = a_{2,\text{in}} + i\sqrt{2\bar{g}_-}b, \tag{6}$$

$$\frac{db}{dt} = -\bar{g}_- b + i\sqrt{2\bar{g}_-}a_{2,\text{in}}, \tag{7}$$

where $\bar{g}_- = (2g_-^2/\kappa)$. Introducing the modes $A_{2,\text{in}}(t) = \sqrt{(2\bar{g}_-/e^{2\bar{g}_- t}-1)}\int_0^t dt' e^{\bar{g}_- t'} a_{2,\text{in}}(t')$, $A_{2,\text{out}}(t) = \sqrt{(2\bar{g}_-/1-e^{-2\bar{g}_- t})}\int_0^t dt' e^{-\bar{g}_- t'} a_{2,\text{out}}(t')$ leads to the simple expression for the solutions of Eqs. (6) and (7) at a time t after the beginning of the red detuned pulse $A_{2,\text{out}}(t) = e^{-\bar{g}_- t}A_{2,\text{in}}(t) + i\sqrt{1-e^{-2\bar{g}_- t}}b(0)$, $b(t) = e^{-\bar{g}_- t}b(0) + i\sqrt{1-e^{-2\bar{g}_- t}}A_{2,\text{in}}(t)$. These solutions can be rewritten as $A_{2,\text{out}} = \tilde{U}_2^\dagger(t)A_{2,\text{in}}\tilde{U}_2(t)$ and $b(t) = \tilde{U}_2^\dagger(t)b(0)\tilde{U}_2(t)$, where the propagator is given by

$$\tilde{U}_2(t) = e^{i\sqrt{e^{2\bar{g}_- t}-1}A_{2,\text{in}} b^\dagger} \times e^{-\bar{g}_- t(A_{2,\text{in}}^\dagger A_{2,\text{in}} - b^\dagger b)} e^{i\sqrt{e^{2\bar{g}_- t}-1}A_{2,\text{in}}^\dagger b}. \tag{8}$$

This corresponds to a process converting a phonon into a photon with probability $1 - e^{-2\bar{g}_- t}$.

Now consider an initial state where both optical modes A_1 and A_2 are empty and where the mechanics is prepared in its ground state. Switching on the blue detuned laser for a time T_1, then the red detuned laser for a time T_2, leads to a photon-photon state in mode $A_{1,\text{out}}$, $A_{2,\text{out}}$ given by $\rho_{A_1,A_2} = \text{Tr}_b \tilde{U}_2(T_2)\tilde{U}_1(T_1)|0,0,0\rangle_{A_{1,\text{in}},A_{2,\text{in}},b}\langle 0,0,0|\tilde{U}_1^\dagger(T_1)\tilde{U}_2^\dagger(T_2)$. In the ideal limit $\bar{g}_- T_2 \to +\infty$, the phonon-photon mapping is perfect and the state ρ_{A_1,A_2} corresponds to a

two-mode squeezed vacuum. In the general case where $\bar{g}_- T_2$ has a finite value, ρ_{A_1,A_2} still corresponds to a squeezed vacuum but where the mode A_2 undergoes loss. This loss can be modeled by a beam splitter with a transmission $T = 1 - e^{-2\bar{g}_- t}$. The next section shows how to reveal the nonlocal content of such a state.

In order to test a Bell inequality with the modes $A_{1,\mathrm{out}}$, $A_{2,\mathrm{out}}$ (the subscript "out" is omitted below), we consider a single-photon detector—which does not resolve the photon number—combined with a displacement operation $D(\alpha)$. We associate the outcome $+1$ (-1) to the absence of detection (to the detection of at least one photon) at least one photon. In the subspace composed of the vacuum and the single-photon Fock state, such a measurement corresponds exactly to the observable σ_z for $\alpha = 0$, while for $\alpha = 1$ $(\alpha = i)$ it is a noisy σ_x (σ_y) [36]. The potential of such measurements for nonlocality detection has been highlighted in Refs. [37,38], for example. Reference [39] has also shown how they can be used for Bell tests in photonic experiments where two-mode squeezed states are produced through spontaneous parametric down-conversion. More recently, they have been used to reveal genuine path entanglement [40]. Further note that a displacement is easy to implement in practice as it requires a coherent state and an unbalanced beam splitter only [41].

The joint probability $P(+1+1|\alpha_1\alpha_2)$ to get the outcomes $+1$ for both A_1 and A_2 when they are analyzed with photon counting with efficiency η preceded by displacements with amplitude α_1 and α_2 for A_1 and A_2, respectively, is given by $P(+1+1|\alpha_1\alpha_2) = \mathrm{Tr}[\rho_{A_1,A_2}\mathcal{O}_\eta(\alpha_1, A_1) \otimes \mathcal{O}_\eta(\alpha_2, A_2)]$, where $\mathcal{O}_\eta(\alpha_i, A_i) = D^\dagger(\alpha_i)(1-\eta)^{A_i^\dagger A_i} D(\alpha_i)$. Such a probability can be computed easily by noting that loss and displacement can be commuted by changing the amplitude of the displacement. In particular, $P(+1+1|\alpha_1\alpha_2) = \mathrm{Tr}[\bar{\rho}_{A_1,A_2}\mathcal{O}_\eta(\alpha_1, A_1) \otimes \mathcal{O}_{\eta'}(\alpha_2\sqrt{T}, A_2)]$, where $\eta' = \eta T$, and $\bar{\rho}_{A_1,A_2} = (1-p)e^{-\sqrt{p}A_1^\dagger A_2^\dagger}|0\rangle_{A_1,A_2}\langle 0|e^{-\sqrt{p}A_1 A_2}$ is simply the two-mode squeezed vacuum. $(1-p = e^{-2\bar{g}_+ T_1}$ is the probability that both modes are empty.) We find

$$P(+1+1|\alpha_1\alpha_2) = \frac{(1-p)}{1-p(1-\eta)(1-\eta')} e^{-\{\eta|\alpha_1|^2[1-(1-\eta')p]+\eta'|\alpha_2|^2 T[1-(1-\eta)p]\}/[1-p(1-\eta)(1-\eta')]} e^{\eta\eta'\sqrt{p}(\alpha_1^*\alpha_2^*+\alpha_1\alpha_2)\sqrt{T}/[1-p(1-\eta)(1-\eta')]}. \tag{9}$$

Together with the marginals

$$P(+1|\alpha_1) = \frac{(1-p)}{1-p(1-\eta)} \times e^{-\eta(1-p)|\alpha_1|^2/[1-p(1-\eta)]},$$
$$P(+1|\alpha_2) = \frac{(1-p)}{1-p(1-\eta')} \times e^{-\eta'(1-p)|\alpha_2|^2 T/[1-p(1-\eta')]},$$

we get the explicit value of the correlator $E^{\alpha_1,\alpha_2} = 1 - 2[P(+1|\alpha_1) + P(+1|\alpha_2)] + 4P(+1+1|\alpha_1\alpha_2)$ to test the Bell-CHSH inequality, $\mathrm{CHSH} = |E^{\alpha_1,\alpha_2} + E^{\alpha_1',\alpha_2} + E^{\alpha_1,\alpha_2'} - E^{\alpha_1',\alpha_2'}| \leq 2$, which holds for any local hidden-variable model.

Figure 2 shows the CHSH values obtained from the optimization over the measurement settings α_i, α_i', $i \in [1,2]$ as a function of the photon-phonon mapping efficiency $T = 1 - e^{-2\bar{g}_- t}$ for various detection efficiencies η. For high enough T and η, we see that the CHSH inequality is violated, hence, showing that the correlations of modes A_1 and A_2 cannot be reproduced by local hidden-variable theories.

In the above discussion, we have assumed that the mechanical system is prepared in its ground state. In the more general case it is in a thermal state with mean occupation number n_0; the expressions of the joint probability $P(+1+1|\alpha_1\alpha_2)$ and the marginals $P(+1|\alpha_i)$ can be derived as before; cf. Ref. [42], part I. The CHSH values resulting from the optimization over the measurement settings are given in Fig. 3 as a function of the phonon-photon mapping efficiency for various mean mechanical occupation numbers assuming unit detection efficiencies. A substantial violation can be obtained if $n_0 \ll 1$.

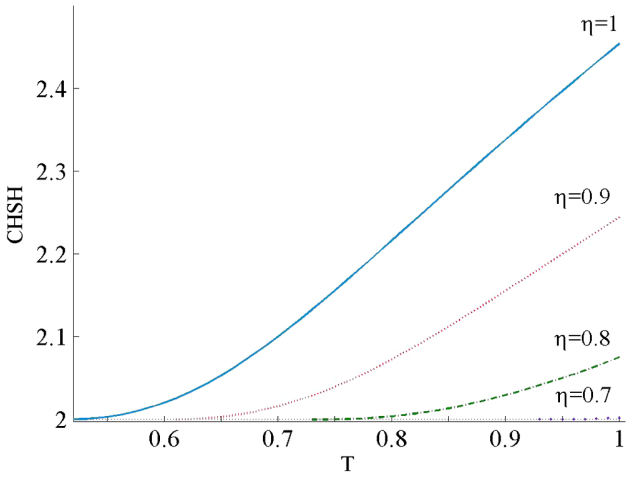

FIG. 2. CHSH values optimized over the measurement settings (α_1, α_2) as a function of the optomechanical mapping efficiency $(T = 1 - e^{-2\bar{g}_- t})$ for various detection efficiencies η. The CHSH value is larger than the local bound 2 for unit detection efficiencies when $T \geq 52\%$, while for unit phonon-photon mapping efficiency, $\eta \geq 66.8\%$ is required.

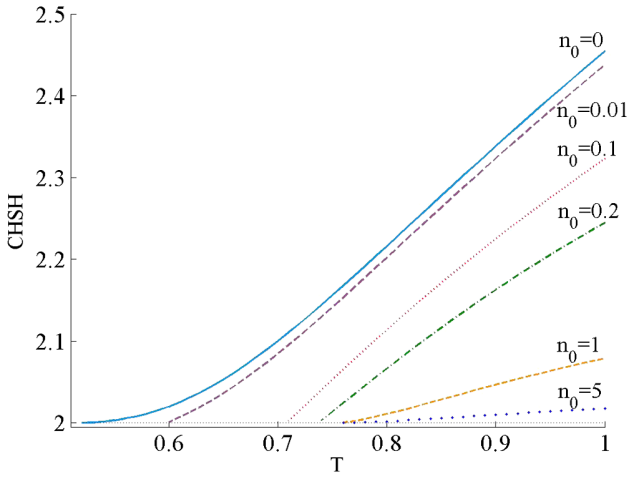

FIG. 3. CHSH values as a function of the optomechanical mapping efficiency ($T = 1 - e^{-2\bar{g}_- t}$) for various mechanical occupation numbers (n_0) assuming unit detection efficiencies ($\eta = 1$).

Feasibility.—In this paragraph, we discuss the experimental feasibility of the proposed Bell test in detail. The requirements for detecting nonlocality are (i) sideband regime $\kappa \ll \Omega_m$, (ii) weak coupling regime $g_0 \ll \kappa$, (iii) ground state cooling $n_0 \ll 1$ and negligible mechanical decoherence during the durations of blue and red detuned laser pulses $T_1 + T_2 \ll (\gamma n_{\rm th})^{-1}$. Given that $n_{\rm th} \propto \Omega_m^{-1}$, these conditions are easier to meet with high Q and high frequency Ω_m oscillators. While superconducting microwave optomechanical cavity systems are promising [44], we focus on an implementation of our Bell test with a photonic crystal nanobeam resonator [6,45,46] that distinguishes itself by a very high mechanical frequency $\Omega_m/2\pi = 5$ GHz. This frequency together with its optical linewidth $\kappa/2\pi < 1$ GHz places this resonator in the resolved sideband regime [45]. The optomechanical coupling rate is large $g_0/2\pi \approx 1$ MHz [45], and mechanical coherence times of the order of 10–100 μs are expected at 4 K and below [45,47]. With a bath temperature $T_{\rm bath} \approx 1.6$ K, an initial occupancy of $n_0 = 0.01$ can be achieved in 100 ns of sideband cooling with 1000 (intracavity) photons corresponding to a peak laser power of 150 μW [34]. For almost squared pulses with rising time of the order of 1 ns, we get pure and noiseless emissions as expected from two-mode squeeezed states [34]. For $T_1 = 25$ ns and $T_2 = 50$ ns, we find CHSH $= 2.19$ assuming $\eta = 90\%$ detection efficiency, fixing $n_- = 250$, and optimizing the CHSH value over $n_+ = 75$, and over the measurement settings. As the present scheme relies on the ability to accurately and repeatedly address the optomechanical sidebands, a continuous monitoring is required to correct the unavoidable broadband frequency noise of the cavity. Furthermore, the scattered photon pairs have to be spectrally filtered from the pump lasers. To account for an imperfect filtering of both the cavity locking and pump lasers, we include a background noise in the detection that we model as dark counts. We found that the CHSH violation (CHSH $= 2.19$) is unchanged if the dark count probability is of $\leq 10^{-3}$. This sets the constraints on the quality of the filtering processes once the intrinsic noise of the detector is determined. Note that for state-of-the-art-detectors, the noise can be of the order of 10^{-7} or 10^{-8} for detection windows of a few tens of ns.

Perspectives.—Our results show how optomechanical systems can be used to test a Bell inequality. They provide an attractive perspective for the experiment reported in Ref. [33], where a mechanical system is combined with photon counting techniques. Achieving high overall detection efficiencies is facilitated by photons emitted in a well-defined spatial mode which may be coupled into a single-mode fiber with a very high efficiency. Moreover, the wavelength of photons at 1550 nm is an appealing asset to perform the Bell test between distant locations, i.e., to close the locality loophole; see Ref. [42] part II. We also note that our results can find interesting perspectives in quantum memory experiments. In the context of light storage, off-resonant Raman scattering can be used to create photon-spin wave pairs in atomic ensembles [48]. The spin-wave state can then be mapped to photons using a resonant Raman process—this mapping is made very efficient thanks to a collective emission. Since the resulting photon-photon state is analog to the one described in this Letter, the Bell test that we propose would allow one to certify that the memory operates in the quantum regime.

We thank K. Hammerer and S. Hofer for having pointed out the interest of an optomechanical Bell test at an early stage of this work. This work was supported by the Swiss National Science Foundation (SNSF), through Grant No. PP00P2-150579, the Swiss NCCR QSIT, and a SNSF Ambizione Fellowship, as well as by the Swiss State Secretariat for Education and Research through the COST Action MP1006.

Note added—While our proposal focuses on optomechanical systems, a Bell test can be performed with electromechanical systems. Recently, we became aware of a proposal along this line by Hofer *et al.* [49].

[1] T. J. Kippenberg and K. J. Vahala, Science **321**, 1172 (2008).
[2] P. Meystre, Ann. Phys. (Berlin) **525**, 215 (2013).
[3] M. Aspelmeyer, T. J. Kippenberg, and F. Marquardt, Rev. Mod. Phys. **86**, 1391 (2014).
[4] A. D. O'Connell, M. Hofheinz, M. Ansmann, R. C. Bial-czak, M. Lenander, E. Lucero, M. Neeley, D. Sank, H. Wang, M. Weides, J. Wenner, J. M. Martinis, and A. N. Cleland, Nature (London) **464**, 697 (2010).

[5] J. D. Teufel, T. Donner, D. Li, J. W. Harlow, M. S. Allman, K. Cicak, A. J. Sirois, J. D. Whittaker, K. W. Lehnert, and R. W. Simmonds, Nature (London) **475**, 359 (2011).
[6] J. Chan, T. P. M. Alegre, A. H. Safavi-Naeini, J. T. Hill, A. Krause, S. Groblacher, M. Aspelmeyer, and O. Painter, Nature (London) **478**, 89 (2011).
[7] G. Anetsberger, E. Gavartin, O. Arcizet, Q. P. Unterreithmeier, E. M. Weig, M. L. Gorodetsky, J. P. Kotthaus, and T. J. Kippenberg, Phys. Rev. A **82**, 061804 (2010).
[8] E. E. Wollman, C. U. Lei, A. J. Weinstein, J. Suh, A. Kronwald, F. Marquart, A. A. Clerk, and K. C. Schwab, Science **349**, 952 (2015).
[9] J.-M. Pirkkalainen, E. Damskagg, M. Brandt, F. Massel, and M. A. Sillanpaa, Phys. Rev. Lett. **115**, 243601 (2015).
[10] T. A. Palomaki, J. D. Teufel, R. W. Simmonds, and K. W. Lehnert, Science **342**, 710 (2013).
[11] A. H. Safavi-Naeini, T. P. M. Alegre, J. Chan, M. Eichenfield, M. Winger, Q. Lin, J. T. Hill, D. E. Chang, and O. Painter, Nature (London) **472**, 69 (2011).
[12] X. Zhou, F. Hocke, A. Schliesser, A. Marx, H. Huebl, R. Gross, and T. J. Kippenberg, Nat. Phys. **9**, 179 (2013).
[13] J. Bochmann, A. Vainsencher, D. D. Awschalom, and A. N. Cleland, Nat. Phys. **9**, 712 (2013).
[14] R. W. Andrews, R. W. Peterson, T. P. Purdy, K. Cicak, R. W. Simmonds, C. A. Regal, and K. W. Lehnert, Nat. Phys. **10**, 321 (2014).
[15] A. H. Safavi-Naeini, S. Groeblacher, J. T. Hill, J. Chan, M. Aspelmeyer, and O. Painter, Nature (London) **500**, 185 (2013).
[16] V. Fiore, Y. Yang, M. C. Kuzyk, R. Barbour, L. Tian, and H. Wang, Phys. Rev. Lett. **107**, 133601 (2011).
[17] S. Bose, K. Jacobs, and P. L. Knight, Phys. Rev. A **59**, 3204 (1999).
[18] W. Marshall, C. Simon, R. Penrose, and D. Bouwmeester, Phys. Rev. Lett. **91**, 130401 (2003).
[19] P. Sekatski, M. Aspelmeyer, and N. Sangouard, Phys. Rev. Lett. **112**, 080502 (2014).
[20] R. Ghobadi, S. Kumar, B. Pepper, D. Bouwmeester, A. I. Lvovsky, and C. Simon, Phys. Rev. Lett. **112**, 080503 (2014).
[21] M. Bahrami, M. Paternostro, A. Bassi, and H. Ulbricht, Phys. Rev. Lett. **112**, 210404 (2014).
[22] S. Nimmrichter, K. Hornberger, and K. Hammerer, Phys. Rev. Lett. **113**, 020405 (2014).
[23] L. Diosi, Phys. Rev. Lett. **114**, 050403 (2015).
[24] N. Brunner, D. Cavalcanti, S. Pironio, V. Scarani, and S. Wehner, Rev. Mod. Phys. **86**, 419 (2014).
[25] J. Ellis, J. S. Hagelin, D. V. Nanopoulos, and M. Srednicki, Nucl. Phys. **B241**, 381 (1984).
[26] G. C. Ghirardi, A. Rimini, and T. Weber, Phys. Rev. D **34**, 470 (1986).
[27] L. Diosi, Phys. Rev. A **40**, 1165 (1989).
[28] R. Penrose, Gen. Relativ. Gravit. **28**, 581 (1996).
[29] C. Pfister, J. Kaniewski, M. Tomamichel, A. Mantri, R. Schmucker, N. McMahon, G. Milburn, and S. Wehner, arXiv:1503.00577.
[30] J. F. Clauser, M. Horne, A. Shimony, and R. A. Holt, Phys. Rev. Lett. **23**, 880 (1969).
[31] R. F. Werner, Phys. Rev. A **40**, 4277 (1989).
[32] V. Scarani, Acta Phys. Slovaca **62**, 347 (2012).
[33] J. D. Cohen, S. M. Meenehan, G. S. MacCabe, S. Groblacher, A. H. Safavi-Naeini, F. Marsili, M. D. Shaw, and O. Painter, Nature (London) **520**, 522 (2015).
[34] C. Galland, N. Sangouard, N. Piro, N. Gisin, and T. J. Kippenberg, Phys. Rev. Lett. **112**, 143602 (2014).
[35] S. G. Hofer, W. Wieczorek, M. Aspelmeyer, and K. Hammerer, Phys. Rev. A **84**, 052327 (2011).
[36] V. Caprara Vivoli, P. Sekatski, J.-D. Bancal, C. C. W. Lim, A. Martin, R. T. Thew, H. Zbinden, N. Gisin, and N Sangouard, New J. Phys. **17**, 023023 (2015).
[37] K. Banaszek and K. Wodkiewicz, Phys. Rev. Lett. **82**, 2009 (1999).
[38] B. Hessmo, P. Usachev, H. Heydari, and G. Björk, Phys. Rev. Lett. **92**, 180401 (2004).
[39] A. Kuzmich, I. A. Walmsley, and L. Mandel, Phys. Rev. Lett. **85**, 1349 (2000).
[40] F. Monteiro, V. C. Vivoli, T. Guerreiro, A. Martin, J.-D. Bancal, H. Zbinden, R. T. Thew, and N. Sangouard, Phys. Rev. Lett. **114**, 170504 (2015).
[41] M. G. A. Paris, Phys. Lett. A **217**, 78 (1996).
[42] See Supplemental Material at http://link.aps.org/supplemental/10.1103/PhysRevLett.116.070405, which includes Refs. [24,31,32,34,43]. Part I gives the joint and marginal probabilities when the mechanical state is not in the vacuum, Part II shows how the locality loophole can be closed.
[43] L. K. Shalm *et al.*, Phys. Rev. Lett. **115**, 250402 (2015).
[44] F. Lecocq, J. D. Teufel, J. Aumentado, and R. W. Simmonds, Nat. Phys. **11**, 635 (2015).
[45] J. Chan, A. H. Safavi-Naeini, J. T. Hill, S. Meenehan, and O. Painter, Appl. Phys. Lett. **101**, 081115 (2012).
[46] E. Kuramochi, H. Taniyama, T. Tanabe, K. Kawasaki, Y.-G. Roh, and M. Notomi, Opt. Express **18**, 15859 (2010).
[47] X. Sun, X. Zhang, C. Schuck, and H. X. Tang, Sci. Rep. **3**, 1436 (2013).
[48] L.-M. Duan, M. D. Lukin, J. I. Cirac, and P. Zoller, Nature (London) **414**, 413 (2001).
[49] S. G. Hofer, K. W. Lehnert, and K. Hammerer, following Letter, Phys. Rev. Lett. **116**, 070406 (2016).

6 What does it take to see entanglement?

What does it take to see entanglement?

Valentina Caprara Vivoli,[1] Pavel Sekatski,[2] and Nicolas Sangouard[3]

[1]*Group of Applied Physics, University of Geneva, CH-1211 Geneva 4, Switzerland*
[2]*Institut for Theoretische Physik, Universitat of Innsbruck, Technikerstraße 25, A-6020 Innsbruck, Austria*
[3]*Department of Physics, University of Basel, Klingelbergstrasse 82, 4056 Basel, Switzerland*

(Dated: February 21, 2016)

Tremendous progress has been realized in quantum optics for engineering and detecting the quantum properties of light. Today, photon pairs are routinely created in entangled states. Entanglement is revealed using single-photon detectors in which a single photon triggers an avalanche current. The resulting signal is then processed and stored in a computer. Here, we propose an approach to get rid of all the electronic devices between the photons and the experimentalist i.e. to use the experimentalist's eye to detect entanglement. We show in particular, that the micro entanglement that is produced by sending a single photon into a beam-splitter can be detected with the eye using the magnifying glass of a displacement in phase space. The feasibility study convincingly demonstrates the possibility to realize the first experiment where entanglement is observed with the eye.

Introduction — The human eye has been widely characterized in the weak light regime. The data presented in Fig. 1 (circles) for example is the result of a well established experiment [1] where an observer was presented with a series of coherent light pulses and asked to report when the pulse is seen (the data have been taken from Ref. [2]). While rod cells are sensitive to single photons [3], these results show unambiguously that one needs to have coherent states with a few hundred photons on average, incident on the eye to systematically see light. As mentioned in Ref. [4], the results of this experiment are very well reproduced by a threshold detector preceded by loss. In particular, the red dashed line has been obtained with a threshold at 7 photons combined with a beamsplitter with 8% transmission efficiency. In the low photon number regime, the vision can thus be described by a positive-operator valued measure (POVM) with two elements $P_{\rm ns}^{\theta,\eta}$ for "not seen"and $P_{\rm s}^{\theta,\eta}$ for "seen"where $\theta = 7$ stands for the threshold, $\eta = 0.08$ for the efficiency, see Appendix, part I. It is interesting to ask what it takes to detect entanglement with such a detector.

Let us note first that such detection characteristics do not prevent the violation of a Bell inequality. In any Bell test, non-local correlations are ultimately revealed by the eye of the experimentalist, be it by analyzing numbers on the screen of a computer or laser light indicating the results of a photon detection. The subtle point is whether the amplification of the signal prior to the eye is reversible. Consider a gedanken experiment where a polarization-entangled two photon state $\frac{1}{\sqrt{2}}(|h\rangle_A|v\rangle_B - |v\rangle_A|h\rangle_B)$ is shared by two protagonists – Alice and Bob – who easily rotate the polarization of their photons with wave plates. Assume that they can amplify the photon number with the help of some unitary transformation U mapping, say, a single photon to a thousand photons while leaving the vacuum unchanged. It is clear that in this case, Alice and Bob can obtain a substantial violation of the Bell-CHSH inequality [5], as the human eye can almost perfectly distinguish a thousand photons from the vacuum. In practice, however, there is no way to properly implement U. Usually, the amplification is realized in an irreversible and entanglement-breaking manner, e.g. in a measure and prepare setting with a single photon detector triggering a laser [6]. In this case however the detection clearly happens before the eye.

One may then wonder whether there is a feasible way to reveal entanglement with the eye in reversible scenarios, i.e. with states, rotations and unitary amplifications that can be accessed experimentally. The task is a priori challenging. For example, the proposal of Ref. [7] where many independent entangled photon pairs are observed does not allow one to violate a Bell inequality with the realistic model of the eye described before. A closer example is the proposal of Ref. [4] where entanglement of a photon pair is amplified through a phase covariant cloning. Entanglement can be revealed with the human eye in this scenario if strong assumptions are made on the source. For example, a separable model based on a measure and prepare scheme, has shown that it is necessary to assume that the source produces true single photons [6, 8]. Here, we go beyond such a proposal by showing that entanglement can be seen without assumption on the detected state. Inspired by a recent work [9], we show that it is possible to detect path entanglement, i.e. entanglement between two optical paths sharing a single photon, with a trusted model of the human eye upgraded by a displacement in phase space. The displacement operation which serves as a photon amplifier, can be implemented with an unbalanced beamsplitter and a coherent state [10]. Our proposal thus relies on simple ingredients. It does not need interferometric stabilization of optical paths and is very resistant to loss. It points towards the first experiment where entanglement is revealed with human

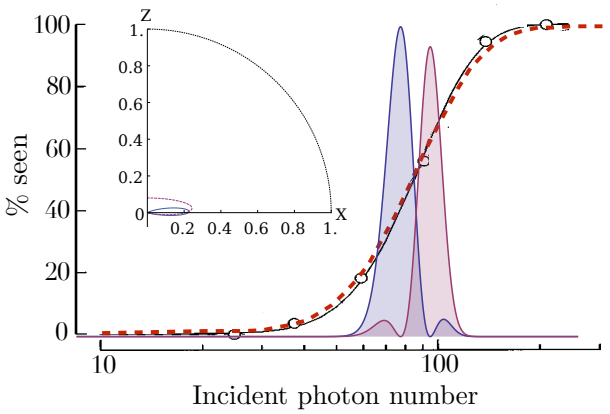

FIG. 1: Experimental results (circles) showing the probability to see coherent light pulses as a function of the mean photon number (taken from Ref. [2]). The black line is a guide for the eye. The dashed red line is the response of a threshold detector with loss (threshold at 7 photons and 8% efficiency). Such a detector can be used to distinguish the states $|0+1\rangle$ and $|0-1\rangle$ when they are displaced in phase space: The displacement operation not only increases the photon number but also makes the photon distribution distinguishable. This is shown through the two bumps which are the photon number distribution of $|D(\alpha)(0+1)\rangle$ and $|D(\alpha)(0-1)\rangle$ respectively for $\alpha \sim \sqrt{100}$. The inset is a quarter of the xz plane of the Bloch sphere having the vacuum and single photon Fock states $\{|0\rangle, |1\rangle\}$ as north and south poles respectively. A perfect qubit measurement corresponds to a projection along a vector with unit length (dotted line). The POVM element "no click"of a measurement combining a single-photon detector with 8% efficiency and a displacement operation defines a non-unit vector on the sphere for which the angle with the z axis can be changed by tuning the amplitude of the displacement (purple dashed curve). For a displacement with a zero amplitude (no displacement), this vector points out in the z direction whereas for an amplitude $\sim \sqrt{12.5}$, the vector points out in the x direction. The POVM element "not seen"of a measurement combining a human eye with a displacement operation also defines a non-unit vector on the sphere. The angle between this vector and the z axis can also be varied by changing the size of the displacement. In particular, for an amplitude of the displacement of $\sim \sqrt{100}$, this vector points out in the x direction and in this case, the measurement with the eye is fairly similar to the measurement with the single-photon detector with the same efficiency. Rotation in the xy plane can be obtained by changing the phase of the displacement operation.

eye-based detectors.

Upgrading the eye with displacement — Our proposal starts with an entangled state between two optical modes A and B

$$|\psi_+\rangle = \frac{1}{\sqrt{2}}\left(|0\rangle_A|1\rangle_B + |1\rangle_A|0\rangle_B\right). \qquad (1)$$

Here $|0\rangle$ and $|1\rangle$ stands for number states filled with the vacuum and a single photon respectively. To detect entanglement in state (1), a method using a photon detector – which does not resolve the photon number ($\theta = 1$) – preceded by a displacement operation has been proposed in Ref. [11] and used later in various experiments [9, 12, 13]. In the $\{|0\rangle, |1\rangle\}$ subspace, this measurement is a two outcome $\{P_{\rm ns}^{1,\eta}$ for "no click", $P_{\rm s}^{1,\eta}$ for "click"$\}$ non-extremal POVM on the Bloch sphere whose direction depends on the amplitude and phase of the displacement [14]. In particular, pretty good measurements can be realized in the x direction. This can be understood by realizing that the photon number distribution of the two states $|\mathcal{D}(\alpha)(0+1)\rangle$ and $|\mathcal{D}(\alpha)(0-1)\rangle$ where $\mathcal{D}(\alpha)$ is the displacement, slightly overlap in the photon number space and their mean photon numbers differ by $2|\alpha|$, see Fig. 1. This means that they can be distinguished, at least partially, with threshold detectors. It is thus interesting to analyze an eye upgraded by a displacement operation. In the $\{|0\rangle, |1\rangle\}$ subspace, we found that the elements $\{P_{\rm ns}^{7,\eta}, P_{\rm s}^{7,\eta}\}$ also constitute a non-extremal POVM, and as before, their direction in the Bloch sphere depends on the amplitude and phase of the displacement. For comparison, the elements "no click"and "not seen"are given in the inset of Fig. 1 considering real displacements and focusing on the case where the efficiency of the photon detector is equal to 8%. While the eye-based measurement cannot perform a measurement in the z direction, it is comparable to the single photon detector for performing measurements along the x direction. Identical results would be obtained in the yz plane for purely imaginary displacements. More generally, the measurement direction can be chosen in the xy plane by changing the phase of the displacement. We present in the next paragraph an entanglement witness suited for such measurements.

Witnessing entanglement with the eye — We consider a scenario where path entanglement is revealed with displacement operations combined with a photon detector on mode A and with the eye on mode B, c.f. Fig. 2. We focus on the following witness

$$W = \int_0^{2\pi} \frac{d\varphi}{2\pi} U_\varphi^\dagger \otimes U_\varphi^\dagger \left(\mathfrak{o}_\alpha^1 \otimes \mathfrak{o}_\beta^7\right) U_\varphi \otimes U_\varphi \qquad (2)$$

where $\mathfrak{o}_\alpha^\theta = D(\alpha)^\dagger \left(2P_{\rm ns}^{\theta,1} - \mathbb{1}\right) D(\alpha)$ is the observable obtained by attributing the value +1 to events corresponding to "no click"("not seen") and -1 to those associated to "click"("seen"). Since we are interested in revealing entanglement at the level of the detection, the inefficiency of the detector can be seen as a loss operating on the state, i.e. the beamsplitter modeling the detector inefficiency acts before the displacement operation whose amplitude is changed accordingly [9]. This greatly simplifies the derivation of the entanglement witness as this allows us to deal with detectors with unit efficiencies ($\eta = 1$). The phase of both displacements α

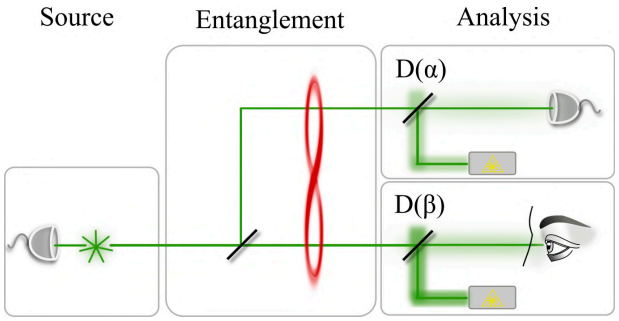

FIG. 2: Scheme of our proposal for detecting entanglement with the human eye. A photon pair source based on spontaneous parametric down conversion is used as a single photon source, the emission of a photon being heralded by the detection of its twin. The heralded photon is then sent into a beamsplitter to create path entanglement, i.e. entanglement between two optical modes sharing a delocalized single photon. The entangled state is subsequently detected using a photon counting detector preceded by a displacement operation on one mode, and using a human eye preceded by a displacement on the other mode. The correlations between the results (click and no click for the photon detector, seen and not seen for the human eye) allows one to conclude about the presence of entanglement, c.f. main text

and β is randomized through the unitary transformation $U_\varphi = e^{i\varphi a^\dagger a}$ for A (where a, $a^\dagger$ are the bosonic operators for the mode A) and similarly for B. The basic idea behind the witness can be understood by noting that for ideal measurements $W_{\text{ideal}} = \int (\cos\varphi\sigma_x + \sin\varphi\sigma_y) \otimes (\cos\varphi\sigma_x + \sin\varphi\sigma_y) \frac{d\varphi}{2\pi}$ equals the sum of coherence terms $|01\rangle\langle 10| + |10\rangle\langle 01|$. Since two qubit separable states stay positive under partial transposition [15, 16], these coherence terms are bounded by $2\sqrt{p_{00}p_{11}}$ for two qubit separable states where p_{ij} is the joint probability for having i photons in A and j photons in B. Any state ρ such that $\text{tr}\left[\rho W_{\text{ideal}}\right] > 2\sqrt{p_{00}p_{11}}$ is thus necessarily entangled. Following a similar procedure, we find that for any two qubit separable states, $\text{tr}\left[W\rho_{\text{sep}}^{\text{qubit}}\right] \leq W_{\text{ppt}}$ where

$$W_{\text{ppt}} = \sum_{i,j=0}^{1} \langle ij|W|ij\rangle p_{ij} + 2|\langle 10|W|01\rangle|\sqrt{p_{00}p_{11}}, \quad (3)$$

see Appendix, part II. The p_{ij}s can be bounded by noting that for well chosen displacement amplitudes, different photon number states lead to different probabilities "not seen"and "no click". For example, we show in the Appendix, part III that

$$p_{00} \leq \frac{P_{AB}(+1{+}1|0\beta_0, \rho_{\text{exp}}) - P_B(+1|\beta_0, |1\rangle) P_A(+1|0, \rho_{\text{exp}})}{P_B(+1|\beta_0, |0\rangle) - P_B(+1|\beta_0, |1\rangle)}.$$

$P_B(+1|\beta_0, \rho_{\text{exp}})$ is the probability "not seen"when looking at the experimental state ρ_{exp} amplified by the displacement β_0. This is a quantity that is measured, unlike $P_B(+1|\beta_0, |1\rangle)$, which is computed from $\frac{1}{2}\left(1 + \langle 1|\sigma^7_{\beta_0}|1\rangle\right)$. β_0 is the amplitude of the displacement such that $P_B(+1|\beta_0, |0\rangle) = P_B(+1|\beta_0, |2\rangle)$. p_{10}, p_{11} and p_{01} can be bounded in a similar way, the two latter requiring another displacement amplitude β_1, see Appendix, part III.

The recipe that we propose for testing the capability of the eye to see entanglement thus consists in four steps. i) Measure the probability that the photon detector in A does not click and of the event "not seen"for two different displacement amplitudes $\{0, \beta_0\}$, $\{0, \beta_1\}$. ii) Upper bound from i) the joint probabilities p_{00}, p_{11} p_{01} and p_{10}. iii) Deduce the maximum value that the witness W would take on separable states W_{ppt}. iv) Measure $\langle W\rangle$. If there are values of α and β such that $\langle W\rangle > W_{\text{ppt}}$, we can conclude that the state is entangled. Note that this conclusion holds if the measurement devices are well characterized, i.e. the models that are used for the detections well reproduce the behavior of single photon detectors and eyes, the displacements are well controlled operations and filtering processes ensure that a single mode of the electromagnetic wave is detected. We have also assumed hitherto that the measured state is well described by two qubits. In the Appendix part IV, we show how to relax this assumption by bounding the contribution from higher photon numbers. We end up with an entanglement witness that is state independent, i.e. valid independently of the dimension of the underlying Hilbert space.

Proposed setup — The experiment that we envision is represented in Fig. 2. A single photon is generated from a photon pair source and its creation is heralded through the detection of its twin photon. Single photons at 532 nm can be created in this way by means of spontaneous parametric down conversion [3]. They can be created in pure states by appropriate filtering of the heralding photon, see e.g. [9]. The heralded photon is then sent into a beamsplitter (with transmission efficiency T) which leads to entanglement between the two output modes. As described before, displacement operations upgrade the photon detection in A and the experimentalist's eye in B. In practice, the local oscillators needed for the displacement can be made indistinguishable from single photons by using a similar non-linear crystal pumped by the same laser but seeded by a coherent state, see e.g. [17]. The relative value $\Delta W = \langle W\rangle - W_{\text{ppt}}$ that would be obtained in such an experiment is given in Fig. 3 as a function of T. We have assumed a transmission efficiency from the source to the detectors $\eta_t = 90\%$, a detector efficiency of 80% in A and an eye with the properties presented before (8% efficiency and a threshold at 7 photons). The results are optimized over the squeezing parameter of the pair source for suitable amplitudes of the displacement

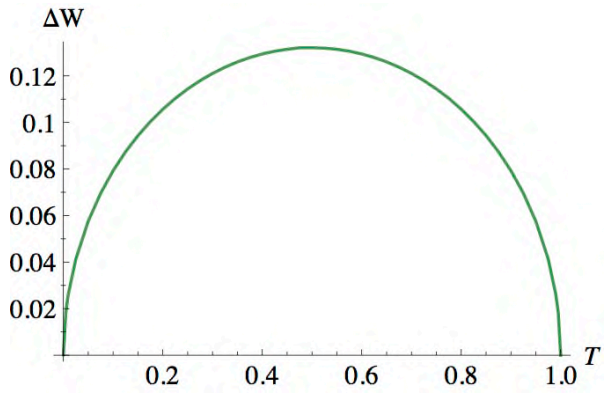

FIG. 3: Value of the witness that would be measured in the setup shown in Fig. 2 relative to the value that would be obtained from state with a positive partial transpose $\Delta W = \langle W\rangle - W_{\rm ppt}$ as a function of the beamsplitter transmission efficiency T under realistic assumption about efficiencies, c.f. main text.

operations, see Appendix, part V. We clearly see that despite low overall efficiencies and multi-photon events that are unavoidable in spontaneous parametric down conversion processes, our entanglement witness can be used to successfully detect entanglement with the eye. Importantly, there is no stabilization issue if the local oscillator that is necessary for the displacement operations is superposed to each mode using a polarization beamsplitter instead of a beamsplitter to create path entanglement, see e.g. [18]. The main challenge is likely the timescale of such an experiment, as the repetition time is inherently limited by the response of the experimentalist, but this might be overcome, at least partially by measuring directly the response of rod cells as in Ref. [3].

Conclusion — Our results help in clarifying the requirements to see entanglement. If entanglement breaking operations are used, as in the experiments performed so far, it is straightforward to see entanglement. In this case, however, the measurement happens before the eyes. In principle, the experimentalist can reveal non-locality directly with the eyes from reversible amplifications, but these unitaries cannot be implemented in practice. What we have shown is that entanglement can be realistically detected with human eyes upgraded by displacement operations in a state-independent way. From a conceptual point of view, it is interesting to wonder whether such experiments can be used to test collapse models in perceptual processes in the spirit of what has been proposed in Refs. [19, 20]. For more applied perpectives, our proposal shows how threshold detectors can be upgraded with a coherent amplification up to the point where they become useful for quantum optics experiments. Anyway, it is safe to say that probing the human vision with quantum light is a *terra incognita*. This makes it an attractive challenge on its own.

Acknowledgements — We thank C. Brukner, W. Dür, F. Fröwis, N. Gisin, K. Hammerer, M. Ho, M. Munsch, R. Schmied, A. Sørensen, P. Treutlein, R. Warburton and P. Zoller for discussions and/or comments on the manuscript. This work was supported by the Swiss National Science Foundation (SNSF) through NCCR QSIT and Grant number PP00P2-150579, by the John Templeton Foundation, and by the Austrian Science Fund (FWF), Grant number J3462 and P24273-N16.

Appendix I In this section, we provide a convenient expression for a threshold detector with non-unit efficiency (threshold θ and efficiency η). By modeling loss by a beamsplitter, the no-click event can be written as $P_{\rm ns}^{\theta,\eta} = C_L^\dagger \sum_{m=0}^{\theta-1} |m\rangle\langle m| C_L$ where $C_L = e^{\tan\gamma\, a c^\dagger} e^{\ln(\cos\gamma) a^\dagger a} |0\rangle_c$ stands for the beam splitter. a, $a^\dagger$ are the bosonic operators for the detected mode and $\cos^2\gamma = \eta$. After straightforward manipulations we can find that

$$P_{\rm ns}^{\theta,\eta} = \frac{\eta^\theta}{(\theta-1)!}\frac{d^{\theta-1}}{d(1-\eta)^{\theta-1}}\frac{(1-\eta)^{a^\dagger a}}{\eta}. \qquad (4)$$

The click event can be deduced from $P_{\rm s}^{\theta,\eta} = \mathbb{1} - P_{\rm ns}^{\theta,\eta}$.

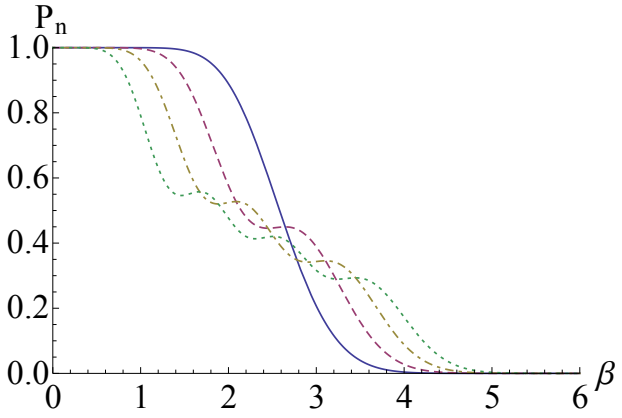

FIG. 4: Probability for having no click on a threshold detector ($\theta = 7$) with a number state $|n\rangle$ that is displaced in phase space as a function of the displacement amplitude β

Appendix II Here we give details on how the entanglement witness has been derived, assuming first that one has qubits. Let's consider a general density matrix P in the subspace $\{|0\rangle, |1\rangle\}$. We look for the maximal value that $\langle W\rangle$ can take over the states staying positive under partial transposition, i.e. we want to optimize $\langle W\rangle$ over P such that i) $P \geq 0$, ii) $\mathrm{tr}(P) = 1$ and iii) $P^{T_b} \geq 0$. Here P^{T_b} stands for the partial transposition over one

party. As $\langle W\rangle$ is non-zero in blocks spanned by $\{|00\rangle\}$, $\{|01\rangle, |10\rangle\}$ and $\{|11\rangle\}$ only, it is straightforward to show that for any separable state

$$W_{\rm ppt} = \sum_{i,j=0}^{1} \langle ij|\, W\, |ij\rangle\, p_{ij} + 2\,|\langle 01|\, W\, |10\rangle|\sqrt{p_{00}p_{11}}, \quad (5)$$

where $p_{ij} = \langle ij|\, P\, |ij\rangle$. Any state $\rho_{\rm exp}$ for which ${\rm tr}(\rho_{\rm exp}\, W) - W_{\rm ppt} > 0$ has a negative partial transpose, i.e. is necessarily entangled. It is important to stress that $W_{\rm ppt}$ depends on the photon number statistics $\vec{p} = p_{ij}$. We show in the next section how they can be bounded.

Appendix III Figure 4 shows the probability for having no click on a threshold detector ($\theta = 7$) with a number state $|n\rangle$ that is displaced in phase space as a function of the displacement amplitude β, $P_B(+1|\beta, |n\rangle)$ for $n = 0$, 1, 2, 3. We show how to bound p_{00}, p_{01}, p_{10}, and p_{11} from these results.

In order to bound p_{00} and p_{01}, let's consider the displacement amplitude β_0 ($\sim$ 2.71) such that $P_B(+1|\beta_0, |0\rangle) = P_B(+1|\beta_0, |2\rangle)$. We have

$$\begin{aligned} P_{AB}(+1+1|0\beta_0, \rho_{\rm exp}) &= \sum_{n=0}^{+\infty} p_{0n} P_B(+1|\beta_0, |n\rangle) \\ &\leq P_B(+1|\beta_0, |1\rangle) p_{0A} + (P_B(+1|\beta_0, |0\rangle) - P_B(+1|\beta_0, |1\rangle)) p_{00}. \end{aligned}$$

using $P_B(+1|\beta_0, |n \geq 2\rangle) < P_B(+1|\beta_0, |1\rangle)$. Note that $p_{0n} = \langle 0n|\, \rho_{\rm exp}\, |0n\rangle$ and $p_{0A} = {\rm tr}(\rho_{\rm exp}\, |0\rangle_A \langle 0|)$. This leads to the upperbound

$$p_{00} \leq \frac{P_{AB}(+1+1|0\beta_0, \rho_{\rm exp}) - P_B(+1|\beta_0, |1\rangle) P_A(+1|0, \rho_{\rm exp})}{P_B(+1|\beta_0, |0\rangle) - P_B(+1|\beta_0, |1\rangle)}.$$

In the same way, we get

$$p_{01} \leq \frac{P_{AB}(-1+1|0\beta_0, \rho_{\rm exp}) - P_B(+1|\beta_0, |1\rangle) P_A(-1|0, \rho_{\rm exp})}{P_B(+1|\beta_0, |0\rangle) - P_B(+1|\beta_0, |1\rangle)}.$$

To bound p_{10} and p_{11} we consider the displacement amplitude β_1 (~ 2.09) such that $P_B(+1|\beta_1, |1\rangle) = P_B(+1|\beta_1, |2\rangle)$ (and $P_B(+1|\beta_1, |n \geq 3\rangle) \leq P_B(+1|\beta_1, |1\rangle)$.) We get

$$p_{10} \leq \frac{P_{AB}(+1+1|0\beta_1, \rho_{\rm exp}) - P_B(+1|\beta_1, |0\rangle) P_A(+1|0, \rho_{\rm exp})}{P_B(+1|\beta_1, |1\rangle) - P_B(+1|\beta_1, |0\rangle)}.$$

$$p_{11} \leq \frac{P_{AB}(-1+1|0\beta_1, \rho_{\rm exp}) - P_B(+1|\beta_1, |0\rangle) P_A(-1|0, \rho_{\rm exp})}{P_B(+1|\beta_1, |1\rangle) - P_B(+1|\beta_1, |0\rangle)}.$$

Note also that for β_2 (~ 2.64) such that $P_B(+1|\beta_2, |0\rangle) = P_B(+1|\beta_2, |1\rangle)$ (and $P_B(+1|\beta_2, |n \geq 2\rangle) < P_B(+1|\beta_2, |0\rangle)$), we have

$$p_{n\geq 2B} = \sum_{n\geq 2} {\rm tr}(\rho_{\rm exp}\, |n\rangle \langle n|_B) \leq \frac{P_B(+1|\beta_2, \rho_{\rm exp}) - P_B(+1|\beta_2, |0\rangle)}{P_B(+1|\beta_2, |3\rangle) - P_B(+1|\beta_2, |0\rangle)} = p_B^*.$$

Note that $p_{n\geq 2A}$ can be bounded from an auto-correlation measurement (see Ref. [13] of the main text). The upperbound on $p_{n\geq 2A}$ is called p_A^*. Importantly, the previous upperbounds hold in the qudit case, i.e. if the modes A and B are filled with more than one photon.

Appendix IV Now consider the case where the state has an arbitrary dimension in the Fock space. We can proceed as follows. A generic state P can be written as

$$P = \begin{pmatrix} P_{n_a\leq 1 \cap n_b \leq 1} & P_{\rm coh} \\ P_{\rm coh}^\dagger & P_{n_a \geq 2 \cup n_b \geq 2} \end{pmatrix}. \quad (6)$$

We focus on the detection of entanglement in the qubit subspace $P_{n_a\leq 1\cap n_b\leq 1}$. By linearity of the trace, we have

$$\begin{aligned}\mathrm{tr}(WP) = &\mathrm{tr}(P_{n_a\leq 1\cap n_b\leq 1}W) + \mathrm{tr}\Big((P_{coh}^{\dagger}+P_{coh})W\Big)\\ &+\mathrm{tr}(P_{n_a\geq 2\cup n_b\geq 2}W). \end{aligned} \quad (7)$$

Let us treat those terms one by one. The maximum algebraic value of W is equal to 1, in such a way that the third term is upperbounded by $\mathrm{tr}(P_{n_a\geq 2\cup n_b\geq 2}W)\leq \mathrm{tr}(P_{n_a\geq 2\cup n_b\geq 2})\leq p_A^*+p_B^*=p^*$.

The first term is the subject of the second section, where we showed that $\mathrm{tr}(WP_{n_a\leq 1\cap n_b\leq 1})\leq W_{\mathrm{ppt}}(\vec{p})$ given in (5).

To bound the second term, let us recall that W does not contain coherences between sectors of different total photon number, in such a way that

$$\mathrm{tr}\Big((P_{coh}^{\dagger}+P_{coh})W\Big)\leq 2(|C_{11}^{20}W_{11}^{20}|+|C_{11}^{02}W_{11}^{02}|),$$

where $C_{ij}^{kl}=\langle ij|\,P\,|kl\rangle$ and $W_{ij}^{kl}=\langle ij|\,W\,|kl\rangle$. The positivity of the state P restricted to the subspace $\{|20\rangle,|02\rangle,|11\rangle\}$ implies $C_{11}^{kl}\leq\sqrt{p_{11}p_{kl}}$. Since $p_{20}\leq p_A^*$ and $p_{02}\leq p_B^*$, we have

$$\mathrm{tr}\Big((P_{coh}^{\dagger}+P_{coh})W\Big)\leq 2\sqrt{p_{11}}\left(|W_{11}^{20}|\sqrt{p_A^*}+|W_{11}^{02}|\sqrt{p_B^*}\right),$$

Finally, any state P, such that its restriction $P_{n_a\leq 1\cap n_b\leq 1}$ remains positive under partial transpose, satisfies

$$\begin{aligned}\mathrm{tr}(WP) &\leq W_{\mathrm{PPT}}\\ &= W_{\mathrm{ppt}}(\vec{p})+2\sqrt{p_{11}}\left(|W_{11}^{20}|\sqrt{p_A^*}+|W_{11}^{02}|\sqrt{p_B^*}\right)\\ &\quad +p^*.\end{aligned}$$

Any state ρ_{exp} such that $\mathrm{tr}(W\rho_{\mathrm{exp}})-W_{\mathrm{PPT}}>0$ is necessary entangled.

Appendix V The value of W that would be observed in the experiment represented in Fig. 2 of the main text can be calculated from

$$\langle W\rangle=\mathrm{tr}\left(\varpi_{\beta}^{7,\eta_b}\varpi_{\alpha}^{1,\eta_a}\rho_h\right),$$

where η_a and η_b are the efficiencies of the detector in mode A and B respectively. ρ_h is the density matrix after the beamsplitter (with transmission T) that is conditioned on a click in the heralding detector. The amplitude of the displacements are chosen such that $\beta=\sqrt{\frac{7}{\eta_b}}$, $\alpha=\frac{1}{\sqrt{\eta_a}}$. Given the efficiency of the heralding detector $\eta_h=1-R_h$ and the squeezing parameter g of the SPDC source, the state that is announced by a click on the heralding detector can be expressed as a difference of two thermal states

$$\frac{1-R_h^2T_g^2}{T_g^2\left(1-R_h^2\right)}\left[\rho_{\mathrm{th}}\left(\bar{n}=\frac{T_g^2}{1-T_g^2}\right)-\frac{1-T_g^2}{1-R_h^2T_g^2}\rho_{\mathrm{th}}\left(\bar{n}=\frac{R_h^2T_g^2}{1-R_h^2T_g^2}\right)\right] \quad (7)$$

where $T_g=\tanh g$ and $\rho_{\mathrm{th}}(\bar{n})=\frac{1}{1+\bar{n}}\sum_k\left(\frac{\bar{n}}{1+\bar{n}}\right)^k|k\rangle\langle k|$. We get

$$\langle W\rangle=\frac{1-R_h^2T_g^2}{T_g^2\left(1-R_h^2\right)}\left[W^{\mathrm{th}}\left(\bar{n}=\frac{T_g^2}{1-T_g^2}\right)-\frac{1-T_g^2}{1-R_h^2T_g^2}W^{\mathrm{th}}\left(\bar{n}=\frac{R_h^2T_g^2}{1-R_h^2T_g^2}\right)\right]$$

where

$$W^{\mathrm{th}}(\bar{n})=\frac{\eta_b^7}{6!}\frac{d^6}{d(1-\eta_b)^6}\frac{1}{\eta_b}\left[1+4\frac{e^{-\eta_a|\alpha|^2-\eta_b|\beta|^2+\frac{\bar{n}|\alpha\eta_a\sqrt{R}+\beta\eta_b\sqrt{T}|^2}{\bar{n}(\eta_aR+T\eta_b)+1}}}{\bar{n}(\eta_aR+T\eta_b)+1}-2\frac{e^{-\frac{\eta_a|\alpha|^2}{\eta_a\bar{n}R+1}}}{\eta_a\bar{n}R+1}-2\frac{e^{-\frac{\eta_b|\beta|^2}{\eta_b\bar{n}T+1}}}{\eta_b\bar{n}T+1}\right].$$

The previous expression can easily be obtained by writing the thermal state as a mixture of coherent states $\rho_{\mathrm{th}}(\bar{n})=\frac{1}{\pi\bar{n}}\int e^{-\frac{|\alpha|^2}{\bar{n}}}|\alpha\rangle\langle\alpha|\,d^2\alpha$, as the expectation value of W on a coherent state $\langle\alpha|\,W\,|\alpha\rangle$ is easily obtained through the formula (4) using $\langle\alpha|\,(1-\eta)^{a^{\dagger}a}\,|\alpha\rangle=e^{-\eta|\alpha|^2}$.

[1] S. Hecht, S. Shlaer, and M. Pirenne, J. Gen. Physiol. **25**, 819 (1942).

[2] F. Rieke and D.A. Baylor, Rev. Mod. Phys. **70**, 1027 (1998).

[3] N.M. Phan, M.F. Cheng, D.A. Bessarab, and L.A. Krivitsky, Phys. Rev. Lett. **112**, 213601 (2014).
[4] P. Sekatski, N. Brunner, C. Branciard, N. Gisin and C. Simon, Phys. Rev. Lett. **103**, 113601 (2009).
[5] J.F. Clauser, M.A. Horne, A. Shimony, and R.A. Holt, Phys. Rev. Lett. **23**, 880 (1969).
[6] E. Pomarico, B. Sanguinetti, P. Sekatski, H. Zbinden, and N. Gisin, New J. Phys. **13**, 063031 (2011).
[7] N. Brunner, C. Branciard, and N. Gisin, Phys. Rev. A **78**, 052110 (2008).
[8] P. Sekatski, B. Sanguinetti, E. Pomarico, N. Gisin, and C. Simon, Phys. Rev. A **82**, 053814 (2010).
[9] F. Monteiro, V. Caprara Vivoli, T. Guerreiro, A. Martin, J.-D. Bancal, H. Zbinden, R. T. Thew, and N. Sangouard, Phys. Rev. Lett. **114**, 170504 (2015).
[10] M.G.A. Paris, Phys. Lett. A **217**, 78 (1996).
[11] K. Banaszek and K. Wodkiewicz, Phys. Rev. Lett. **82**, 2009 (1998).
[12] A. Kuzmich, I. A. Walmsley, and L. Mandel, Phys. Rev. Lett. **85**, 1349 (2000).
[13] B. Hessmo, P. Usachev, H. Heydari, and G. Björk, Phys. Rev. Lett. **92**, 180401 (2004).
[14] V. Caprara Vivoli, P. Sekatski, J.-D. Bancal, C.C.W. Lim, A. Martin, R. T. Thew, H. Zbinden, N. Gisin and N. Sangouard, New J. Phys. **17** 023023 (2015).
[15] A. Peres, Phys. Rev. Lett. **77**, 1413 (1996).
[16] M. Horodecki, P. Horodecki, and R. Horodecki, Phys. Lett. A **223**, 1 (1996).
[17] N. Bruno, A. Martin, P. Sekatski, N. Sangouard, R. Thew, and N. Gisin, Nature Phys. **9**, 545 (2013).
[18] O. Morin, J.-D. Bancal, M. Ho, P. Sekatski, V. D'Auria, N. Gisin, J. Laurat, and N. Sangouard, Phys. Rev. Lett. **110**, 130401 (2013).
[19] G. C. Ghirardi, Phys. Lett. A **262**, 1 (1999).
[20] F. H. Thaheld, BioSystems **71**, 305 (2003).

Acknowledgments

At the end of my PhD experience, I am naturally induced to look back and draw some conclusions concerning my scientific and human growth. Although this thesis is conceived as a presentation of the results of my research, I would like to express here my thankfulness to the persons who played an important role in my scientific and human life during the last four years.
I wish, first of all, to thank my supervisors, Nicolas Gisin and Nicolas Sangouard. They offered me a constant support stimulating, at the same time, the development of my own research skills.
During the four years of my PhD, I had the occasion of sharing my scientific ideas with many valuables scientists. Among them, I feel the real pleasure to express my gratitude to Gilles Puetz, Tomer Barnea, Charles Lim, Anthony Martin, and Yeong-Cherng Liang. They gave different and strong contributions to my scientific growth and approach to research.
Finally, I must acknowledge that these four years of work would have been much harder without the presence of my friends. I would like, firstly, to thank my "old" friends from Palermo, that supported me all the time, especially because of my personal life issues. In particular, among them, I would like to cite Riccardo, Nicoletta, and Laura.
Secondly, I would like to thank the "new" friends that I have made in Geneva and that have accompanied my experience here. I would like to thank Natalia, Giulia, Tomer, Tommasso, Gianluca, and Ephanielle.
Lastly, I would like to thank all the members of my family. You are my strength, now and forever.